ABSTRACT

WHITE, ERIC LOUIS. Use of UAS Technology and Imaging Sensors for Optimization of Target Weed Control in Vegetation Management Scenarios (Under the direction of Drs. Robert J. Richardson and Ramon Leon Gonzalez).

Undesirable vegetation in rights-of-way scenarios if not managed properly negatively impact powerlines and railroad systems inflicting billions of dollars on taxpayers. Power outage expenditures are federally mandated and cost millions of dollars for each individual power outage. An overwhelming majority of power outages are caused from vegetation. Integrated vegetation management (IVM) is necessary to prevent damages and power outages from occurring. Management practices can vary across landscape and range from mechanical, chemical, cropping, and grazing techniques. Chemical treatments have become a popular method of control of nuisance species. This method is efficient and effective, however can become a cumbersome task with using backpack sprayers over vast distances. In remote locations other methods of using aerial spray systems are more feasible than with locating each specimen within the treatment zones. Advancements in small Unmanned Aerial Systems and machine learning provide vegetation managers the ability to autonomously detect and manage undesirable vegetation and even administer herbicides with sUAS systems. This research focuses on machine learning techniques with remotely sensed data to produce autonomous methods to detect undesirable vegetation.

Two common nuisances within the piedmont and coastal region of North Carolina transmission rights-of-way scenarios are *Pinus taeda* and *Liquidambar styraciflua*. These two species in these scenarios are low growing and unable to be detected with large scale satellite data with current resolutions available. However, our object was to evaluate machine learning techniques for autonomously detecting *Pinus taeda* and *Liquidambar styraciflua* within rights-

of-ways. The results obtained provided evidence to support *Pinus taeda* and *Liquidambar styraciflua* are in fact capable of being autonomously detected with data obtained from small Unmanned Aerial Systems and computer vision.

Use of sUAS Technology and Imaging Sensors for Optimization of Target Weed Control in Vegetation Management Scenarios

by
Eric Louis White

A thesis submitted to the Graduate Faculty of
North Carolina State University
in partial fulfillment of the
requirements for the degree of
Master of Science

Fisheries, Wildlife and Conservation Biology &
Crop Science

Raleigh, North Carolina
2021

APPROVED BY:

_____	_____
Dr. Robert Richardson Committee Co-Chair	Dr. Ramon Leon Gonzalez Committee Co-Chair
_____	_____
Dr. Stacy A. C. Nelson	Dr. Scott Ferguson
_____	
Dr. David Spak External Member	

DEDICATION

I dedicate this to my wife, Malissa Elliott White, and my daughter, Daughtry Rose White, to my mom and dad. Thank you all for your love and support throughout my endeavors with this journey. I appreciate everything you done that allowed me to pursue this dream of mine and for me to continue to do for me each day. Without you, none of this would have been possible.

BIOGRAPHY

Eric White was born in Knoxville, TN and was raised in Seymour, TN. He began his undergraduate academic career at a small liberal arts college nestled in the southwestern portion of Virginia, called The University of Virginia's College at Wise, obtaining a B.S. in Environmental Science with a concentration in Biology. During his undergraduate degree he researched Green Salamanders (*Aneides aeneus)* and the impact of land degradation from natural resource extraction in this species habitat. Along with this, he joined a research team focused on water quality monitoring of acid mine drainage on reclaimed minelands. During his field offseason, time was spent helping the local Southern Appalachian Maple Research and Activities (SAMaRA) team performing interdisciplinary research to conserve sugar maple and assess potential alternative maple species for the sugaring industry.

Upon graduation Eric worked as an independent research consultant with NASA DEVELOP and utilized remote sensing to address environmental issues with local, state, and federal agencies across the country. This experience broadened his horizon and sparked interest in him to apply to NCSU.

ACKNOWLEDGMENTS

I would like to acknowledge my advisor Dr. Robert Richardson for guiding me along this journey to obtain my M.S. I would also like to thank all of those apart of the Richardson lab and those who were always there when I needed it during my time at NCSU. I would like to especially acknowledge my loving wife Elliott for her continuous support throughout this entire journey.

TABLE OF CONTENTS

LIST OF TABLES

LIST OF FIGURES

CHAPTER 1

Techniques for Computer Vision Applications in Aquatic Plant Management

Abstract

Until recently, major advancements in artificial intelligence (AI) have been limited due to inadequate computational power. Today, AI is rapidly advancing due to the graphical processing unit (GPU) revolution which has allowed computers to process larger and more complex objects than they were previously able to (Oh & Jung, 2004). As a result, rapid integration of AI and convolutional neural networks (CNNs) to address engineering and science problems have increased internationally since the mid-2000s. One industry beginning to integrate this technology into its research and development strategies is that of aquatic plant management. Proper procedures for implementing, designing, and training CNNs for aquatic plant management are absent. Such methods for CNN development can determine the viability and success of the created models. This paper explores the guidelines for the creation of successful CNN models and the challenges of applying them in aquatic settings.

Introduction

New technologies and open-sourced community efforts have brought forth several integral components that have allowed for the rapid development of improved artificial intelligence (AI). One such component is the convolutional neural network (CNN). CNNs were first developed in the 1980s to train a neural network to detect handwritten digits (Fukushima, 1988). Since the inception, CNNs have been trained for computer vision, speech recognition, facial recognition, and several other applications. These are capable to be trained with CCNs

because they are feedforward networks, meaning information flows in one direction from the inputs to outputs. CNNs were designed to mimic the human visual cortex and its functionality to process visualize and imagery based on a hierarchical structure (German, 1999). The human visual cortex contains alternating layers and both simple and complex cells (Hubel, 1959 ; Hubel & Wiesel, 1962), thus a CNN has several simple and complex layers within its own architecture to mimic human vision (LeCun et al., 1998). CNNs achieve these simple and complex layers with convolution and pooling layers (Fukushima, 1988). The pooling layer immediately follows a convolutional layer to down sample the output to reduce the number of parameters to be learned by the network. Further, deep modules are formed by stacking these subsampled layers on top of each other. In a CNN, a computer visualizes a window over the input image and flows over each of the image's pixels. During this process, the computer selects and extracts important features and forms a new layer. Next, a pooling technique selects additional values to enhance features. By enhancing features, differentiating between different types of objects is more achievable.

The field of aquatic plant management could greatly benefit from the use of AI and applied CNNs. Wu et al. (2014) used neural networks and hyperspectral sensors to monitor turbidity and found the neural networks to outperform the regression models. Their work provides opportunity for remote monitoring of water bodies. CNNs can be applied to research similar to Wu et al. (2014) with image classifications for long term monitoring efforts. These efforts could improve the early detection and rapid response of nuisance species. Due to the immense diversity of aquatic macrophytes, the development of a CNN that could successfully identify these species would be challenging. These challenges include differentiating between

similar phenological stages of different species, working with species of differing growth habits of submersed, floating, or emergent, and the geographical localities of these species of interest.

In general, computer vision can be performed using one of three major categories: image classification, object detection, or semantic segmentation. If it is only necessary to distinguish aquatic plants by their growth habit and not down to the species level, image classification can be used. Image classification is the basis for other forms of computer vision such as localization, detection, segmentation. Image classification assigns a categorical class label to an image and does not bound the classification with any insight to what is classified as the target. Object detection is an image processing technology that detects occurrences of semantic objects in digital media files. Object detection is feasible with several different species of floating aquatic macrophytes. Lastly, semantic segmentation, a more precise method of object detection, simplifies and changes the representations of the multiple segments for easier analysis by labelling each pixel within the digital files (Long et al., 2015). Further, instance segmentation, a form of semantic segmentation, may be applied to predict and identify each object individually rather than classifying each pixel by segmentation masks (Romera-Paredes & Torr, 2016). Selecting the correct image classification scheme is important, especially with determining desired outcome with data collection.

To adequately differentiate species, capturing a large amount of imagery for each individual species is necessary. To determine the appropriate number of images to capture, it is important to consider model integrity and model parameters and the results obtained after training. When high volumes of images are needed to successfully run a model, it is advantageous to utilize transfer learning. Transfer learning allows for quicker training and is adapted from datasets and models that have already been trained with classified data, thus

reducing the amount of imagery needed to train. As such, with transfer learning, basic models have the ability to represent the objects of interest without relying on robust datasets. This reduction of imagery allows for the computational requirements to be greatly reduced as well.

As trainable data are increased in number, computational limitations will occur. To alleviate, smaller batch sizes and larger amounts of epochs for training will be required to reduce computational limitations. As this occurs, training on larger GPUs and or utilizing a cloud computing platform, such as Google Collaboratory, should be explored. As more resources become readily available, vegetation managers will have more possibilities and near limitless potential to achieve goals such as the early detection rapid response (EDRR) to nuisance plant invasions.

Methods

Data Acquisition

The first proposed CNN was neocognitron that was self-organized into a structure similar to a proposed visual human cortex by Hubel and Wiesel (1962). This original CNN built upon the previous work of a self-organizing multilayered neural network (Fukushima, 1975). Because of the design, the first self-organizing multilayered neural network recognized geometrically similar patterns. As systems and frameworks evolved (LeCun et al., 1989), brought forth new potential in computer vision tasks through CNNs.

Before CNNs frameworks are constructed, data collection is inevitable. There are publicly available datasets for the use of transfer learning such as but not limited to LeNet (LeCun et al., 1998), AlexNet (Krizhevsky et al., 2012), and GoogLeNet (Szegedy et al., 2015). These pre-labeled data provide an opportunity for transfer learning (Torrey & Shavlik, 2010).

Selecting the right dataset for transfer learning should align with the data going to be classified, thus not all datasets will transfer learning efficiently.

When collecting data for a CNN, a comprehensive wholistic approach consisting of data comprising of multiple backgrounds, different environments, and diverse object appearance can be an excellent starting point. This should provide enough variation for a comprehensive overview of the object being studied. Methods to increase data diversity during image acquisition include variance in the image angle, time of day, shadowing, time of year, and if vegetation is being captured different phenological stages. Traditional image augmentations such as clipping, flipping, rotating, shearing (O'Gorman & Kasturi, 1995), can also increase accuracy and traditional image augmentations

Capturing imagery within an aquatic setting can be complicated by light reflection on the water surface and light penetration into water column. In the optical spectral region radiometric signals are greatly absorbed and plant reflectance for submersed macrophytes are found to be lower (Dierssen et al., 2003; Everitt et al., 1999; Fyfe, 2003; Han & Rundquist, 2003; Heege et al., 2003; Paringit et al., 2003). The amount of sunlight reflectance off the plants being observed will alter the pixel values within the image. If data are comprised of red, green, and blue wave imagery, diversification of solar radiance within the data will allow for the CNN to weigh color accordingly during its learning process. If submersed aquatic vegetation is a target object, capturing data near near solar noon, the time of day when sunlight is directly perpendicular to Earth's surface at the location of interest, will allow the user to capture data with maximized light penetration into the water column. With this, the detection of submersed macrophytes may be improved without significantly compromising data integrity. For consistency, image acquisition of emergent and floating macrophytes should also occur at solar noon.

Capturing data at multiple angles to provide a near 360-degree view of the specimen is one way to increase data diversification. Varying angles are inclusive to potential key identifying characteristics of the target object. While these varied angles are important, it is also important to remember other factors, such as solar radiance, will also alter learning capabilities. Accessibility to floating macrophyte communities can be limited in surveys (Vis et al., 2003), so remote sensing and other applications such as a small unmanned aerial system might be appropriate for data collection, however Thamaga & Dube found their hierarchical classification to outperform a segmentation CNN using earth observations (2020), however their system was using a MultiResUnet semantic segmentation which uses a backbone from images for medical images (Ibtehaz & Rahman, 2020).

Along with solar radiance, the overall health of the plants should not be consistent throughout the dataset. This will allow the model not to rely to heavily on the color of the macrophyte because due to global nutrient fluctuations, plant health and morphological characteristics will differ from geographic location and time of year. Varying morphological data and adjusting the amount of sunlight within the image will create a structurally sound dataset which is necessary for a holistic model. Diversified data with varied tinting and shading also needs adequate representation to avoid convergence issues within the weights and layers of the model. These training data need to ultimately support and optimize the model's learning ability, while simultaneously limiting the constriction of learning.

Data Processing

During the data processing phase, it is important to consider methods that prevent overfitting. Overfitting is a phenomenon that occurs when the training data incorporates noise

into the model by memorizing anomalies rather than learning general features (Dietterich, 1995). Randomization of training datasets, image augmentation, and the incorporation of dropouts (Hinton, 2012b) can be applied to prevent overfitting. Training time with image augmentation can performed outside of training to increase training speed (Chilimbi, 2014). Randomization of the training and testing data does decrease observer bias and provides benefits with training. The reduction of observer bias is important to allow the machine to adequately learn the species in a wholistic approach and reduce overfitting. As models begin to overfit, geometric data augmentations such as flipping, cropping, color space, rotation, translation, noise injection, and color space transformations can be incorporated to reduce overfitting (Moreno-Barea et al., 2018; Shorten & Khoshgoftaar, 2019). Different networks possess different augmentation capabilities, and the accessible options should be explored for each network to eliminate overfitting.

Incorporation of dropout mechanisms to randomly deactivating a percentage of neurons and their associated connected weights reduces overfitting from introduction of generalization and regulations into the model (Ketkar 2017a; Ketkar, 2017c). Dropouts select random units, both visible and invisible within the model's architecture, and temporarily removes them (Srivastava et al., 2014). This process forces the machines to adjust its learning process and ameliorates the computer's learning capabilities. The machine will continually advance in the network and attempt to learn new features while other features are not allowed to be used within the layer is visualizing. Dropouts grant CNNs an enormous learning opportunity especially with integration with convolutions.

A convolution is an operation applied to an input resulting in dot-product operation between weights and spatial localities and maps the activations from one layer to the next (Aggarwal, 2018a; Aggarwal, 2018b) Convolutions are an excellent operation for image data,

because images possess large amounts of spatial data. These connections are sparse due to a decreased amount of spatial region from the previous layer being activated in the new layer, increasing understanding of impactful portions from images (Aggarwal, 2018a). More primitive features are captured in lower-level convolutions, and as more convolutions are applied more intricate details are captured (Aggarwal, 2018a). As more layers are assembled, a more enhanced feature is available for the computer to visualize and differentiate data similar in size, shape, and closely resembled identifying characteristics. There are 1D, 2D, and 3D convolutions. 1D convolutions produce a kernel that is convolved over a singular dimension to produce an output; 2D convolves over two dimensions, and 3D over three different dimensions (Gulli & Pal, 2017).

The 2D convolutions are comprised of a small matrix of weights from the image. A selected kernel size flows over the 2D input and performs elementwise multiplications for each pixel it intersects and summarizes the results into an output pixel creating powerful descriptors (Krizhevsky et al., 2012). The kernel repeats the process for each location and each layer until the image is completed. These new features with the images can become more complex in nature, and reliable outputs have been shown to be extracted at each layer (Zhou et al., 2014). Once convolved, the images are able to be subdued by a pooling layer.

A pooling layer is performed at the level of each activation map on small, gridded regions within each layer to produce a new layer (Aggarwal, 2018c). There are several types of pooling layers, one example is max pooling. Max pooled layers bring forth the largest number within the gridded regions of the activation map on the image within the layer to create a newly refined image. Pooling occurs independently on a feature map and increases the receptive field while spatial footprints on the layer being pooled decreases. For data possessing complex and large

regions will require larger receptive fields for layers deeper into the model's layers. Thus, pooling and convolutions are independent of each other and not interchangeable in operations.

Integration of convolutions, dropouts, and data augmentations reduce the chances of the model's overfitting. The location of overfitting within the architecture is complex. However, during training, overfitting within the model is classified by high levels of training and validation accuracy and high levels of training and validation loss. Additional weights and layers will add parameters for the architecture but also increase training time. As parameters increase, computational requirements will increase as well, however ReLU activation function allows increased training speeds for more dense networks noticed in LeCun et al.'s (1998) LeNet-5 model of around 1 million parameters, Krizhevsky et al.'s (2012) model achieving first place at the ImageNet competition with 60 million parameters, Deepface processing 120 million parameters (Taigman et al., 2014), Coates et al. (2013) was able to train a model with around 10 billion parameters. As neurons increase and more layers are added, opportunities for additional dropouts will need to be tested in the model's training. Upon completion of training the model should be rigorously tested with an external validation dataset using a Precision-Recall Curve (PRC) and average Precision (AP). The PRC and AP have been standardized for several object detection studies (Franklin, 2018; Han et al., 2014; Ketkar, 2017d; Zhang et al., 2014).

Building the Model

The model should be built with the complexity of the objects being studied. The number of layers should best represent the data while still providing enough layers to avoid overfitting. The architectural design of the model is dependent of the data. The data composition should include several object classifications within each model of similar species to help differentiate

objects closely resembling themselves. The correct identification of the target species depends upon several factors within the architecture of the model. Comparison of the different results of the varying combinations of optimizers, activation functions, and loss functions provide insight to the model and its ability to maximize its efficiency for detection of aquatic macrophytes.

Optimization algorithms

Selecting the correct optimization algorithm will improve the model's functionality of minimizing or maximizing an object function. An object function is a mathematical operation that depends upon the model's learnable parameters. Learnable parameters are the target values, or weights, that are based on the predictors within the model. The weights correct the optimizer when it is not learning in the right direction when moving along the descent. A smaller learning rate provides insurance for not skipping over the local minima during training (Ketkar, 2017b). Optimization algorithms are integral in the training process of the neural network model and selecting the correct optimizer for the model being trained is vital to the model's success.

There are two major categories in optimizers, first order and second order optimizers, and should be selected based on the model's goal. There are advantages to both optimizers. The first order optimizers are less computationally intensive than the second order optimizers requiring less time and allowing for the ability to cover larger data sets more quickly than second order optimizers. Second order optimizers fail to neglect surface curvature in its computations, and if computational limitations are not of concern should be considered (Tan & Lim, 2019). This article will cover first order optimizers, and if second order optimizers are wanting to be explored, Tan & Lim (2019) provide an overview of different second-order optimization methods feasibility and performance of 6 different second-order optimization techniques.

First Order Optimizers

First order optimization algorithms contain Gradient Descent optimizers, which are also the most common. Gradient Descent optimizers are one of the most integral techniques in machine learning. Gradient descent's original inception was designed for human perception (Rosenblatt, 1958). Due to neural networks ability to backpropagate, neural networks carrying errors will update weight values with Gradient Descent as an optimizer (Moolayil, 2019). Gradient descent is calculated by $\theta = \theta - \eta \cdot \nabla \mathrm{J}(\theta)$ (Ruder, 2016) and has been attributed to success in neural networks (Darken et al., 1992; Deng et al., 2013; Graves et al., 2013; Hinton & Salakhutdinov, 2006; Hinton et al., 2012a; Krizhevsky et al., 2012; Robbins & Monro, 1951). In this equation η is the learning rate, $\nabla J(\theta)$ is the Gradient of Loss function-$J(\theta)$ with respect to parameter θ. Stochastic gradient descent (SGD) updates the parameters for the individual training examples. SGD is typically faster than a normal Gradient Descent optimizer (Robbins & Monro, 1951). The frequent updates in the training examples create high variances. The fluctuating differences in the intensity of the loss function is caused by the frequent updates. This allows for potential new local minima to be discovered and improve the model. However, due to the frequent updates, the convergence for the exact minimum is complicated. The SGD is calculated by $\theta = \theta - \eta \cdot \nabla_{\theta} \mathrm{J}(\theta; \mathrm{x}^{(\mathrm{i})}; \mathrm{y}^{(\mathrm{i})})$, where $\mathrm{x}^{(\mathrm{i})}$are the training examples and label $\mathrm{y}^{(\mathrm{i})}$ (Ruder, 2016). Mini-batch gradient descents remediates SGD faults. Mini-batch gradient descent is a method of training neural networks that is growing in popularity because of its efficiency (Bottou, 2010; Cui et al., 2020; Ghadimi & Lan; 2013; Ghadimi et al., 2016; Huo & Huang, 2017; Lan, 2012; Nemirovski et al., 2009;), especially during new learning. The convergence of mini-batch Gradient Descents is more stable due to the reduction in variance during parameter updates

(Cotter et al., 2011). Proper gradient descent selection is an increasingly difficult challenge provided the variable learning rates.

Optimizer learning rates impact the model's capability to converge when necessary. Learning rates that are too large will alter convergence and the loss of function will fluctuate near the minimum in computations. Learning rates that are too small can drastically increase time of training by failing to locate the optimal parameter to minimize loss. To avoid using inappropriate learning rates, default options should be selected for optimal convergence.

Difficult convergence of a SGD model is related to variance in oscillations, and to correct this, momentum method (Polyak, 1964; Qian, 1999) is a technique for accelerating Gradient Descent (GD), while still dampening the oscillation when local minima are nearby. This is achievable by following the relevant direction and the reduction in the oscillations that move in the incorrect directions. Mathematically, it adds a fraction γ to the equation. This fraction is added to the updated vector of the previous step to the current updated vector. Visually it is $v_{(t)} = \gamma v_{(t-1)} + \eta \nabla J(\theta)$ (Ruder, 2016). Momentum only performs parameter updates for relevant examples, thus possesses the potential inability to slow down which could create difficulties during training. Due to this, Nesterov Accelerated Gradient (NAG), created by Yurri Neserov, was developed to provide a futuristic approach to the descent by using $\gamma v_{(t-1)}$ to move the weigh parameters θ in respect to future steps. To determine the next position of the parameter on the curve, $\theta - \gamma v_{(t-1)}$ is computed. After this, calculation of gradient descent is done effectively with $v(t) = \gamma v_{(t-1)} + \eta \nabla J(\theta - \gamma v_{(t-1)})$ (Ruder, 2016). Parameters are required to be updated with $\theta = \theta - v_{(t)}$. The learning rate is not always consistent and is dependent upon sparse datasets.

Sparse datasets can be implemented with Adagrad. This is because the learning rate in Adagrad adapts by making larger updates for parameters that are infrequent to learning and smaller updates for parameters that are frequent (Duchi et al., 2011). The learning rate is modified at a rate based upon time step t for each parameter θ(i) . This is visualized as $\theta_{t+1,i} = \theta_{t,i} - \frac{\eta}{\sqrt{G_{t,ii}+\varepsilon}} \cdot g_{t,i}$ (Ruder, 2016). The $g_{t,i}$ is set as the gradient of the loss function this is with respect to the parameter $\theta_{(i)}$ at time t. Division by zero needs to be avoided, so a smoothing function is added, ε. G_t is a diagonal matrix with each diagonal element i, i being the sum of the squares of the gradients with respect to $\theta_{(i)}$ up to time t (Duichi et al., 2011; Ruder, 2016). The benefit of using Adagrad is that the learning rate does not need to be adjusted with each training step because the learning rate is decaying.

A favorable optimizer is the Adaptive Moment Estimation, or Adam optimizer, because of its adaptive learning rate capabilities. The Adam optimizer is a combination of the RMSProp and Adagrad gradients. This allows Adam to have unique advantages, including parameter updates that become invariant to rescaling of its gradient. Adam optimizer can handle sparse gradients and non-stationary objectives and requires little memory. Mathematically, the parameter update is represented by $\theta_{t+1} = \theta_t - \frac{\eta}{\sqrt{\hat{v}_t}+\varepsilon} \cdot \hat{m}_t$ (Kingma & Ba, 2014). Sparse data sets should incorporate the Adam optimizer because the optimization algorithm converges faster than other adaptive techniques and minimizes loss within the function by tuning internal parameters. The step size hyper-parameters bound the step size within the individual iterations in the Adam optimizer proving advantageous in determining learning rate hyper-parameter. However, Adam's convergence is not always in its most optimal solution. Selecting the correct optimizer is dependent upon the data and the desired outcome of the model.

Significantly increased training speeds allow for faster implementation and convergence on the local minima can be improved with the correct optimizer. However, the optimizers discussed all possess pitfalls and limitations. As new optimizers continually emerge, assessment of the model's architecture with each new optimizer is critical to determine if the model can be improved.

Activation function

Activation functions are functions of a node which define the output based on the inputs. These functions allow the model to compute and transfer necessary information to the next node in the framework. Activation functions are comprised of different properties: nonlinear, continuously differentiable, monotonic, smooth functions with a monotonic derivative, and approximate identity near the origin (Ketkar, 2017a). If an activation function is non-linear, in theory, a two-layer Neural Network can approximate any function. Differentiable gradients progress due to activation functions finding parameters that minimize the loss function. Gradient-based methods are more stable with a function's range being finite in comparison to an infinite range. Lastly activation functions are symmetric around the origin, to prevent gradients altering directions, and are similar to identity functions ($f(x) = x$) (Ketkar, 2017a). One of the most common activation functions is the rectified linear unit, hereafter known as ReLU. Differences in activation functions allow for flexibility in models and differentiate with learning abilities and potentials, however non-linear activation functions are essential for datasets possessing high dimensionality.

The only activation function being thoroughly discussed in this article is the ReLU activation. ReLU is desirable because it is less computationally intensive in comparison to other

activation functions because it is not complicated mathematically. The ReLU model converges quickly because of its linearity as demonstrated by Krizhevsky et al. (2012). The linearity in this function means the slope does not plateau as the x value continually increases. ReLU's speed is desirable because the input, if negative, is not activated from the ReLU function. Sparsity in these models possess improved predictive power (Glorot, 2011), especially in comparison to binary units and process variations more naturally (Nair & Hinton, 2010).

This sparsity within the data is desirable for computational speed, however this increase in speed does contains inactivated neurons. As total number of layers and neurons increase, sparsity in data will need to occur due to memory limitations (Kepner et al., 2018). Weights that are set to zero inflict little to no effect on performance and still reduce computational costs (Iandola et al., 2016). Shi & Chu (2017) tested the ability of ReLUs in skipping zero-valued neurons and found several ReLU layers to contain 70% of the neurons output on LeNet (LeCun et al., 1998), AlexNet (Krizhevsky et al., 2012) for Cifar10, AlexNet (Krizhevsky et al., 2012) for ImageNet, GoogLeNet (Szegedy et al., 2015) to be zero-valued outputs. Sparsity in Shi & Chu was for each layer the ratio of zero-valued inputs over the total number of inputs (2017). A cascade model designed by Liu et al. pruned object detection windows with each image and achieved 5 times faster speed with almost no drop in accuracy with not calculating zeroed values (2015). In a study testing 6 different publicly available datasets in modelzoo on average 44% of the runtime calculated of all neurons were zero (Albericio et al., 2016). Because ReLU transforms negative values to zero, computation times are greatly reduced. Selecting the correct activation function should be done through experimentation within the model itself. The process of activation function selection should begin with the basic ReLU function.

Loss Functions

CNNs calculate the training and test rates through loss functions. Loss functions measure the performances of the architecture and inconsistencies between the actual y and the predicited $\hat{y}$ values which ultimately allows the user to determine how accurate their model is (Murugan, 2018). As model performance increases, the differences between the y and $\hat{y}$ should decrease (Murugan, 2018). These differences, rather than over a singular data point, are calculated over several data points. When measuring the disagreement, loss functions can be computed via a binary classification, multi-classification, or regression. Loss functions are derived using Maximum Likelihood. Common loss functions from Maximum Likelihood are squared error, binary cross entropy, and categorical cross entropy.

Squared error is mathematically computed with the equation $\sum_{i=1}^{n}(y-\hat{y})^2$ (Ketkar & Santana, 2017). The model is designed to predict the value of y**,** and the difference between the predicted and actual y is assumed to have a Gaussian distribution with zero mean and a variance of σ^2 for the assumptions of Maximum Likelihood to be met (Ketkar & Santana, 2017). The activation function selected when using squared error will possess a single unit, so a sigmoid activation function is adequate.

Binary cross entropy is a loss function in the context of binary classifications. The function of binary classifications is $-\sum_{i=1}^{n} y_i \log\ f(x_i,\theta) + (1-y)\log\,(1-f(x_i,\theta))$ (Ketkar & Santana, 2017). Binary classifications should by default implement this loss function and the framework should be inferenced from Maximum Likelihood. The activation function with this model should be sigmoid activation if binary cross entropy is selected.

Categorical cross entropy loss function is used in multiclass classifications. For this formula y is a vector comprised zeros except where it encodes becomes a 1 and the probabilities

of the feature belonging to a class from an applied SoftMax function is denoted by x (Paszke et al., 2019). The overall categorical cross entropy loss function formula can be visualized as $\text{Loss}(x, y) = \sum_{i=1}^{n} y_i \log(x_i)$ (Paszke et al., 2019). The categorical cross entropy loss function is a recommended for multi-class classification and should be selected by default. The activation function selected should be a SoftMax function. The loss function selection within the model is ultimately dependent upon the model and its data. These selections will differ from models and frameworks. The end model should be optimized for its learning and recognition ability.

Testing and Inferencing the Model

After successful completion of data processing and model creation, a validation dataset should be generated. The validation dataset provides the model data to evaluate the model's ability and to tune hyperparameters. Validation datasets should be randomized similar to that of the testing and training datasets. Inference datasets are datasets comprised of imagery or data not used in testing, training, or validation. The inference datasets should be comprised of images containing targets of interest and other targets outside of the training data that share similar characteristics. These images should be unique to those that were used for training and should represent the diversity of environments in which the species may be found. This way, the validation dataset can accurately test the model's capabilities of detecting the species outside of your training and testing datasets.

Selecting an external data set of roughly 5% of the amount of training data will allow for adequate validation. Images selected for inferencing should not be from the testing, validation, and training data. Inferencing data should comprise of varying backgrounds, foregrounds, and landscapes. Inferencing data will provide visual insight to which data are underrepresented in the

model. Diversified inferencing data will bring forth areas of strengths and weaknesses within the model's hyperparameters and how it identifies its desired target. The model's capabilities and strengths can also become weaknesses of the model. If the model becomes too reliant on specific identifiable characteristics of objects, it will not correctly identify the object if not presented with those characteristics. Implementing multiple dropout layers in the framework can help to correct this issue as dropout layers remove connecting neurons and force the model to identify new characteristics.

Discussion and Conclusion

CNNs have become increasingly more popular in automating tasks from identifying handwritten digits, facial recognition, autonomous driving, and even food classifications (Fukushima, 1988; Matsugu et al., 2003; Wu et al., 2012; Yanai & Kawano, 2015). As new activation, loss, optimizers, and hardware within computers improve, newer models will continually outperform previous models. Increasing computational possibilities with emerging technologies such as tensor processing units, quantum computers, and hybrid approaches such as TensorFlow Quantum (Broughton et al., 2020) will propel object-based detection with CNNs forward.

As computational limitations are continually addressed with newer technology and datasets, advanced opportunities with CNNs become a reality. The abundance of applications that CNNs possess will generate new tools that will be beneficial to many industries, especially that of the aquatic plant management field as newer technologies emerge. Such technologies include autonomous aquatic herbicide applications from a vessel (Richardson et al., 2018). Coupling this technology with an onboard system to rapidly classify and administer herbicides to

nuisance species could provide new management approaches to problematic species. CNNs models can be more diverse for aquatic plant managers than a classical image classification. CNNs and deep neural networks can be trained for management techniques from detecting effective plant control, plant health following treatments, suitable locations for revegetation habitats, and plant disease.

However, there are limitations with using these models related to data collection. If datasets do not possess imagery containing the desired results of the data, then computer vision is not feasible. In this event, remember that neural networks are still an option. As newer technologies such as fast.ai are created, tabular data, such as time series data, are more relevant and should be explored. Integration of CNN with aquatic plant management and its success are reliant upon proper data collection, proper model selection, and architecture creation.

REFERENCES

Aggarwal, C. C. (2018a). *Neural networks and deep learning* (pp. 41). Springer.

Aggarwal, C. C. (2018b). *Neural networks and deep learning* (pp. 316). Springer.

Aggarwal, C. C. (2018c). *Neural networks and deep learning* (pp. 326-327). Springer.

Albericio, J., Judd, P., Hetherington, T., Aamodt, T., Jerger, N. E., & Moshovos, A. (2016). Cnvlutin: Ineffectual-neuron-free deep neural network computing. *ACM SIGARCH Computer Architecture News*, *44*(3), 1-13.

Bottou, L. (2010). Large-scale machine learning with stochastic gradient descent. In *Proceedings of COMPSTAT'2010* (pp. 177-186). Physica-Verlag HD.

Broughton, M., Verdon, G., McCourt, T., Martinez, A. J., Yoo, J. H., Isakov, S. V., ... & Mohseni, M. (2020). Tensorflow quantum: A software framework for quantum machine learning. *arXiv preprint arXiv:2003.02989*.

Chilimbi, T., Suzue, Y., Apacible, J., & Kalyanaraman, K. (2014). Project adam: Building an efficient and scalable deep learning training system. In *11th {USENIX} Symposium on Operating Systems Design and Implementation ({OSDI} 14)* (pp. 571-582).

Coates, A., Huval, B., Wang, T., Wu, D., Catanzaro, B., & Andrew, N. (2013, February). Deep learning with COTS HPC systems. In *International conference on machine learning* (pp. 1337-1345).

Cotter, A., Shamir, O., Srebro, N., & Sridharan, K. (2011). Better mini-batch algorithms via accelerated gradient methods. In *Advances in neural information processing systems* (pp. 1647-1655).

Cui, Y., Wu, D., & Huang, J. (2020). Optimize TSK fuzzy systems for classification problems: Mini-batch gradient descent with uniform regularization and batch normalization. *IEEE Transactions on Fuzzy Systems*.

Darken, C., Chang, J., & Moody, J. (1992, August). Learning rate schedules for faster stochastic gradient search. In *Neural networks for signal processing* (Vol. 2).

Deng, L., Li, J., Huang, J. T., Yao, K., Yu, D., Seide, F., ... & Acero, A. (2013, May). Recent advances in deep learning for speech research at Microsoft. In *2013 IEEE International Conference on Acoustics, Speech and Signal Processing* (pp. 8604-8608). IEEE.

Dierssen, H. M., Zimmerman, R. C., Leathers, R. A., Downes, T. V., & Davis, C. O. (2003). Ocean color remote sensing of seagrass and bathymetry in the Bahamas Banks by high-resolution airborne imagery. *Limnology and oceanography*, *48*(1part2), 444-455.

Dietterich, T. (1995). Overfitting and undercomputing in machine learning. *ACM computing surveys (CSUR)*, *27*(3), 326-327.

Duchi, J., Hazan, E., & Singer, Y. (2011). Adaptive subgradient methods for online learning and stochastic optimization. *Journal of machine learning research*, *12*(Jul), 2121-2159.

Everitt, J. H., Yang, C., Escobar, D. E., Webster, C. F., Lonard, R. I., & Davis, M. R. (1999). Using remote sensing and spatial information technologies to detect and map two aquatic macrophytes. *Journal of Aquatic Plant Management*, *37*, 71-80.

Franklin, S. E. (2018). Pixel-and object-based multispectral classification of forest tree species from small unmanned aerial vehicles. *Journal of Unmanned Vehicle Systems*, *6*(4), 195-211.

Fukushima, K. (1988). Neocognitron: A hierarchical neural network capable of visual pattern recognition. *Neural networks*, *1*(2), 119-130.

Fyfe, S. K. (2003). Spatial and temporal variation in spectral reflectance: Are seagrass species spectrally distinct?. *Limnology and Oceanography*, *48*(1part2), 464-479.

Geman, S. (1999). Hierarchy in machine and natural vision. In *Proceedings of the Scandinavian Conference on Image Analysis* (Vol. 1, pp. 179-184).

Ghadimi, S., & Lan, G. (2013). Stochastic first-and zeroth-order methods for nonconvex stochastic programming. *SIAM Journal on Optimization*, *23*(4), 2341-2368.

Ghadimi, S., Lan, G., & Zhang, H. (2016). Mini-batch stochastic approximation methods for nonconvex stochastic composite optimization. *Mathematical Programming*, *155*(1-2), 267-305.

Glorot, X., Bordes, A., & Bengio, Y. (2011, June). Deep sparse rectifier neural networks. In *Proceedings of the fourteenth international conference on artificial intelligence and statistics* (pp. 315-323).

Graves, A., Mohamed, A. R., & Hinton, G. (2013, May). Speech recognition with deep recurrent neural networks. In *2013 IEEE international conference on acoustics, speech and signal processing* (pp. 6645-6649). IEEE.

Gulli, A., & Pal, S. (2017). *Deep learning with Keras*. Packt Publishing Ltd.

Han, J., Zhang, D., Cheng, G., Guo, L., & Ren, J. (2014). Object detection in optical remote sensing images based on weakly supervised learning and high-level feature learning. *IEEE Transactions on Geoscience and Remote Sensing*, *53*(6), 3325-3337.

Han, L., & Rundquist, D. C. (2003). The spectral responses of Ceratophyllum demersum at varying depths in an experimental tank. *International Journal of Remote Sensing*, *24*(4), 859-864.

Heege, T., Bogner, A., & Pinnel, N. (2004, February). Mapping of submerged aquatic vegetation with a physically based process chain. In *Remote Sensing of the Ocean and Sea Ice 2003* (Vol. 5233, pp. 43-50). International Society for Optics and Photonics.

Hinton, G., Deng, L., Yu, D., Dahl, G. E., Mohamed, A. R., Jaitly, N., ... & Kingsbury, B. (2012a). Deep neural networks for acoustic modeling in speech recognition: The shared views of four research groups. *IEEE Signal processing magazine*, *29*(6), 82-97.

Hinton, G. E., & Salakhutdinov, R. R. (2006). Reducing the dimensionality of data with neural networks. *science*, *313*(5786), 504-507.

Hinton, G. E., Srivastava, N., Krizhevsky, A., Sutskever, I., & Salakhutdinov, R. R. (2012b). Improving neural networks by preventing co-adaptation of feature detectors. *arXiv preprint arXiv:1207.0580*.

Huo, Z., & Huang, H. (2017, February). Asynchronous mini-batch gradient descent with variance reduction for non-convex optimization. In *Proceedings of the AAAI Conference on Artificial Intelligence* (Vol. 31, No. 1).

Hubel, D. H. (1959). Single unit activity in striate cortex of unrestrained cats. *The Journal of Physiology*, *147*(2), 226-238.

Hubel, D. H., & Wiesel, T. N. (1962). Receptive fields, binocular interaction and functional architecture in the cat's visual cortex. *The Journal of Physiology*, *160*(1), 106-154.

Iandola, F. N., Han, S., Moskewicz, M. W., Ashraf, K., Dally, W. J., & Keutzer, K. (2016). SqueezeNet: AlexNet-level accuracy with 50x fewer parameters and< 0.5 MB model size. *arXiv preprint arXiv:1602.07360*.

Ibtehaz, N., & Rahman, M. S. (2020). MultiResUNet: Rethinking the U-Net architecture for multimodal biomedical image segmentation. *Neural Networks*, *121*, 74-87.

Kepner, J., Gadepally, V., Jananthan, H., Milechin, L., & Samsi, S. (2018, September). Sparse deep neural network exact solutions. In *2018 IEEE High Performance extreme Computing Conference (HPEC)* (pp. 1-8). IEEE.

Ketkar, N. (2017a). Introduction to keras. In *Deep learning with Python* (pp. 27-30). Apress, Berkeley, CA.

Ketkar, N. (2017b). Introduction to keras. In *Deep learning with Python* (pp. 118). Apress, Berkeley, CA.

Ketkar, N. (2017c). Introduction to keras. In *Deep learning with Python* (pp. 141-142). Apress, Berkeley, CA.

Ketkar, N. (2017d). Introduction to pytorch. In *Deep learning with python* (pp. 195-208). Apress, Berkeley, CA.

Ketkar, N., & Santana, E. (2017). *Deep Learning with Python* (Vol. 1 pp. 24-26). Berkeley, CA: Apress.

Kingma, D. P., & Ba, J. (2014). Adam: A method for stochastic optimization. *arXiv preprint arXiv:1412.6980*.

Krizhevsky, A., Sutskever, I., & Hinton, G. E. (2012). Imagenet classification with deep convolutional neural networks. In *Advances in neural information processing systems* (pp. 1097-1105).

Lan, G. (2012). An optimal method for stochastic composite optimization. *Mathematical Programming*, *133*(1-2), 365-397.

LeCun, Y., Boser, B., Denker, J. S., Henderson, D., Howard, R. E., Hubbard, W., & Jackel, L. D. (1989). Backpropagation applied to handwritten zip code recognition. *Neural computation*, *1*(4), 541-551.

LeCun, Y., Bottou, L., Bengio, Y., & Haffner, P. (1998). Gradient-based learning applied to document recognition. *Proceedings of the IEEE, 86*(11), 2278-2324.

Long, J., Shelhamer, E., & Darrell, T. (2015). Fully convolutional networks for semantic segmentation. In *Proceedings of the IEEE conference on computer vision and pattern recognition* (pp. 3431-3440).

Matsugu, M., Mori, K., Mitari, Y., & Kaneda, Y. (2003). Subject independent facial expression recognition with robust face detection using a convolutional neural network. *Neural Networks*, *16*(5-6), 555-559.

Moolayil, J. (2019). *Learn Keras for Deep Neural Networks* (pp. 34-37). Apress.

Moreno-Barea, F. J., Strazzera, F., Jerez, J. M., Urda, D., & Franco, L. (2018, November). Forward noise adjustment scheme for data augmentation. In *2018 IEEE Symposium Series on Computational Intelligence (SSCI)* (pp. 728-734). IEEE.

Murugan, P. (2018). Implementation of deep convolutional neural network in multi-class categorical image classification. *arXiv preprint arXiv:1801.01397*.

Nair, V., & Hinton, G. E. (2010). Rectified linear units improve restricted boltzmann machines. In *Proceedings of the 27th international conference on machine learning (ICML-10)* (pp. 807-814).

Nemirovski, A., Juditsky, A., Lan, G., & Shapiro, A. (2009). Robust stochastic approximation approach to stochastic programming. *SIAM Journal on optimization*, *19*(4), 1574-1609.

O'Gorman, L., & Kasturi, R. (1995). *Document image analysis* (Vol. 39). Los Alamitos: IEEE Computer Society Press.

Oh, K. S., & Jung, K. (2004). GPU implementation of neural networks. *Pattern Recognition*, *37*(6), 1311-1314.

Polyak, B. T. (1964). Some methods of speeding up the convergence of iteration methods. *USSR Computational Mathematics and Mathematical Physics*, *4*(5), 1-17.

Paringit, E. C., Nadaoka, K., Fortes, M. D., Harii, S., Tamura, H., Mistui, J., et al. (2003). Multiangular and hyperspectral reflectance modeling of seagrass beds for remote sensing studies. In *Proceedings of the International Geoscience and Remote Sensing Symposium '03* (Vol. 3. pp. 21–25).

Paszke, A., Gross, S., Massa, F., Lerer, A., Bradbury, J., Chanan, G., ... & Chintala, S. (2019). Pytorch: An imperative style, high-performance deep learning library. In *Advances in neural information processing systems* (pp. 8026-8037).

Pinnel, N., Heege, T., & Zimmermann, S. (2004). Spectral discrimination of submerged macrophytes in lakes using hyperspectral remote sensing data. *SPIE Proceedings on Ocean Optics XVII*, *1*, 1-16.

Qian, N. (1999). On the momentum term in gradient descent learning algorithms. *Neural networks*, *12*(1), 145-151.

Richardson Jr, R. J., Hoyle, S. T., & Nawrocki, J. J. (2018). *U.S. Patent Application No. 15/763,144*.

Robbins, H., & Monro, S. (1951). A stochastic approximation method. *The annals of mathematical statistics*, 400-407.

Romera-Paredes, B., & Torr, P. H. S. (2016, October). Recurrent instance segmentation. In *European conference on computer vision* (pp. 312-329). Springer, Cham.

Ruder, S. (2016). An overview of gradient descent optimization algorithms. *arXiv preprint arXiv:1609.04747*.

Shi, S., & Chu, X. (2017). Speeding up convolutional neural networks by exploiting the sparsity of rectifier units. *arXiv preprint arXiv:1704.07724*.

Shorten, C., & Khoshgoftaar, T. M. (2019). A survey on image data augmentation for deep learning. *Journal of Big Data*, *6*(1), 60.

Srivastava, N., Hinton, G., Krizhevsky, A., Sutskever, I., & Salakhutdinov, R. (2014). Dropout: a simple way to prevent neural networks from overfitting. *The journal of machine learning research*, *15*(1), 1929-1958.

Szegedy, C., Liu, W., Jia, Y., Sermanet, P., Reed, S., Anguelov, D., ... & Rabinovich, A. (2015). Going deeper with convolutions. In *Proceedings of the IEEE conference on computer vision and pattern recognition* (pp. 1-9).

Taigman, Y., Yang, M., Ranzato, M. A., & Wolf, L. (2014). Deepface: Closing the gap to human-level performance in face verification. In *Proceedings of the IEEE conference on computer vision and pattern recognition* (pp. 1701-1708).

Thamaga, K. H., & Dube, T. (2018). Remote sensing of invasive water hyacinth (Eichhornia crassipes): A review on applications and challenges. *Remote Sensing Applications: Society and Environment*, *10*, 36-46.

Torrey, L., & Shavlik, J. (2010). Transfer learning. In *Handbook of research on machine learning applications and trends: algorithms, methods, and techniques* (pp. 242-264). IGI global.

Vis, C., Hudon, C., & Carignan, R. (2003). An evaluation of approaches used to determine the distribution and biomass of emergent and submerged aquatic macrophytes over large spatial scales. *Aquatic Botany*, *77*(3), 187-201.

Wu, B., Iandola, F., Jin, P. H., & Keutzer, K. (2017). Squeezedet: Unified, small, low power fully convolutional neural networks for real-time object detection for autonomous driving. In *Proceedings of the IEEE Conference on Computer Vision and Pattern Recognition Workshops* (pp. 129-137).

Wu, J., Ho, C., Huang, C., Srivastav, A. L., Tzeng, J., & Lin, Y. (2014). Hyperspectral sensing for turbid water quality monitoring in freshwater rivers: Empirical relationship between reflectance and turbidity and total solids. *Sensors, 14*(12), 22670-22688. doi:http://dx.doi.org.prox.lib.ncsu.edu/10.3390/s141222670

Yanai, K., & Kawano, Y. (2015, June). Food image recognition using deep convolutional network with pre-training and fine-tuning. In *2015 IEEE International Conference on Multimedia & Expo Workshops (ICMEW)* (pp. 1-6). IEEE.

Zhang, D., Han, J., Cheng, G., Liu, Z., Bu, S., & Guo, L. (2014). Weakly supervised learning for target detection in remote sensing images. *IEEE Geoscience and Remote Sensing Letters*, *12*(4), 701-705.

Zhou, B., Khosla, A., Lapedriza, A., Oliva, A., & Torralba, A. (2014). Object detectors emerge in deep scene cnns. *arXiv preprint arXiv:1412.6856*.

CHAPTER 2

sUAS Technology and Convolutional Neural Networks for Optimization of Target Weed Control in Vegetation Management Scenarios

Abstract

Small Unmanned Aerial Systems (sUAS) were flown to obtain imagery mimicking rights-of-way (ROW) scenarios in North Carolina, USA to autonomously detect two tree species: *Pinus taeda* and *Liquidambar styraciflua*. Pytorch and toolbox MMdetection were utilized to train the model for autonomous detection using FasterRCNN with a framework of resnet50. The sUAS imagery were collected at 4 field sites, obtaining 3000 images of varying heights. These images were labelled with LabelImg in Pascal VOC format. Data were trained for 100 epochs and accuracy was 98.6855% accuracy with a loss rate of 0.1374. These data were subject to multiple flights at varying heights. *Pinus taeda* average precision was 0.599, while *Liquidambar styraciflua* was 0.558. *Pinus taeda* recall was 0.707 while the recall for *Liquidambar styraciflua* was 0.603. The *m*AP was 0.579 for the training. The model was successful in autonomously detecting these two desirable tree species in ROW scenarios, however there are improvements in training, testing, and validation data with inclusion of more field sites and other images possessing less dense vegetation. The lower precision scores are primarily from false negatives from *Pinus taeda* and *Liquidambar styraciflua*. There are several inference images containing few instances of false positives of *Liquidambar styraciflua* and *Pinus taeda*. These data should be revisited with data collected in ROW scenarios to adequately determine if the model produced works within a ROW scenario. Data obtained in ROW scenarios outside of the Piedmont region

of North Carolina, USA need to be tested against our model to determine if new data in these regions will need to be collected.

Introduction

Technological advancements in sUAS have generated an improved, practical environmental remote sensing tool. These sUAS provide a complimentary tool for current remote sensing efforts in environmental science applications. sUAS can provide spatially precise data to sample temperature and relative humidity in the atmosphere at 2500 meters above ground level (Greatwood et al., 2017). As technological advances continue, the challenges mentioned in Hardin & Jensen (2011) were revisited in Hardin et al. (2019) and provided insight to how large imagery volume, on-board power, and paucity of commercially available sensors, are becoming less cumbersome on sUAS units. A study in Precision Viticulture integrated sUAS into their agronomy practices (Matese et al., 2015). Their study addressed the use of sUAS and large-scale satellites to monitor and implement effective Precision Viticulture management strategies. Systems using sUAS detected areas with small vegetation gradients and vegetation patchiness, which possessed a notable lack of characterization from low resolution satellite imagery. These observations resulted from the high spatial resolution from provided by the sUAS imagery. However, higher spatial resolution is not the only advantage of using sUAS; a relatively low cost is an important advantage of this type of equipment (Thomas et al., 2017). As spectral detail increase and cost continually decrease, the integration of sUAS platforms and large satellite sensors provide an inherent approach for vegetation management.

Large scale satellite data are continuously used across the globe for vegetation management practices from modeling phenology across growing seasons to vegetation

classification. These data are excellent sources for historical trends but possess draw backs. Large scale satellite imagery contains missing data due to cloud cover, spatial resolution, and temporal resolution. Algorithms have been developed for data fusion to incorporate IKONOS, Landsat, and MODIS data to produce high spatial and temporal resolution imagery (Gray & Song, 2012). These algorithms are still only capable at local to regional ecosystem scale. Large Earth observing satellite data are excellent sources for historical datasets, but coarse spatial resolution and missing temporal data are plaguing issues with these remotely sensed data. The combination of sUAS platforms ease of use, low cost, and repetitive field site visits provide an alternative solution or complimentary tool to large scale artificial satellites.

sUAS datasets provide an opportunity for rapid repetitive field visits while producing a more detailed image bringing forth features diminished by larger satellite data. The spatial resolutions on each sUAS flight are different because of flight height but can still possess centimeter level resolution. This increase in resolution has become desirable to vegetation managers. These abilities of sUAS imagery were leveraged to classify deciduous tree species performing unsupervised ISODATA clustering classifications of UAV-based imagery and achieved an accuracy of around 45%-50% (Franklin, 2018). Object based image analysis, random forest, and an automated tree crown delineation classification achieved an 80% accuracy rating (Franklin, 2018). These results were promising for the inclusion of new emergent sUAS technology into remotely sensing tree species.

Enhanced analysis techniques and sUAS data provide opportunities to revolutionize remotely sensed data with computer vision, specifically object detection. Object detection software allows computers to statistically visualize results and learn textures previously not utilized in classification techniques.

This research aimed to combine object detection with remotely sensed data collected with a sUAS to selectively identify weeds in ROW settings. The species of interest in utility ROW were sweetgum (*Liquidambar styraciflua)* and loblolly pine (*Pinus taeda*), which are undesirable species in ROW. Each year millions of miles of ROW are subjected to unwanted and undesirable vegetative growth requiring management.

Integrated Vegetation Management (IVM) programs on ROW are critical for utility managers and landowners. Transmission owner's vegetation management programs specify strategies to maximize the use of the active transmission line ROW. These methods of removing vegetation can include mechanical clearing, selective mechanical tree removal, low-volume foliar selective herbicide treatment, and side pruning (NERC, 2010). Best management strategies for IVM in ROW are to set objectives for identifying desirable and compatible vegetation within the active and inactive ROW. Control methods with these are designed for each ROW owner by land use, site characteristics, security, economics, and several other factors (NERC, 2010). IVM contains 6 elements: setting objectives, evaluation of the site, defining action thresholds, evaluation and selection of control methods, implementation of the IVM, and monitoring and quality assurance. IVM programs are considered one of the most appropriate techniques for use in electric ROW projects.

Comprehensive site evaluations of sites provide excellent data for management decisions but can become impractical for utilities with small budgets and a vast index of species. An alternative to overcome this is point sampling (NERC, 2010). Point sampling equally divides management areas into units to randomly sample to sufficiently describe workloads and species inventory. These transmission owners are required to specify a vegetation inspection frequency of at least one time per calendar year accounting for environmental and local factors. These plans

help craft an IVM program to practice and promote low-growing, stable, and desirable plants. Because of this practice, tall-growing vegetation and invasive species are selected for control by appropriate methods. After treatments are implemented, monitoring is required to provide prove that the vegetation control was completed to specifications (NERC, 2010). These efforts from IVM programs provide benefits of cost, control, public health, environmental quality, and regulatory compliance. With implementation of IVM programs on utility ROW, companies are working to create a conducive environment of low growing vegetation to promote safe and reliable energy transmission for ROW to minimize power outages.

Reduction of operational costs are important not only to utility companies, but also the U.S. economy. The Electric Power Research Institute (EPRI) and the U.S. Department of Defense in 2003 estimated almost 120 billion US dollars a year lost in the U.S. economy due to power outages, and several more billions are required to repair these outages (EPRI and U.S. Department of Defense, 2003). Prevention of power outages can be achieved with proper IVM practices. A complimentary tool for use of monitoring species in ROW are sUAS. These tools revealed in ROW scenarios in Brazil to detection of potential vegetative risk to the ROW structures (Jardini et al., 2017). The implementation of sUAS for vegetation management introduce new possibilities of workload reduction from monitoring efforts, assessments, and even vegetation control. Being able to autonomously detect specific undesirable vegetation growth in ROW will provide IVM programs an advantageous tool to reduce operational costs. Coupling object detection with emergent technologies including imaging sUAS will provide vegetation management increased efficiency for vegetation management strategies in utility ROW. This research aimed to generate an object detection model using the MMdetection toolbox in Pytorch with remotely sensed data collected from four field sites in North Carolina,

USA using both a DJI Phantom 4 Pro and DJI Phantom 4 Advance quadcopters to identify *Liquidambar styraciflua* and *Pinus taeda* in utility ROW scenarios.

Materials and Methods

A DJI Phantom 4 Pro and a DJI Phantom 4 Advanced were the two sUAS utilized for imaging purposes for this research. Both systems used a one-inch CMOS sensor capturing 20-megapixel still shots. These units were flown at varying heights ranging from 18.288 meters to and not exceeding 121.92 meters. Flying at several heights allowed for determination of the best suitable height for detection of loblolly pines and sweetgums. Field sites were targeted to mimic simulated rights-of-way (ROW) settings containing natural vegetative growth of loblolly pine and sweetgum. Images were obtained at four separate locations across the state of North Carolina, USA. These images were collected abiding by all laws according to 14 code of Federal Regulation (CFR) part 107 and North Carolina Department of Transportation. Images were collected seasonally throughout spring, summer, fall, and winter. As a result, images provided a wide range of phenological stages and background vegetation variability allowing for a more diversified training and validation dataset.

Flight plans were created using DJI Go 4 and Pix4D. These flight plans were generated once and then used repeatedly during the period of this study. The flight plans for each field site remained the same flight path, however the height for each flight flown varied. The variation of heights during image collection were selected to for diversification of training data, and still abided by FAA standards with height limitations flying no higher than 121.92 meters. Flights were not flown less than 18.288 meters at each site due to potentially hazardous flying conditions from varying topography and vegetation heights.

After collection, images were then sliced equally into four separate images. Slicing images prior to labelling the image significantly reduced the total number of pixels lost when the software resizes prior to training, while increasing the total training data quantity. MMdetection resizes the imagery prior to training and labels with the same scale factor. The imagery after slicing remained in the same format to eliminate any further compression or loss of image integrity. A total of 3000 images were labelled for training.

The images were labelled with LabelIMG (Tzutalin, 2015), an open-source software available on github. To avoid confusion with common names, species were labelled with binomial nomenclature with abbreviated genus and full species name. To ensure the proper species were labelled, weed targets were identified in the field prior to labelling within LabelImg. The deep learning library selected for this project was Pytorch. This framework is an open-source machine learning library based on Torch Library Ketkar, 2017, and the toolbox MMdetection was selected for computer vision, specifically object detection. This platform was selected because of its modular design, support of multiple frameworks, and its high efficiency (Chen et al., 2019). Several other platforms were considered prior to selecting MMDetection, however due to ease of use and performance, MMDetection was selected.

The object detection software employed during this research was PyTorch. This framework is an open-sourced python package providing two high-level features. These two features are tensor computation and deep neural networks built upon a tape-based autograd system. PyTorch implements reverse-mode auto-differentiation allowing control over the network's behavior. This technique is not the first created, however PyTorch is among the fastest implementations. The tape-based autograd dynamic neural network approach PyTorch uses along with the custom memory allocators for the graphical processing unit, or GPU, optimizes

the memory efficiency for local deep learning models. This research was provided access to a local hardware set up as follows: OS is Ubuntu Server 18.04, CPU AMD Ryzen Threadripper 2950X 16-Core Processor, motherboard ROG ZENITH EXTREME ALPHA, Memory 128 GiB of Corsair Vengeance LPX DDR4, and GPU Nvidia Titan RTX. This local set up was powerful enough to allow for adequate training and testing of the model created. The local hardware set up, integration of sUAS data, and object detection platform provided an avenue to process the large data volume and memory size of sUAS data.

The sUAS data were randomly selected through excel and assigned to either a training validation directory or a testing directory. The training and validation datasets were separated with 70% of imagery used for training and 30% for testing. These data comprised of around 2,100 images in training and validation directory and 900 in testing dataset. These images once trained in a dataset were not moved to another folder unless an entire new randomization of data for each training, validation, and testing data were desired. The model in this research selected an architecture of FasterRCNN with a framework of resnet50. FasterRCNN was selected due to the results found in Körez & Barışçı (2020) with their low-capacity GPU system (Körez & Barışçı, 2020). This model was trained for 100 epochs, with inference of 30 images. Once the model training was completed, the validation images were processed and ran through the system to assess the total number of correctly detected objects within the validation imagery. The Precision and recall were determined with true positives (TP), false positives (FP), and false negatives (FN). The PRC and average Precision (AP) have been standardized for several object detection studies (Franklin, 2018; Han et al., 2014; Ketkar, 2017; Zhang et al., 2014). To determine the accuracy, Precision-Recall Curve (PRC) was used to determine the proportions of the TP. The formula used to obtain the Precision and recall are as follows:

$$Precision = \frac{TP}{(TP + FP)}$$

$$Recall = \frac{TP}{(TP + FN)}$$

$$mAP = \frac{1}{N}\sum_{i=1}^{N} AP_i$$

Results

The model trained for 100 epochs and the best results obtained during training was the 50th epoch. The training results were 98.685% accuracy while obtaining a total loss rate of 0.1374. The bounding box loss was 0.0163, the loss for classification was 0.0314, and the bounding box loss was 0.0889. The AP for *P. taeda* was 0.599 and for *L. styraciflua* was 0.558. The recall for *P. taeda* was 0.707 while the recall for *L. styraciflua* was 0.603 as seen in **Table 2.1**. The mean average precision (*mAP*) is $Recall = 0$ to $Recall = 1$ calculated average value of precision of recalls at 11 points by calculating the area under the PRC. The *m*AP 0.579. Thus, larger *m*AP scores are indicative of better performance of the model.

Our model detected both loblolly pines and sweetgums within our inference dataset. These data are comprised of imagery not previously seen from the model and did include variations of phenological stages of the target species. In **Figures 2.1-2.5** the detection of species proved to differentiate between other hardwood tree species other than sweetgums and omit these from its detection. However, there were some false negatives regarding both species.

Discussion

We set out to perform computer vision to detect two tree species commonly found in rights-of-way scenarios in North Carolina, USA with imagery captured by an sUAS. This methodology should be considered as an option for integration in vegetation management for conducting weed inventories, monitoring programs of weed locations, management efforts and with model improvements acreage infested. This model's ability to detect species from sUAS imagery proves the feasibility of integrating new technologies to autonomously detect tree species, also shown in Santos et al. (2019). Unlike Santos et al. (2019) this research did not use their five-folding technique and used a Resenet50 backbone. The model generated in this research consisted of training on a dataset comprised of several other species outside of our target species loblolly pines and sweetgums found in their natural habitats. These imagery in the dataset were that of nearly 2600 more total images in size compared to Santos et al. (2019) data providing a diversified approach to learning. Santos et al. (2019) did produce a higher precision than found in this research using TensorFlow and Faster-RCNN with an average precision of 0.8248 in comparison to this research's results of an average precision of 0.579 across both species. A potential reason for their increased precision can potentially be attributed to overfitting of their data from their folding approach. Their methods were unclear to whether their folding technique was performed during the same training, and not in separate trainings. Their approach with image folding should be considered in future research projects using object detection and sUAS imagery, however it is important to not intermingle training, testing, and validation data within the same training session. If folds are rotated during the same training session overfitting will occur and not produce a model capable of truly detecting species outside of the testing, training, and validation data.

The size of data provides the ability for the model to reduce overfitting by diversifying testing and training imagery, however more data are still needed to include other regions of loblolly pines and sweetgums respective habitat ranges. The concept of object detection with remotely sensed imagery has been previously accomplished in other research outside of vegetation management scenarios to detect airport runways within remotely sensed imagery (Cheng et al., 2013), however Ševo and Avramović (2016) used object detection and image classification from satellite imagery to detect a singular species (Ševo & Avramović, 2016). The model generated in the present research detects sweetgum at an acceptable recall score. Similar to that of sweetgum recall score, loblolly pine performed well but still possessed several false negatives for classifications. The false negatives in these images pertaining to loblolly pines are due to the lack of training data with the differentiating phenological characteristics found within the training, testing, and validation data. These inferencing images were captured in May of 2019 during the spring season and loblolly pines did contain microstrobili and megastrobili. These two reproductive features will need more data collection and further labelling for the model to correctly detect loblolly pines with these reproductive features present. These two reproductive features are not typically found on those species found growing in a utility ROW.

Lower growing specimens of sweetgum and loblolly pines were used in the training data, thus if taller and more robust trees were needed to be identified, this model will need to be retrained with imagery more applicable to desired phenology of the tree. Detection of larger specimens are seen in Santos et al. (2019) utilizing TensorFlow, thus is feasible. Their results yielded an accuracy lesser than what was obtained using the toolbox MMdetection within Pytorch.

To further improve these results in the model in this study, more labelling of imagery not from the current four field sites are needed. These four field sites are indicative of the Piedmont region of North Carolina, rather than the coastal and mountain regions. This model will be able to generate results in these regions, however, data collected in areas outside the Piedmont region of North Carolina will potentially have different phenological characteristics and result in lower precision and recall. This object detection model is designed for sUAS imagery and should be used for sUAS imagery. The integration of this model will be able to increase effectiveness of IVM management plans and potentially immediately reduce cost of management over large areas. Inclusion of this model with management practices could include extraction of global positioning system (GPS) coordinates of each bounding box to generate a precise spray map to prioritize management techniques. This model coupled with real-time kinematic techniques and agriculture sUAS could provide fast, efficient, and precise applications for herbicide control in hazardous terrains for ground crews. This model could also be used to monitor escapes after control measures in vegetation management scenarios and provide an excellent rapid monitoring tool.

The use of overhead arial imagery found in large-scale satellite data and modifications of objection frameworks have provided some insight of improvements in overhead imagery and object detection (Van Etten, 2018). Van Etten's research aimed to implement a fully convolution neural network pipeline for detection of five classes in satellite imagery. This methodology did produce a model capable of detection of their classes not only on their same sensor, but on a different sensor not utilized in training. This research provides enough evidence to generate spatial data from our data through photogrammetry software to then utilize in an object detection model and use in other geospatial applications. This would provide the ability to generate data

usable with geospatial software to produce other desired maps. This is important in the generation of weed density maps, extraction of GPS coordinates of detected objects, and priority treatment maps for vegetation managers.

Creation of additional data of weed density maps, priority treatment maps, and the extraction of GPS coordinates of detected objects provide an avenue for use of agriculture sUAS systems capable of administering herbicides. Weed density maps would provide vegetation managers information on species distribution to better allocate resources to control vegetation, and better determine prescription maps for herbicide applications. Priority treatment maps could then be produced from the prescription maps to determine areas of higher interest or in urgent need of control. These maps could prove to be beneficial especially in areas of high-density during drought years that would otherwise increase fire risks. The generation of a model that detects and then exports the GPS coordinates of the detection would provide precise and accurate locations of data for use in systems similar to the DJI AGRAS T16 (DJI, 2020). This sUAS uses real-time kinematic (RTK) positioning to increase precision of its positional data. This unit's capability is limited to using a sUAS imaging unit with RTK technology to generate a precise map capable of centimeter level accuracy. This RTK imaging technology, RTK spray technology, and a model generated to produce precise GPS coordinates would be able to provide the necessary tools for vegetation managers to optimize management practices by autonomously detecting target weeds for control in vegetation management scenarios.

REFERENCES

Chen, K., Wang, J., Pang, J., Cao, Y., Xiong, Y., Li, X., ... & Zhang, Z. (2019). Mmdetection: Open mmlab detection toolbox and benchmark. *arXiv preprint arXiv:1906.07155*.

Cheng, G., Han, J., Guo, L., Qian, X., Zhou, P., Yao, X., & Hu, X. (2013). Object detection in remote sensing imagery using a discriminatively trained mixture model. *ISPRS Journal of Photogrammetry and Remote Sensing*, *85*, 32-43.

DJI (2020). Agras t16. Available at: https://www.dji.com/t16

EPRI & U.S. Department of Defense (2003). *Complex Interactive Networks/Systems Initiative: Final Summary Report: Overview and Summary Report for Joint EPRI and U.S. Department of Defense University Research Initiative*, EPRI, Palo Alto, CA, and U.S. Department of Defense, Washington DC: 2003. Product ID.

Franklin, S. E. (2018). Pixel-and object-based multispectral classification of forest tree species from small unmanned aerial vehicles. *Journal of Unmanned Vehicle Systems*, *6*(4), 195-211.

Gray, J., & Song, C. (2012). Mapping leaf area index using spatial, spectral, and temporal information from multiple sensors. *Remote Sensing of Environment*, *119*, 173-183.

Greatwood, C., Richardson, T. S., Freer, J., Thomas, R. M., MacKenzie, A. R., Brownlow, R., ... & Nisbet, E. G. (2017). Atmospheric sampling on ascension island using multirotor UAVs. *Sensors*, *17*(6), 1189.

Han, J., Zhang, D., Cheng, G., Guo, L., & Ren, J. (2014). Object detection in optical remote sensing images based on weakly supervised learning and high-level feature learning. *IEEE Transactions on Geoscience and Remote Sensing*, *53*(6), 3325-3337.

Hardin, Perry J., and Ryan R. Jensen. "Small-scale unmanned aerial vehicles in environmental remote sensing: Challenges and opportunities." *GIScience & Remote Sensing* 48.1 (2011): 99-111.

Hardin, P. J., Lulla, V., Jensen, R. R., & Jensen, J. R. (2019). Small Unmanned Aerial Systems (sUAS) for environmental remote sensing: challenges and opportunities revisited. *GIScience & Remote Sensing*, *56*(2), 309-322.

Jardini, M. G., Simões, A. J. M., Jardini, J. A., de Souza, J. M. S., & Crispino, F. (2017, December). Practical Experience of the Use of RGB Camera Images in UAV for the Generation of 3D Images in the Accurate Detection Distance of Vegetation Risk in Right-of-Way Transmission Line. In *International Conference on Geo-Spatial Knowledge and Intelligence* (pp. 152-160). Springer, Singapore.

Ketkar, N. (2017). Introduction to pytorch. In *Deep learning with python* (pp. 195-208). Apress, Berkeley, CA.

Körez, A., & Barışçı, N. (2020). Object Detection with Low Capacity GPU Systems Using Improved Faster R-CNN. *Applied Sciences*, *10*(1), 83.

Matese, A., Toscano, P., Di Gennaro, S. F., Genesio, L., Vaccari, F. P., Primicerio, J., ... & Gioli, B. (2015). Intercomparison of UAV, aircraft and satellite remote sensing platforms for precision viticulture. *Remote Sensing*, *7*(3), 2971-2990.

NERC (2010). Transmission Vegetation Management NERC Standard FAC-003-2 Technical Reference. Available at https://www.nerc.com/pa/Stand/Project%20200707%20Transmission%20Vegetation%20Management/FAC-003-2_TR_December_17_2010.pdf.

Santos, A. A. D., Marcato Junior, J., Araújo, M. S., Di Martini, D. R., Tetila, E. C., Siqueira, H. L., ... & Feitosa, R. Q. (2019). Assessment of CNN-based methods for individual tree detection on images captured by RGB cameras attached to UAVs. *Sensors*, *19*(16), 3595.

Ševo, I., & Avramović, A. (2016). Convolutional neural network based automatic object detection on aerial images. *IEEE geoscience and remote sensing letters*, *13*(5), 740-744.

Thomas, O. H., Smith, C. E., & Wilkinson, B. E. (2017). Economics of mapping using small manned and unmanned aerial vehicles. *Photogrammetric Engineering & Remote Sensing*, *83*(8), 581-591.

Tzutalin. LabelImg. Git code (2015). https://github.com/tzutalin/labelImg

Van Etten, A. (2018). You only look twice: Rapid multi-scale object detection in satellite imagery. *arXiv preprint arXiv:1805.09512*.

Zhang, D., Han, J., Cheng, G., Liu, Z., Bu, S., & Guo, L. (2014). Weakly supervised learning for target detection in remote sensing images. *IEEE Geoscience and Remote Sensing Letters*, *12*(4), 701-705.

Tables and Figures

Table 2.1. Results from MMDetection training on the Faster RCNN architecture using a ResNet backbone to detect *Liquidambar styraciflua* and *Pinus taeda*. These results are from the 50th training epoch. This epoch had an accuracy of 98.6855 and a total loss of 0.1374. Results were generated from MMdetection.

50th Epoch Training Results				
Class	Ground Truths	Detections	Recall	Average Precision
Liquidambar styraciflua	2098	1923	0.603	0.558
Pinus taeda	2542	2739	0.707	0.599
mAP				0.579

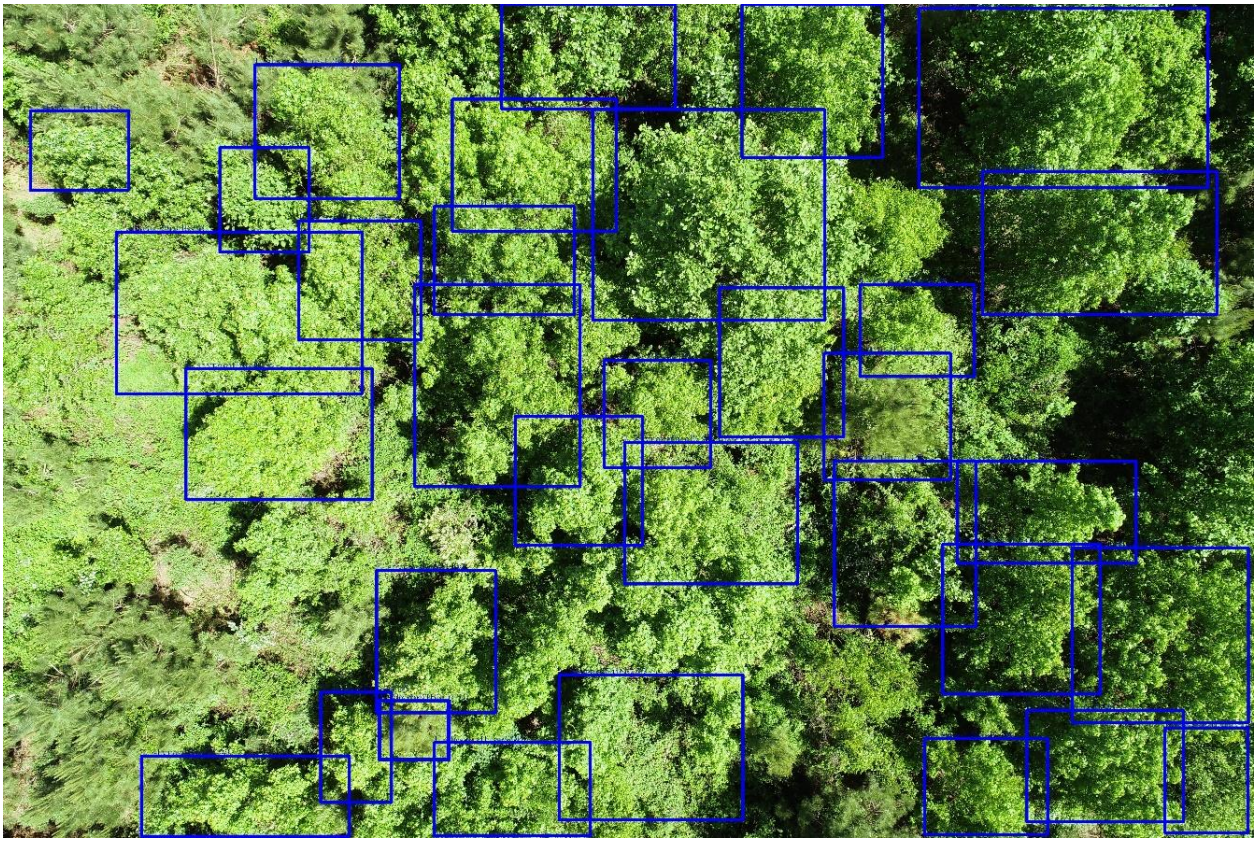

Figure 2.1. Image collected from field site in Wake County, NC USA during the month of June during 2019.

Figure 2.2. Image collected from field site in Johnston County, NC USA during the month of June during 2019.

Figure 2.3. Image collected from field site in Wake County, NC USA during the month of January during 2019. This image depicts larger growing specimens of *Pinus taeda* not being detected.

Figure 2.4. Image collected from field site in Granville County, NC USA during the month of May during 2019. This image depicts vegetation similarly found in a ROW growing next to an open field.

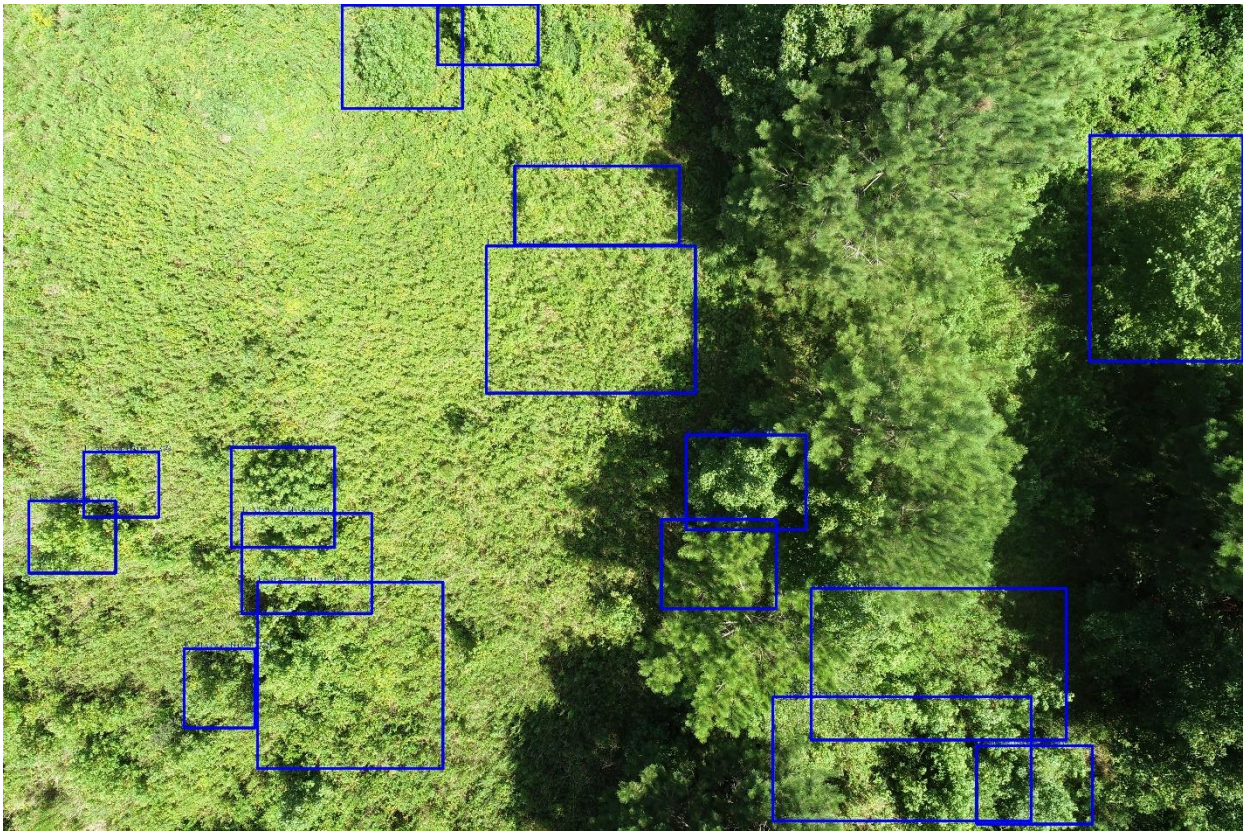

Figure 2.5. Image collected from field site in Granville County, NC USA during the month of May during 2019. This image depicts larger growing specimens of *Pinus taeda* not being detected. There are also False negatives of *Liquidambar styraciflua.*

CHAPTER 3

Implementation of the Automatic Color Thresholding Application, Canopeo, to Quantify Herbicide Efficacy in Floating Aquatic Macrophytes

Abstract

Salivinia molesta (giant salvinia) is a free-floating aquatic fern native to South America which exhibits high reproductive rates outside its native range. Giant salvinia's high grows in dense mats that make difficult to implement control measures. Early detection and rapid response are key to prevent the spread and eradication of new infestations of giant salvinia. A potential tool for monitoring giant salvinia control is an automatic color thresholding tool called Canopeo. This tool was developed by Oklahoma State University to measure fractional green canopy cover percentage by calculating green pixels from RGB imagery. In the present study, Canopeo was used to measure herbicide symptomology progression in *Salvinia molesta* during two separate herbicide trials. The first trial evaluated the effectiveness of Aquastrike (diquat dibromide and dipotassium salt of endothall) herbicide on giant salvinia along with multiple rates and exposures of diquat (0.25 – 0.36 ppm), glyphosate and diquat (96 fl oz A^{-1}, 32 fl oz A^{-1} and 0.25% v/v), endothall (1.2-1.8 ppm), endothall and diquat (1.2-1.8 ppm and 0.25-0.36 ppm), and lastly diquat and endothall (4.5 – 6.5 qts/A -ft). The second trial aimed to determine what herbicides would be an adequate control measure for subsequent in water applications using fluridone (5.0-10.0 ppb), glyphosate (48-96 lb a.e. gal^{-1} 1% v/v), penoxsulam (5.0 – 10.0 ppb), and diquat (0.125 -0.25 ppm) to treat giant salvinia with in water rates. Trial 1, all rates and exposures were effective in controlling giant salvinia except those of only endothall at all rates and exposures at the 4 weeks after treatment evaluations. Trial 2 found diquat at 0.25 ppm to be the most effective

against giant salvinia for submersed in water applications. The diquat 0.125 ppm rates reduced biomass and showed some control, however were not as effective as diquat at 0.25 ppm. Fluridone 10 ppb showed substantial reduction in dry weight biomass in comparison to one control group, however regrowth from buds were present. There were little to no differences of biomass in comparison to controls in the penoxsulam 10 ppb, penoxsulam 5 ppb, fluridone 5 ppb samples. Canopeo measurements tracked the herbicide symptomology development in giant salvinia in Trial 2 effectively. Conversion of the fractional green canopy cover to percent change allowed for a direct comparison of change of green pixels within each individual treatment. This application was able to monitor herbicide symptomology and it can be implemented in both laboratory and field settings using consistent measurement techniques throughout monitoring efforts.

Introduction

The invasive aquatic fern in this study, *Salvinia molesta* (giant salvinia) is native to Brazil and northern Argentina. Giant salvinia's introduction is believed to have occurred from aquarium trade and was first documented in 1995 in South Carolina, USA (Johnson, 1995). Since its first documentation, giant salvinia and since has spread throughout most of the southeastern United States. This species and other invasive aquatic macrophytes have been found to be sold online throughout the United States and internationally (Kay & Hoyle 2001). Discarding of these unwanted invasive macrophytes into ditches, ponds, and other waterbodies with favorable growing conditions have been attributed to the spread of invasive aquatic macrophytes (Kay & Hoyle 2001). Due to plant morphology and rapid growth characteristics of giant salvinia, this macrophyte is difficult to control after introducing. Giant salvinia forms free-floating dense colonies of modules (ramets) held together by a submersed horizontal rhizome; an

intact module possesses three distinct fronds (McFarland et al., 2004). Two of these fronds are located above the surface covered in trichomes, while a third is located below the surface and is elongated resembling a root mass to aid in resistance and stabilizes the plant (McFarland et al., 2004). These trichome resemble eggbeaters or kitchen whisks aiding in flotation by repelling water and trapping air. Amongst these fronds are four to five buds. The vegetative buds of giant salvinia may survive stress underneath the water's surface (Whiteman & Room, 1991), and these buds at a size of at least 0.2 cm and as little as 30% moisture content can have sufficient nutrients and carbohydrates stored to produce new growth (Owens et al., 2004). An anomaly at meiosis prevents fertile haploid gametes (Mitchell & Gopal 1991), thus giant salvinia reproduces asexually through their apical and axillary buds. In optimal growing condition, giant salvinia can double its biomass and individuals in as little as 3 days (Harley and Mitchell 1981; Barrett 1989), thus timely responses are necessary in controlling this aquatic nuisance. Previous studies found similar growth rates in giant salvinia when measuring number of leaves with up to 22% per day and 17% per day increase in dry weight (Mitchel & Tur, 1975). A doubling time of around 14 days with a growth rate of 5% per day in acceptable conditions, giant salvinia could produce anywhere from 45 – 109 dry tonnes ha^{-1} yr^{-1} (Mitchell &Tur 1975; Ranni and Bhambi 1983) in the right conditions. These characteristics of rapid reproduction provide a challenge of control once this species is introduced to a foreign body of water.

This aquatic fern has three different phenological growth stages comprising of the primary (survival stage), secondary (colonizing stage), and the tertiary (mat) stage (Ashton and Mitchell 1989). The primary stage, the plant is slow growing and progresses to a colonizing stage where giant salvinia's growth rate increases and can be found in more open waters. The final phenological growth stage is the mat growth stage (Oliver, 1993). Giant salvinia mats have

been recorded to reach up to 1 meter in thickness (Thomas & Room, 1986), thus providing another challenge for its control via foliar applications by establishing contact with the entirety of mat. The rapid growth and the large quantities of trichomes on the surface of the plant can prevent herbicide penetration to the ferns surface (Holm et al., 1977; Oliver, 1993). The combination of dense mats and trichomes preventing herbicide penetration to the ferns surface provide a multitude of challenges to control this highly invasive species.

There are several means of controlling this aquatic nuisance including mechanical, biological, and chemical. Biological methods of control include the introduction of the of the *Cyrtobagous salviniae* (salvinia weevil). The salvinia weevil is host specific to giant salvinia, and starvation will occur before finding a new host plant (Forno et al. 1983, Thomas and Room 1986), however a case where the salvinia weevil found a new host plant was documented in Forno et al. (1983). The introduction of the salvinia weevil to control giant salvinia has been shown to increase the dissolved oxygen levels in waterways and had a highly successful rates of control at sites, however salvinia weevil at sites did take longer for visual impacts and even up to a year (Flores & Carlson, 2006). Maintenance of these species might be needed in areas experiencing more below freezing temperatures during winter months (Tipping et al., 2008). The salvinia weevil has been proven to control giant salvinia in areas in Texas, USA, however, for maintaining an active population in temperate climates can become a challenge in other parts of the United States. A combination approach of introducing the salvinia weevil and chemical treatments of giant salvinia found a reduction of biomass up to 68% introducing only the salvinia weevil, however a combination of flumioxazin, flumioxazin plus giant salvinia weevil, penoxsulam, and penoxsulam plus giant salvinia weevil treatments resulted in 98 to 100%

control of plants in a 6 weeks after treatment evaluation in a mesocosm study (Mudge et al., 2013).

Chemical treatment is one of, if not the most common method of controlling this invasive plant in the United States. A frequently used field treatment is foliar application of diquat and glyphosate (Mudge et al., 2016; Mudge & Sartain, 2018). However, in a previous study using diquat, endothall, and glyphosate to control giant salvinia achieved an 80% control rating in foliar applications using a trigger pump sprayer in combination with a non-ionic surfactant (Thayer & Haller, 1985). Using foliar applied contact herbicides for control of giant salvinia becomes less effective with dense mats preventing herbicide contact each layer of the mat. During winter months, these mats are less thick than during the growing season, thus winter applied herbicide treatments were proven advantageous and showed herbicides are a useful tool in giant salvinia control in colder months (Mudge & Sartain, 2018). Increasing herbicidal contact in dense mats is desired for increased control of giant salvinia. Herbicidal response of giant salvinia to 32 different herbicides with varying surfactants, rates, and application methods were studied by Nelson et al. (2001). From their findings, diquat was identified as the most effective measure for control using either submersed or foliar applications regardless of rates and surfactants. Nelson et al. (2001) also noted copper, endothall-k, and endothall amine final evaluations were not synonymous with their initial treatment ratings. High rates of endothall amine, endothall-k, and a low rate of endothall amine and copper decreased in control because of regrowth observed later in the study. Longer evaluations provided this information in a laboratory setting. This study also noted diquat as an effective submerged application method at all the rates 0.5 mg L^{-1} and a water depth of 0.46 m.

Visual observations of herbicide symptomology can be performed by several individuals and lead to several different results varying upon opinion. Tracking herbicide symptomology progression with a different method than visual observations could prove effective in monitoring control in herbicide trials. These new methods could provide beneficial insights to applications where regrowth is occurring that decrease control noted in Nelson et al. (2001). With technology rapidly evolving, new tools and applications have emerged with the potential to improve evaluations and measurements. An application which can be used for monitoring herbicide symptomology is Canopeo. Canopeo is an application, developed in MATLAB, that measures fractional green canopy cover (FGCC). This application was designed to monitor terrestrial crops by utilizing automatic color threshold (ACT) (Patrignani & Ochsner, 2015). FGCC in this application is classified on,

$R/G < P_1 \; and \; B/G < P_2 \; and \; 2G - R - B > P_3$ where $P_1 = 0.95,\ P_2 = 0.95$, $P_3 = 20$,(Patrignani & Ochsner, 2015). Unlike the Normalized Difference Vegetation Index (NDVI), which measures in the near infrared part of the spectrum to determine healthy vegetation; Canopeo measures FGCC to assess the canopy development and light inception. This study's main objectives were to determine the effectiveness of Canopeo in assessing herbicide symptomology in giant salvinia and determine what herbicides could be used for submersed in water applications in control of giant salvinia and determine Aquastrike's control on giant salvinia.

Methods

Trial 1:

In the first part of this study a single run with four replicates was performed to determine the effectiveness of a new pre-mix herbicide formulation in controlling giant salvinia. This pre-mix is a combination of active ingredients diquat dibromide and dipotassium salt of endothall (trade name: Aquastrike). Salvinia plants were propagated from greenhouse stock populations prior to treatment. Fronds of similar size, approximately 2-3 g fresh weight, were excised from stock populations and acclimated in test vessels for 3 days prior to treatment. Experimental setup followed a complete randomized block design with four replicates. Treatments were carried out in 500 ml plastic vessels with 350 ml of dechlorinated tap water. Visual ratings were performed with percent control ranging from 0% to 100% control with 100% control being complete desiccation. These visual estimates were performed at two (2 WAT) and four weeks after treatment (4 WAT). Glyphosate is inactive in-water, and as such treatments are exclusively foliar-applied in the field. To best mimic a foliar field application, the glyphosate was applied using a calibrated pressurized spray chamber.

Plants were exposed to all treatments for differential periods of 1, 3, 5 and 7 days. Following the designated exposure period, plants were washed for 10 seconds under a soft stream of untreated tap water and moved to a clean vessel containing 350 ml of dechlorinated tap water. Untreated controls were washed and moved in the same manner as treated plants after 7 days in the initial untreated vessel. Four replicate plants were harvested prior to treatment and dried to a constant mass at 70°C.

Treatment efficacy was assessed with a combination of visual ratings and image analysis at 2 WAT and 4 WAT. A dry biomass analysis was also performed at 4 WAT and dried to a

constant mass at 70°C. Images were captured following the methodology of Patrignani and Ochsner (2015) with slight modifications. These modifications included maintaining camera height by utilizing a stand to reduce height variability between measurements. The images collected were taken using a custom-built stand providing a nadir view towards the vessel of interest. This stand was designed to limit shadowing effects and maintain a consistent distance between lens and water surface and camera angle throughout the study. This was fundemental for the study to eliminate any potential variances between measurements. The camera utilized for this study was a Panasonic Lumix DMC-TS1 12.1-megapixel digital camera. The images collected were captured during three separate stages: pretreatment, 2 WAT, and 4 WAT to monitor the efficacy of the herbicide. Dry biomass data were collected at the conclusion of the experiment 4 WAT.

Trial 2:

The second part of this study aimed at determining if subsequent in water applications of diquat, endothall, and penoxsulam would be effective in controlling giant salvinia, while still delving further into monitoring the progression of herbicide symptomology using Canopeo. Giant salvinia plants were propagated as described in Trial 1. Plant fronds of approximately 3 g fresh weight were excised from greenhouse cultures. Treatments were performed in two runs with four replicates each utilizing a randomized complete block design.

Static treatments were carried out in 500 ml plastic vessels with 350 ml of dechlorinated tap water. All treatments were carried out with their respective in-water rates injected into the water with sterile syringes, except for the glyphosate treatments. In water application was chosen to determine if the rates and herbicides chosen would be adequate in controlling giant salvinia

with in water applications to help eliminate escapes following foliar applications in a field setting. Treatments containing glyphosate were administered via pressurized spray chamber to mimic field applications and not submersed because of the rapid degradation of glyphosate in water (Rueppel et al., 1977).

Efficacy of these static treatments were assessed using a combination of image analysis and dry biomass data. Imaging techniques and equipment were consistent with those utilized in trial 1, however images were captured during six separate stages: pretreatment, three days after treatment (3 DAT), one week (1 WAT), two weeks (2 WAT), three weeks (3 WAT), and four weeks after treatment (4 WAT). Capturing images more frequently during this trial as compared to trial 1 was to effectively capture early onset symptomology and track its progression or regenerative growth to monitor the percent difference. Plants were harvested and dry weights were recorded like trial 1.

Image analysis:

Images from trial 1 and trial 2 were analyzed using Canopeo. The rapid automatic color thresholding tool provided a new method of observing herbicide control typically administered by visual observers. This fractional green canopy cover (FGCC) rating measures the percent of green pixels within the image. This measurement was then converted into a percent change measurement to adequately quantify the difference in greenness in each individual specimen being observed from pretreatment observation till the final observation.

Data Analysis:

All data were statistically analyzed using analysis of variance (ANOVA) and compared with a Tukey's HSD means with JMP Pro 14.3. Herbicide formulation, herbicide rate, and replication were used as fixed effects in the ANOVA model. Percent control and percent change were associated with significant values in quantifying association with herbicide treatments. Images were clipped down to the size of the mouth of the cup prior to processing through Canopeo. This was done to eliminate any background pixels to be classified as green pixels.

Results

Trial 1:

Giant salvinia control at 2 WAT was greatest with any formulation containing diquat in comparison to the control treatments exhibiting no significant block effects (**Tables 3.1**-**3.2**). Endothall treatments of the highest rate of 1.8 ppm at a three-day exposure did not provide significant injury in comparison to the control (**Table 3.3; Figure 3.1**) at 2 WAT. The 4 WAT visual evaluations revealed significant difference between the treatments, and no significant block effect were noted in the 4 WAT evaluation. Diquat treatments were different than the control groups. However, a seven day, five-day of 1.2 ppm and a 5-day exposure of 1.8 ppm endothall provided injury levels different from untreated controls, but not significantly different.

The dry biomass of giant salvinia was lowest in all treatments with diquat (0.36 ppm five-day exposure). Following this was glyphosate (96 fl-oz/A) and diquat (32 fl-oz/A and MSO 0.25% v/v) at a five-day exposure. The premix diquat and endothall combination treatments were lowest with a three-day exposure (4.5 qts / A-Ft). Endothall and diquat tank mixture biomass

values were similar with no significant difference in comparison to the premixed. Endothall alone was least effective and provided little to no control (**Table 3.4**).

These data were also compared in JMP Pro 14 using the fractional green canopy cover ratings obtained from Canopeo. The application's fractional green canopy cover rating was recorded and then converted to a percent change,

$$Percent\ Change = \left(\frac{observation - pretreatment}{pretreatment}\right) * 100$$

, to adequately represent objects decreasing an increasing in greenness. The percent change ratings were used to determine if herbicide symptomology could be tracked throughout the study.

There was a significant replicate effect noted for 2 WAT injury also not observed in the visual analysis (**Tables 3.5-3.6**). The results of the means separation analysis indicated that at 2 WAT for all exposures and treatments except those of only endothall showed signs of significant control in comparison to untreated controls (**Figure 3.2)**. The 4 WAT analysis showed a difference (**Tables 3.7-3.8**), and upon this all-pairs Tukey-Kramer HSD was performed. Every treatment excluding endothall only treatments from the untreated control groups were significantly different. Endothall only treatments provided little to no control of giant salvinia during this trial (**Figure 3.3**).

Trial 2:

Oneway anova tests were run (**Tables 3.9-3.11**), and there were no significant differences among treatment groups during the 3 DAT observation, however some control began to emerge with the glyphosate (48 LBAE/GAL 1% v/v), glyphosate (96 LBAE/GAL 1% v/v), penoxsulam (10ppb), diquat (0.125 ppm), and diquat (0.25 ppm) treatments. No significant differences between the groups were observed during the 1 WAT observation (**Tables 3.12-3.14**). However,

glyphosate (48 LBAE/GAL 1% v/v), glyphosate (96 LBAE/GAL 1% v/v), penoxsulam (10ppb), penoxsulam (10 ppb), diquat (0.125 ppm), and diquat (0.25 ppm) treatments exhibited herbicide symptomology. 2 WAT observations did reveal a significant difference between groups glyphosate (48 LBAE/GAL 1% v/v), glyphosate (96 LBAE/GAL 1% v/v), and diquat (0.25 ppm) (**Figure 3.4**) in direct comparison to the control, and no difference between both rates of glyphosate and diquat (0.25) ppm treatments (**Tables 3.15-3.18**). This reveals in water applications of diquat at a rate of 0.25 ppm is statistically indifferent from foliar applied glyphosate in this trial at a 2 WAT rating. Other herbicides did not show any difference from the control groups in the fluridone (5-10 ppb), penoxsulam (5 -10 ppb), and diquat (0.125 ppm) (**Figure 3.4**). The 3 WAT treatment evaluations found similar results to the 2 WAT evaluations (**Tables 3.19-23.2; Figure 3.5**). There was an increase of treatments significantly different in comparison to other treatments in 3 WAT, however no new treatments were significantly different in comparison to the controls (**Figure 3.5**). There were notable increases in comparison to the controls in the diquat (0.125 ppm), fluridone (10 ppb), and penoxsulam (10 ppb). The 4 WAT results revealed diquat (0.25 ppm), glyphosate (48 LBAE/GAL 1% v/v), and glyphosate (96 LBAE/GAL 1% v/v) to be significantly different from both control groups (**Tables 3.23-3.26; Figure 3.6**). Although penoxsulam (10.0 ppb) and diquat (0.125 ppm) had notable control on giant salvinia, there were no statistical differences from control groups. Fluridone (5 ppb) and penoxsulam (5 ppb) treatments had little to no control in comparison to control groups and however there was a noticeable difference between the fluridone (10 ppb) and control groups.

Biomass results revealed diquat 0.125 ppm, diquat 0.25 ppm, glyphosate 48 LBAE/GAL 1% v/v, and glyphosate 96 LBAE/GAL 1% v/v to be significantly different than that of both control groups. There were no statistical differences between both diquat rates and the two

glyphosate rates when compared to each other. Penoxsulam 10 ppb provided a notable difference in comparison to the control groups with Canopeo measurements, and little to no difference between the penoxsulam 5 ppb and 10 ppb measurements. There were little to no differences between the penoxsulam (5 - 10 ppb) and both control groups. There were no differences between the biomass of fluridone 5 ppb and the control groups. There were notable biomass decreases of in the fluridone 10 ppb treatments in comparison to the controls, however these showed increases in greenness observed by Canopeo. The biomass of fluridone 10 ppb in comparison to penoxsulam 10 ppb showed little to no difference in biomass (**Tables 3.27-3.30**; **Figure 3.7**).

The progression of herbicide symptomology was tracked in trial 2 effectively by reducing the time in between evaluations in comparison to Trial 1. In **Figure 3.8**, the fluridone treatments of 10 ppb revealed a higher percent difference in comparison to fluridone 5 ppb and the control treatments. This change can be attributed to early herbicide control that caused desiccation of the salvinia plant, however regrowth occurred and was visible in the 3 DAT treatment evaluation. Because of the lower control on the fluridone 5 ppb treatments, the midrib on the fronds were still growing close together, thus exposing less foliage to the camera angle. The fluridone 10 ppb treatments new regrowth had higher amounts of green foliage growing parallel to the water's surface, increasing the image's total area of green foliage visible to the camera. These new fronds were accompanied by older foliage that did exhibit herbicide symptomology. The penoxsulam treatments at the 2 WAT evaluation had an increase in greenness, and then more herbicide symptomology is seen within 3 WAT and 4 WAT in both treatments (**Figure 3.9**). Both glyphosate rates were effective against salvinia and were quick to control reduce the Canopeo rating to 0.00% in as early as the 2 WAT ratings and all raters registering 0.00% at the

4 WAT measurements (**Figure 3.10**). Similar to penoxsulam, the diquat 0.125 ppm measurements increased in greenness and reduced its greenness to almost where the original measurements were recorded by the 4 WAT mark, however the biomass was significantly different than the control groups (**Figure 3.11**). The diquat 0.25 ppm rate showed quick control and by the 2 WAT rating almost all replicates were registering 0.00%. The 4 WAT ratings all specimens rated 0.00%. After further evaluation with the dry weight results (**Figure 3.12**), the fluridone 5 ppb had a range of biomass higher than that of both control groups, and the fluridone 10 ppb had less biomass than the fluridone 5 ppb and both control groups. In comparison to the 4 WAT and dry biomass comparisons, there was a discrepancy with the Fluridone 10 ppb evaluations with increased greenness, but still having a decrease in biomass in comparison to the fluridone 5 ppb treatments (**Figure 3.13**).

Discussion and Conclusion

Giant salvinia control varied by treatments, however the foliar applications of glyphosate presented the best overall control in trial 2 with percent change ratings at the 2 WAT mark being -100, indicating these species greenness from the beginning of this trial were completely gone. These results were the same at the 4 WAT after treatment measurements. From the results of this study submersed applications to treat giant salvinia should incorporate diquat 0.25 ppm in combination with foliar applications using diquat, glyphosate, or a combination of diquat and endothall. Submersed in water applications of diquat 0.25 ppm proved to control giant salvinia and could provide an application measure to help improve the contact of herbicide with giant salvinia mats located below the water's surface. Higher rates of fluridone and penoxsulam should be revisited at higher rates of 10 ppb but still abide by the label limits to test against giant

salvinia for in water applications. Submersed in water applications of diquat at a rate of 0.5 mg L^{-1} were seen in Nelson et al. (2001) to control giant salvinia, and similar results were found at rates of diquat at 0.25 ppm. In trial 1 diquat and endothall treatments did control giant salvinia effectively. In trial 1, Aquastrike across all rates and exposures were effective in controlling giant salvinia.

Utilization of Canopeo in these herbicide trials allowed for a method to track each individual treatment herbicide symptomology progression for direct comparison to other herbicides. Converting the FGCC to percent change allowed results to represent a degree of change over time to represent the herbicide symptomology from the pretreatment measurements to each evaluation period. This is important because of the continual growth of the giant salvinia control groups. The treatment groups are typically labelled as 0.00 % in control measurements; however, these measurements do not adequately represent the growth of salvinia in control groups. Using this application to measure the herbicide symptomology also allowed for a more precise measurement of control groups by adequately measuring the increase of greenness. This allowed for a comparison of controls of where growth is typically not measured. By not including the growth of control groups, observational bias is introduced.

Observer bias in herbicide control is based upon observer experience and knowledge of symptomology, macrophyte, and herbicides being administered; thus, it creates multiple avenues of observational bias. Incorporation of Canopeo in measuring and quantifying herbicide was seen in Abreu et al. (2019) measuring herbicide injury in bermudagrass, and found visual observations lower in control ratings than that of Canopeo measurements. Observational bias in this study was attributed to Canopeo quantifying a specific green wavelength at a pixel based level, and visual observations influenced by eye cone receptors in each individual and ambient lighting.

Controlling the observations at a standardized level will eliminate observer bias and provide a newfangled approach monitoring herbicide symptomology. This method does contain its limitations within the application. These limitations are easily overcome with performing a percent change equation to adequately represent the species or target being observed. The user does possess the ability to control the red to green and blue to green ratio within the application, thus allowing the potential introduction of observer bias. However, proper documentation and observer consistency with each treatment's settings will diminish this.

By tracking and monitoring the efficacy of herbicides through Canopeo measurements, observing the herbicide symptomology progression is possible. As noted in Nelson et al. (2001), monitoring treatment efficacy with time is important, and Canopeo demonstrated in these trials its ability to monitor herbicide symptomologies adequately and effectively during treatment. Furthermore, this application does not adequately represent true plant health because it does not measure plant health through a Normalized Difference Vegetation Index, or NDVI. This application does not adequately represent the dry biomass as witnessed with the fluridone 10 ppb treatments. This application's ability to measure foliar greenness contains its limitations in comparison to other methods, especially with a plant morphology containing thicker, waxier cuticles which would increase light reflection off of the surface, dampening Canopeo's ability to register green pixels. Adjustments within the application can reduce the noise, but for precision and accuracy of the application in monitoring herbicide sympotology, adjustments need to be consistent and implemented for each consecutive rating and kept for each measurement. Maintaining consistency with image augmentation, green to red ratios, green to blue ratios, and noise reduction is essential for the optimal functionality and reduction of bias within laboratory herbicide trials. Field trials using this tool should avoid altering the height, angle, and

manipulation of ratios from pretreatment measurements to the conclusion of observations. This tool will need to be tested against multiple field trials to determine if this tool can be effectively used in a field trial setting.

This application is a well-balanced tool which possessing its own challenges; however, it is extremely beneficial and has tremendous upside. The possibilities with this application provide several uses outside of its intended original purpose. One of these is proved in this study to monitor herbicide symptomology in laboratory trials for giant salvinia.

REFERENCES

Abreu, L. F., Rocateli, A. C., Manuchehri, M. R., Arnall, B., & Antonangelo, J. (2019, November). Assessing Gyphosate Injury and Forage Bermudagrass Regrowth Using Canopeo. In *ASA, CSSA and SSSA International Annual Meetings (2019)*. ASA-CSSA-SSSA.

Ashton, P.J. & Mitchell, D. S. (1989). Aquatic plants: pattern and modes of invasion, attributes of invading species and assessment of control programmes. Pages 111-154 in J. A. Drake, H. A. Mooney, F. di Castri, R. H. Groves, F. J. Kruger, M. Rejmanek, and M. Williamson, eds. *Biological Invasions: a Global Perspective*. Wiley and Sons, New York.

Barrett, S. C. (1989). Waterweed invasions. *Scientific American*, *261*(4), 90-97.

Flores, D., & Carlson, J. W. (2006). Biological control of giant salvinia in East Texas waterways and the impact on dissolved oxygen levels.

Forno, I. W., Sands, D. P. A., & Sexton, W. (1983). Distribution, biology and host specificity of *Cyrtobagous singularis* Hustache (Coleoptera: Curculionidae) for the biological control of *Salvinia molesta*. *Bulletin of Entomological Research*, *73*(1), 85-95.

Harley, K. L. S., & Mitchell, D. S. (1981). "The biology of Australian weeds. 6. Salvinia molesta D. S. Mitchell," *Journal of the Australian Institute of Agricultural Science* 47, 67-76.

Holm, L. G., Plucknett, D. L., Pancho, J. V., & Herberger, J. P. (1977). *The world's worst weeds. Distribution and biology*. University press of Hawaii.

Johnson, D. 1995. Giant salvinia found in South Carolina. *Aquatics* 17(4):22.

Kay, S. H., & Hoyle, S. T. (2001). Mail order, the internet, and invasive aquatic weeds. *Journal of Aquatic Plant Management*, *39*(1), 88-91.

McFarland, D. G., Nelson, L. S., Grodowitz, M. J., Smart, R. M., & Owens, C. S. (2004). *Salvinia molesta DS Mitchell (Giant Salvinia) in the United States: A review of species ecology and approaches to management* (No. ERDC/EL-SR-04-2). ENGINEER RESEARCH AND DEVELOPMENT CENTER VICKSBURG MS ENVIRONMENTAL LAB.

Mitchell, D. S., & Gopal, B. (1991). Invasion of tropical freshwaters by alien aquatic plants. *Ecology of biological invasion in the tropics.*, 139-155.

Mitchell, D. S., & Tur, N. M. (1975). The rate of growth of *Salvinia molesta* (S. auriculata Auct.) in laboratory and natural conditions. *Journal of Applied Ecology*, 213-225.

Mudge, C. R., Harms, N. E., & Nachtrieb, J. G. (2013). Interactions of herbicides, surfactants, and the giant salvinia weevil (*Cyrtobagous salviniae*) for control of giant salvinia (*Salvinia molesta*). *J. Aquat. Plant Manage*, *51*, 77-83.

Mudge, C. R., Perret, A. J., & Winslow, J. R. (2016). Evaluation of foliar herbicide and surfactant combinations for control of giant salvinia at three application timings. *J Aquat Plant Manag*, *54*, 32-36.

Mudge, C. R., & Sartain, B. T. (2018). Influence of winter on herbicide efficacy for control of giant salvinia (*Salvinia molesta*). *J Aquat Plant Manag*, *56*, 68-71.

Nelson, L. S., Skogerboe, J. G., & Getsinger, K. D. (2001). Herbicide evaluation against giant salvinia. *Journal of Aquatic Plant Management*, *39*, 48-53.

Oliver, J. D. (1993). A review of the biology of giant salvinia (*Salvinia molesta* Mitchell). *Journal of Aquatic Plant Management 31*, 227–231.

Owens, C. S., Smart, R. M., & Dick, G. O. (2004). Regeneration of giant Salvinia from apical and axillary buds following desiccation or physical damage. *Journal of Aquatic Plant Management*, *42*, 117-119.

Patrignani, A., & Ochsner, T. E. (2015). Canopeo: A powerful new tool for measuring fractional green canopy cover. *Agronomy Journal*, *107*(6), 2312-2320.

Rani, V. U., & Bhambie, S. (1983). A study on the growth of Salvinia molesta Mitchell in relation to light and temperature. *Aquatic Botany*, *17*(2), 119-124.

Rueppel, M. L., Brightwell, B. B., Schaefer, J., & Marvel, J. T. (1977). Metabolism and degradation of glyphosate in soil and water. *Journal of agricultural and food chemistry*, *25*(3), 517-528.

Tipping, P. W., Martin, M. R., Center, T. D., & Davern, T. M. (2008). Suppression of *Salvinia molesta* Mitchell in Texas and Louisiana by *Cyrtobagous salviniae* Calder and Sands. *Aquatic Botany*, *88*(3), 196-202.

Thayer, D. D., & Haller, W. T. (1985). Effect of herbicides on floating aquatic plants. *Journal of Aquatic Plant Management*, *23*, 94-95.

Thomas, P. A., & Room, P. M. (1986). Taxonomy and control of *Salvinia molesta*. *Nature*, *320*(6063), 581-584.

Whiteman, J. B., & Room, P. M. (1991). Temperatures lethal to *Salvinia molesta* Mitchell. *Aquatic Botany*, *40*(1), 27-35.

Table 3.1. Trial 1 oneway anova summary of fit for 2 WAT visual observation ratings

Oneway Anova	
Summary of Fit	
Rsquare	0.990618
Adj Rsquare	0.987256
Root Mean Square Error	3.924219
Mean of Response	77.62195
Observations (or Sum Weights)	164

Table 3.2. Trial 1 oneway anova analysis of variance for 2 WAT visual observation ratings

Analysis of Variance					
Source	**DF**	**Sum of Squares**	**Mean Squares**	**F Ratio**	**Prob > F**
Herbicide and Rate	40	195046.06	4879.15	316.6437	<.0001*
Replicate	3	76.56	25.52	1.6572	0.1799
Error	120	1847.94	15.40		
Corrected Total	163	196970.56			

Table 3.3. 2 WAT visual observations percent control connecting letters report oneway anova and all pairs Tukey-Kramer HSD

2 WAT Connecting Letters Report Oneway Anova

Herbicide	Rate	Exposure Days	Letter			Mean
Aquathol K **Reward**	1.2 ppm 0.25 ppm	3	A			97.50
Glyphosate **Reward** **MSO**	96 fl-oz/ac 32 fl-oz/ac 0.25% v/v	1	A			97.25
Glyphosate **Reward** **MSO**	96 fl-oz/ac 32 fl-oz/ac 0.25% v/v	7	A			97.00
Reward	0.36 ppm	7	A			96.75
Glyphosate **Reward** **MSO**	96 fl-oz/ac 32 fl-oz/ac 0.25% v/v	3	A			96.50
Aquastrike	4.5 qts / A-Ft	3	A			96.50
Glyphosate **Reward** **MSO**	96 fl-oz/ac 32 fl-oz/ac 0.25% v/v	5	A			96.50
Aquathol K **Reward**	1.2 ppm 0.25 ppm	5	A			96.50
Aquastrike	5.5 qts/ A-Ft	3	A			96.50
Reward	0.36 ppm	5	A			96.50
Aquastrike	6.5 qts / A-Ft	3	A			96.50
Reward	0.36 ppm	3	A			96.50
Aquathol K **Reward**	1.8 ppm 0.36 ppm	5	A			96.00
Aquathol K **Reward**	1.8 ppm 0.36 ppm	1	A			96.00
Aquastrike	4.5 qts / A-Ft	1	A			95.75
Aquastrike	4.5 qts / A-Ft	7	A			95.75
Aquastrike	5.5 qts/ A-Ft	5	A			95.75
Aquastrike	5.5 qts/ A-Ft	7	A			95.75
Aquathol K **Reward**	1.2 ppm 0.25 ppm	1	A			95.75
Reward	0.25 ppm	7	A			95.75
Aquastrike	6.5 qts / A-Ft	1	A			95.75
Aquathol K **Reward**	1.8 ppm 0.36 ppm	7	A			95.00
Aquathol K **Reward**	1.8 ppm 0.36 ppm	3	A			95.00
Aquathol K **Reward**	1.2 ppm 0.25 ppm	7	A			95.00
Aquastrike	6.5 qts / A-Ft	7	A			95.00
Reward	0.25 ppm	1	A			95.00
Reward	0.25 ppm	3	A			95.00
Reward	0.25 ppm	5	A			95.00
Reward	0.36 ppm	1	A			95.00
Aquastrike	6.5 qts / A-Ft	5	A			95.00
Aquastrike	4.5 qts / A-Ft	1	A			95.00
Aquastrike	5.5 qts/ A-Ft	1	A			94.50
Aquathol K	1.2 ppm	5		B		20.00
Aquathol K	1.2 ppm	7		B		17.50
Aquathol K	1.8 ppm	1		B		15.00
Aquathol K	1.8 ppm	5		B		15.00
Aquathol K	1.2 ppm	1		B		12.50
Aquathol K	1.2 ppm	3		B		12.50
Aquathol K	1.8 ppm	7		B		12.50
Aquathol K	1.8 ppm	3		B	C	10.00
Untreated Control	0	0			C	0.00

Levels not connected by same letter are significantly different

Tukey's HSD (honestly significant difference), is a single-step multiple comparison statistical test to find means that are significantly different from each other.

Table 3.4. Dry biomass in grams Trial 1

Dry Biomass in Grams Trial 1

Herbicide	Rate	Exposure Days	Weight (g)
Aquastrike	4.5 qts / A-Ft	1	0.079
Aquastrike	4.5 qts / A-Ft	3	0.065
Aquastrike	4.5 qts / A-Ft	5	0.073
Aquastrike	4.5 qts / A-Ft	7	0.103
Aquastrike	5.5 qts/ A-Ft	1	0.080
Aquastrike	5.5 qts/ A-Ft	3	0.083
Aquastrike	5.5 qts/ A-Ft	5	0.072
Aquastrike	5.5 qts/ A-Ft	7	0.086
Aquastrike	6.5 qts / A-Ft	1	0.087
Aquastrike	6.5 qts / A-Ft	3	0.745
Aquastrike	6.5 qts / A-Ft	5	0.083
Aquastrike	6.5 qts / A-Ft	7	0.078
Aquathol K **Reward**	1.2 ppm 0.25 ppm	1	0.089
Aquathol K **Reward**	1.2 ppm 0.25 ppm	3	0.104
Aquathol K **Reward**	1.2 ppm 0.25 ppm	5	0.085
Aquathol K **Reward**	1.2 ppm 0.25 ppm	7	0.095
Aquathol K **Reward**	1.8 ppm 0.36 ppm	3	0.086
Aquathol K **Reward**	1.8 ppm 0.36 ppm	3	0.078
Aquathol K **Reward**	1.8 ppm 0.36 ppm	5	0.064
Aquathol K **Reward**	1.8 ppm 0.36 ppm	7	0.103
Aquathol K	1.2 ppm	1	0.260
Aquathol K	1.2 ppm	3	0.237
Aquathol K	1.2 ppm	5	0.215
Aquathol K	1.2 ppm	7	0.212
Aquathol K	1.8 ppm	1	0.236
Aquathol K	1.8 ppm	3	0.254
Aquathol K	1.8 ppm	5	0.224
Aquathol K	1.8 ppm	7	0.221
Glyphosate **Reward** **MSO**	96 fl-oz/ac 32 fl-oz/ac 0.25% v/v	1	0.085
Glyphosate **Reward** **MSO**	96 fl-oz/ac 32 fl-oz/ac 0.25% v/v	3	0.094
Glyphosate **Reward** **MSO**	96 fl-oz/ac 32 fl-oz/ac 0.25% v/v	5	0.061
Glyphosate **Reward** **MSO**	96 fl-oz/ac 32 fl-oz/ac 0.25% v/v	7	0.070
Reward	0.25 ppm	1	0.073
Reward	0.25 ppm	3	0.108
Reward	0.25 ppm	5	0.076
Reward	0.25 ppm	7	0.091
Reward	0.36 ppm	1	0.085
Reward	0.36 ppm	3	0.068
Reward	0.36 ppm	5	0.049
Reward	0.36 ppm	7	0.080
Untreated Control	0	0	0.244

Table 3.5. Trial 1 oneway anova summary of fit for 2 WAT Canopeo percent change rating

Oneway Anova	
Summary of Fit	
Rsquare	0.695301
Adj Rsquare	0.586118
Root Mean Square Error	56.80919
Mean of Response	-59.9483
Observations (or Sum Weights)	164

Table 3.6. Trial 1 oneway anova analysis of variance for 2 WAT Canopeo percent change rating

Analysis of Variance					
Source	**DF**	**Sum of Squares**	**Mean Squares**	**F Ratio**	**Prob > F**
Herbicide and Rate	40	848344.8	21208.6	6.5717	<.0001*
Replicate	3	35388.2	11796.1	3.6551	0.0145*
Error	120	387274.1	3227.3		
Corrected Total	163	1271007.2			

Table 3.7. Trial 1 oneway anova summary of fit for 4 WAT Canopeo percent change

Oneway Anova	
Summary of Fit	
Rsquare	0.587881
Adj Rsquare	0.440205
Root Mean Square Error	90.60184
Mean of Response	-55.2579
Observations (or Sum Weights)	164

Table 3.8. Trial 1 oneway anova analysis of variance for 4 WAT Canopeo percent change

Analysis of Variance					
Source	**DF**	**Sum of Squares**	**Mean Squares**	**F Ratio**	**Prob > F**
Herbicide and Rate	40	1388411.8	34710.3	4.2285	<.0001*
Replicate	3	167380.0	5579.3	0.6797	0.5661
Error	120	985043.2	8208.7		
Corrected Total	163	2390193.0			

Table 3.9. Trial 2 oneway anova summary of fit for 3 DAT Canopeo percent change

Oneway Anova	
Summary of Fit	
Rsquare	0.14687
Adj Rsquare	-0.00593
Root Mean Square Error	39.66684
Mean of Response	-1.8405
Observations (or Sum Weights)	80

Table 3.10. Trial 2 oneway anova analysis of variance for 3 DAT Canopeo percent change

Analysis of Variance

Source	DF	Sum of Squares	Mean Squares	F Ratio	Prob > F
Herbicide	9	10517.17	1168.57	0.7427	0.6686
Replicate	3	7631.58	2543.86	1.6167	0.1937
Error	67	105421.70	1573.46		
Corrected Total	79	123570.45			

Table 3.11. Trial 2 oneway anova analysis of variance for 3 DAT Canopeo percent change

Means for Oneway Anova

Level	Number	Mean	Standard Error	Lower 95%	Upper 95%
Control 00	8	8.253	14.024	-19.74	36.246
Control 01	8	-5.296	14.024	-33.29	22.697
Fluridone 10 ppb	8	9.968	14.024	-18.02	37.961
Fluridone 5 ppb	8	12.711	14.024	-15.28	40.703
Glyphosate 48 LBAE/GAL 1% v/v	8	-18.197	14.024	-46.19	9.795
Glyphosate 96 LBAE/GAL 1% v/v	8	-16.940	14.024	-44.93	11.052
Penoxsulam 10 ppb	8	-11.046	14.024	-39.04	16.947
Penoxsulam 5 ppb	8	13.616	14.024	-14.38	41.609
Diquat 0.125 ppm	8	-5.568	14.024	-33.56	22.425
Diquat 0.25 ppm	8	-5.907	14.024	-33.90	22.086

Standard error uses a pooled estimate of error variance

Table 3.12. Trial 2 oneway anova summary of fit for 1 WAT Canopeo percent change

Oneway Anova	
Summary of Fit	
Rsquare	0.238601
Adj Rsquare	0.10223
Root Mean Square Error	69.50691
Mean of Response	0.81674
Observations (or Sum Weights)	80

Table 3.13. Trial 2 oneway anova analysis of variance for 1 WAT Canopeo percent change

Analysis of Variance					
Source	**DF**	**Sum of Squares**	**Mean Squares**	**F Ratio**	**Prob > F**
Herbicide	9	84188.22	9354.25	1.9362	0.0614
Replicate	3	17247.19	5749.06	1.1900	0.3203
Error	67	323691.14	4831.21		
Corrected Total	79	425126.55			

Table 3.14. Trial 2 oneway anova analysis of variance for 1 WAT Canopeo percent change

Means for Oneway Anova					
Level	**Number**	**Mean**	**Standard Error**	**Lower 95%**	**Upper 95%**
Control 00	8	45.664	24.574	-3.4	94.72
Control 01	8	-2.735	24.574	-51.8	46.32
Fluridone 10 ppb	8	38.852	24.574	-10.2	87.90
Fluridone 5 ppb	8	15.925	24.574	-33.1	64.98
Glyphosate 48 LBAE/GAL 1% v/v	8	-23.455	24.574	-72.5	25.60
Glyphosate 96 LBAE/GAL 1% v/v	8	-56.325	24.574	-105.4	-7.27
Penoxsulam 10 ppb	8	-11.978	24.574	-61.0	37.07
Penoxsulam 5 ppb	8	43.117	24.574	-5.9	92.17
Diquat 0.125 ppm	8	-12.937	24.574	-62.0	36.11
Diquat 0.25 ppm	8	-27.961	24.574	-77.0	21.09

Standard error uses a pooled estimate of error variance

Table 3.15. Trial 2 oneway anova summary of fit for 2 WAT Canopeo percent change

Oneway Anova	
Summary of Fit	
Rsquare	0.238601
Adj Rsquare	0.10223
Root Mean Square Error	69.50691
Mean of Response	0.81674
Observations (or Sum Weights)	80

Table 3.16. Trial 2 oneway anova analysis of variance for 2 WAT Canopeo percent change

Analysis of Variance

Source	DF	Sum of Squares	Mean Squares	F Ratio	Prob > F
Herbicide	9	506644.1	56293.8	7.4009	<.0001*
Replicate	3	29925.9	9975.3	1.3114	0.2780
Error	67	509623.1	7606.3		
Corrected Total	79	1046193.0			

Table 3.17. Trial 2 oneway anova analysis of variance for 2 WAT Canopeo percent change

Means for Oneway Anova

Level	Number	Mean	Standard Error	Lower 95%	Upper 95%
Control 00	8	130.84	30.835	69.3	192.38
Control 01	8	101.93	30.835	40.4	163.47
Fluridone 10 ppb	8	175.82	30.835	114.3	237.37
Fluridone 5 ppb	8	111.02	30.835	49.5	172.57
Glyphosate 48 LBAE/GAL 1% v/v	8	-50.11	30.835	-111.7	11.44
Glyphosate 96 LBAE/GAL 1% v/v	8	-60.31	30.835	-121.9	1.23
Penoxsulam 10 ppb	8	37.77	30.835	-23.8	99.32
Penoxsulam 5 ppb	8	97.68	30.835	36.1	159.23
Diquat 0.125 ppm	8	9.60	30.835	-51.9	71.15
Diquat 0.25 ppm	8	-41.19	30.835	-102.7	20.36

Standard error uses a pooled estimate of error variance

Table 3.18. Trial 2 connecting letters report for 2 WAT Canopeo percent change

Means for Oneway Anova						
Level	**Rate**					**Mean**
Fluridone	10 ppb	A				175.82
Control 00	0	A	B			130.84
Fluridone	5 ppb	A	B			111.02
Control 01	0	A	B			101.93
Penoxsulam	5 ppb	A	B	C		97.68
Penoxsulam	10 ppb	A	B	C	D	37.77
Diquat	0.125 ppm		B	C	D	9.60
Diquat	0.25 ppm			C	D	-41.19
Glyphosate	48 LBAE/GAL 1% v/v				D	-50.11
Glyphosate	96 LBAE/GAL 1% v/v				D	-60.31

Levels not connected by same letter are significantly different
Tukey's HSD (honestly significant difference), is a single-step multiple comparison statistical test to find means that are significantly different from each other.

Table 3.19. Trial 2 oneway anova summary of fit 3 WAT Canopeo percent change

Oneway Anova	
Summary of Fit	
Rsquare	0.550673
Adj Rsquare	0.470197
Root Mean Square Error	95.90241
Mean of Response	54.06075
Observations (or Sum Weights)	80

Table 3.20. Trial 2 oneway anova analysis of variance for 3 WAT Canopeo percent change

Analysis of Variance					
Source	**DF**	**Sum of Squares**	**Mean Squares**	**F Ratio**	**Prob > F**
Herbicide	9	723943.1	80438.1	8.7459	<.0001*
Replicate	3	31262.5	10420.8	1.330	0.3421
Error	67	616217.2	9197.3		
Corrected Total	79	1371422.8			

Table 3.21. Trial 2 oneway anova analysis of variance for 3 WAT Canopeo percent change

Means for Oneway Anova

Level	Number	Mean	Standard Error	Lower 95%	Upper 95%
Control 00	8	143.54	33.907	75.9	211.2
Control 01	8	118.82	33.907	51.1	186.5
Fluridone 10 ppb	8	216.23	33.907	148.5	283.9
Fluridone 5 ppb	8	114.49	33.907	46.8	182.2
Glyphosate 48 LBAE/GAL 1% v/v	8	-72.88	33.907	-140.6	-5.2
Glyphosate 96 LBAE/GAL 1% v/v	8	-77.70	33.907	-145.4	-10.0
Penoxsulam 10 ppb	8	33.27	33.907	-34.4	100.9
Penoxsulam 5 ppb	8	100.17	33.907	32.5	167.8
Diquat 0.125 ppm	8	14.13	33.907	-53.5	81.8
Diquat 0.25 ppm	8	-49.46	33.907	-117.1	18.2

Standard error uses a pooled estimate of error variance

Table 3.22. Trial 2 connecting letters report for 3 WAT Canopeo percent change

Means for Oneway Anova

Level	Rate					Mean
Fluridone	10 ppb	A				216.23
Control 00	0	A	B			143.54
Control 01	0	A	B			118.82
Fluridone	5 ppb	A	B			114.49
Penoxsulam	5 ppb	A	B	C		100.17
Penoxsulam	10 ppb		B	C	D	33.27
Diquat	0.125 ppm		B	C	D	14.13
Diquat	0.25 ppm			C	D	-49.46
Glyphosate	48 LBAE/GAL 1% v/v				D	-72.88
Glyphosate	96 LBAE/GAL 1% v/v				D	-77.70

Levels not connected by same letter are significantly different

Tukey's HSD (honestly significant difference), is a single-step multiple comparison statistical test to find means that are significantly different from each other.

Table 3.23. Trial 2 oneway anova summary of fit for 4 WAT Canopeo percent change

Oneway Anova	
Summary of Fit	
Rsquare	0.628146
Adj Rsquare	0.561545
Root Mean Square Error	91.50802
Mean of Response	48.80948
Observations (or Sum Weights)	80

Table 3.24: Trial 2 oneway anova analysis of variance for 4 WAT Canopeo percent change

Analysis of Variance					
Source	**DF**	**Sum of Squares**	**Mean Squares**	**F Ratio**	**Prob > F**
Herbicide	9	913254.0	101473	12.1180	<.0001*
Replicate	3	34469.2	11490	1.3721	0.2588
Error	67	561039.1	8374		
Corrected Total	79	1508762.3			

Table 3.25. Trial 2 oneway anova analysis of variance for 4 WAT Canopeo percent change

Means for Oneway Anova					
Level	**Number**	**Mean**	**Standard Error**	**Lower 95%**	**Upper 95%**
Control 00	8	148.33	32.353	83.8	212.9
Control 01	8	135.41	32.353	70.8	200.0
Fluridone 10 ppb	8	232.86	32.353	168.3	297.4
Fluridone 5 ppb	8	121.78	32.353	57.2	186.4
Glyphosate 48 LBAE/GAL 1% v/v	8	-96.26	32.353	-160.8	-31.7
Glyphosate 96 LBAE/GAL 1% v/v	8	-93.44	32.353	-158.0	-28.9
Penoxsulam 10 ppb	8	14.24	32.353	-50.3	78.8
Penoxsulam 5 ppb	8	80.87	32.353	16.3	145.4
Diquat 0.125 ppm	8	6.04	32.353	-58.5	70.6
Diquat 0.25 ppm	8	-61.73	32.353	-126.3	2.8

Standard error uses a pooled estimate of error variance

Table 3.26. Trial 2 connecting letters report for 4 WAT Canopeo percent change

Means for Oneway Anova						
Level	**Rate**					**Mean**
Fluridone	10 ppb	A				232.86
Control 00	0	A	B			148.33
Control 01	0	A	B			135.41
Fluridone	5 ppb	A	B			121.78
Penoxsulam	5 ppb		B	C		80.87
Penoxsulam	10 ppb		B	C	D	14.24
Diquat	0.125 ppm		B	C	D	6.04
Diquat	0.25 ppm			C	D	-61.73
Glyphosate	96 LBAE/GAL 1% v/v				D	-93.43
Glyphosate	48 LBAE/GAL 1% v/v				D	-96.26

Levels not connected by same letter are significantly different
Tukey's HSD (honestly significant difference), is a single-step multiple comparison statistical test to find means that are significantly different from each other.

Table 3.27. Trial 2 oneway anova summary of fit biomass by herbicide

Oneway Anova	
Summary of Fit	
Rsquare	0.593703
Adj Rsquare	0.520934
Root Mean Square Error	0.048614
Mean of Response	0.183175
Observations (or Sum Weights)	80

Table 3.28. Trial 2 oneway anova analysis of variance biomass by herbicide

Analysis of Variance					
Source	**DF**	**Sum of Squares**	**Mean Squares**	**F Ratio**	**Prob > F**
Herbicide	9	0.22855680	0.025395	10.7456	<.0001*
Replicate	3	0.00282095	0.000940	0.3979	0.7549
Error	67	0.15834180	0.002363		
Corrected Total	79	0.38971955			

Table 3.29. Trial 2 oneway anova analysis of variance for biomass in grams by herbicide

Means for Oneway Anova

Level	Number	Mean	Standard Error	Lower 95%	Upper 95%
Control 00	8	0.249625	0.01719	0.21532	0.28393
Control 01	8	0.239875	0.01719	0.20557	0.27418
Fluridone 10 ppb	8	0.191500	0.01719	0.15719	0.22581
Fluridone 5 ppb	8	0.246125	0.01719	0.21182	0.28043
Glyphosate 48 LBAE/GAL 1% v/v	8	0.112750	0.01719	0.07844	0.14706
Glyphosate 96 LBAE/GAL 1% v/v	8	0.119875	0.01719	0.08557	0.15418
Penoxsulam 10 ppb	8	0.206750	0.01719	0.17244	0.24106
Penoxsulam 5 ppb	8	0.208625	0.01719	0.17432	0.24293
Diquat 0.125 ppm	8	0.147250	0.01719	0.11294	0.18156
Diquat 0.25 ppm	8	0.109375	0.01719	0.07507	0.14368

Standard error uses a pooled estimate of error variance

Table 3.30. Trial 2 connecting letters report for dry biomass weight in grams

Means for Oneway Anova

Level	Rate					Mean
Control 00	0	A				0.249625
Fluridone	5 ppb	A				0.246125
Control 01	0	A				0.239875
Penoxsulam	5 ppb	A	B			0.208625
Penoxsulam	10 ppb	A	B			0.206750
Fluridone	10 ppb	A	B	C		0.191500
Diquat	0.125 ppm		B	C	D	0.147250
Glyphosate	96 LBAE/GAL 1% v/v			C	D	0.119875
Glyphosate	48 LBAE/GAL 1% v/v			C	D	0.112750
Diquat	0.25 ppm				D	0.109375

Levels not connected by same letter are significantly different

Tukey's HSD (honestly significant difference), is a single-step multiple comparison statistical test to find means that are significantly different from each other.

Connecting Letters Report

Level					Mean
Reward0.36 ppm5	A				99.250000
Glyphosate Reward MSO100 fl oz/A, 32 floz/A and 0.25% v/v1	A				99.000000
Reward0.36 ppm3	A				99.000000
Aquastrike 4.5 qts / A-Ft3	A				98.750000
Aquathol K and Reward1.8 ppm and 0.36 ppm5	A				98.750000
Glyphosate Reward MSO100 fl oz/A, 32 floz/A and 0.25% v/v3	A				98.750000
Aquastrike6.5 qts / A-ft3	A				98.750000
Glyphosate Reward MSO100 fl oz/A, 32 floz/A and 0.25% v/v7	A				98.750000
Glyphosate Reward MSO100 fl oz/A, 32 floz/A and 0.25% v/v5	A				98.500000
Aquastrike 4.5 qts / A-Ft5	A				98.250000
Aquastrike5.5 qts/ A-ft3	A				98.250000
Aquathol K and Reward1.8 ppm and 0.36 ppm1	A				98.250000
Aquastrike5.5 qts/ A-ft7	A				98.250000
Aquastrike 4.5 qts / A-Ft1	A				97.750000
Aquathol K and Reward1.2 ppm and 0.25 ppm5	A				97.750000
Reward0.36 ppm7	A				97.750000
Aquastrike5.5 qts/ A-ft1	A				97.500000
Reward0.25 ppm5	A				97.500000
Aquastrike 4.5 qts / A-Ft7	A				97.250000
Aquathol K and Reward1.8 ppm and 0.36 ppm7	A				97.250000
Aquathol K and Reward1.8 ppm and 0.36 ppm3	A				97.000000
Aquathol K and Reward1.2 ppm and 0.25 ppm1	A				97.000000
Reward0.25 ppm1	A				97.000000
Reward0.25 ppm3	A				97.000000
Reward0.25 ppm7	A				97.000000
Reward0.36 ppm1	A				97.000000
Aquastrike5.5 qts/ A-ft5	A				96.750000
Aquastrike6.5 qts / A-ft1	A				96.750000
Aquathol K and Reward1.2 ppm and 0.25 ppm3	A				96.750000
Aquastrike6.5 qts / A-ft5	A				96.500000
Aquastrike6.5 qts / A-ft7	A				96.250000
Aquathol K and Reward1.2 ppm and 0.25 ppm7	A				96.000000
Aquathol K1.8 ppm5		B			15.000000
Aquathol K1.2 ppm5		B	C		12.500000
Aquathol K1.2 ppm7		B	C		11.250000
Aquathol K1.2 ppm3		B	C	D	8.750000
Aquathol K1.8 ppm1		B	C	D	6.250000
Aquathol K1.8 ppm7		B	C	D	6.250000
Aquathol K1.2 ppm1			C	D	5.000000
Aquathol K1.8 ppm3			C	D	3.750000
Untreated Control00				D	0.000000

Levels not connected by same letter are significantly different
Tukey's HSD (honestly significant difference), is a single-step multiple comparison statistical test to find means that are significantly different from each other.

Figure 3.1. Connecting letters report after running oneway anova and all pairs Tukey-Kramer HSD from trial one 4 WAT evaluation from visual observers.

Connecting Letters Report			
Level			Mean
Aquathol K1.8 ppm1	A		164.1500
Untreated Control00	A		116.4700
Aquathol K1.8 ppm7	A		97.7425
Aquathol K1.2 ppm1	A	B	52.2400
Aquathol K1.2 ppm5	A	B	47.8575
Aquathol K1.2 ppm3	A	B	45.4150
Aquathol K1.8 ppm3	A	B	43.7750
Aquathol K1.2 ppm7	A	B	37.5850
Aquathol K1.8 ppm5	A	B	25.5300
Aquathol K and Reward1.8 ppm and 0.36 ppm5		B	-87.0275
Reward0.36 ppm7		B	-92.7625
Aquastrike 4.5 qts / A-Ft3		B	-94.1875
Aquathol K and Reward1.8 ppm and 0.36 ppm1		B	-94.1925
Aquastrike5.5 qts/ A-ft5		B	-94.2775
Aquathol K and Reward1.2 ppm and 0.25 ppm5		B	-94.4025
Aquathol K and Reward1.2 ppm and 0.25 ppm7		B	-94.8425
Aquathol K and Reward1.2 ppm and 0.25 ppm3		B	-94.8900
Reward0.25 ppm1		B	-95.3025
Aquathol K and Reward1.2 ppm and 0.25 ppm1		B	-95.7550
Reward0.36 ppm1		B	-95.8075
Glyphosate Reward MSO100 fl oz/A, 32 floz/A and 0.25% v/v3		B	-96.0775
Reward0.25 ppm7		B	-96.1625
Aquastrike 4.5 qts / A-Ft1		B	-96.5750
Glyphosate Reward MSO100 fl oz/A, 32 floz/A and 0.25% v/v7		B	-96.7825
Aquastrike 4.5 qts / A-Ft5		B	-97.3075
Aquastrike6.5 qts / A-ft5		B	-97.3500
Aquastrike5.5 qts/ A-ft1		B	-97.4200
Glyphosate Reward MSO100 fl oz/A, 32 floz/A and 0.25% v/v1		B	-97.5025
Aquastrike5.5 qts/ A-ft7		B	-97.5550
Aquastrike6.5 qts / A-ft3		B	-97.7975
Aquathol K and Reward1.8 ppm and 0.36 ppm3		B	-97.9150
Aquathol K and Reward1.8 ppm and 0.36 ppm7		B	-98.1100
Glyphosate Reward MSO100 fl oz/A, 32 floz/A and 0.25% v/v5		B	-98.1700
Reward0.36 ppm5		B	-98.2325
Reward0.25 ppm5		B	-98.4850
Aquastrike6.5 qts / A-ft7		B	-98.5225
Aquastrike 4.5 qts / A-Ft7		B	-98.9125
Aquastrike6.5 qts / A-ft1		B	-98.9800
Reward0.25 ppm3		B	-99.0600
Aquastrike5.5 qts/ A-ft3		B	-99.1050
Reward0.36 ppm3		B	-99.1750

Levels not connected by same letter are significantly different
Tukey's HSD (honestly significant difference), is a single-step multiple comparison statistical test to find means that are significantly different from each other.

Figure 3.2. Connecting letters report after running oneway anova and all pairs Tukey-Kramer HSD from trial 1 Canopeo ratings 2 WAT.

Connecting Letters Report

Level					Mean
Reward0.36 ppm5	A				99.250000
Glyphosate Reward MSO100 fl oz/A, 32 floz/A and 0.25% v/v1	A				99.000000
Reward0.36 ppm3	A				99.000000
Aquastrike 4.5 qts / A-Ft3	A				98.750000
Aquathol K and Reward1.8 ppm and 0.36 ppm5	A				98.750000
Glyphosate Reward MSO100 fl oz/A, 32 floz/A and 0.25% v/v3	A				98.750000
Aquastrike6.5 qts / A-ft3	A				98.750000
Glyphosate Reward MSO100 fl oz/A, 32 floz/A and 0.25% v/v7	A				98.750000
Glyphosate Reward MSO100 fl oz/A, 32 floz/A and 0.25% v/v5	A				98.500000
Aquastrike 4.5 qts / A-Ft5	A				98.250000
Aquastrike5.5 qts/ A-ft3	A				98.250000
Aquathol K and Reward1.8 ppm and 0.36 ppm1	A				98.250000
Aquastrike5.5 qts/ A-ft7	A				98.250000
Aquastrike 4.5 qts / A-Ft1	A				97.750000
Aquathol K and Reward1.2 ppm and 0.25 ppm5	A				97.750000
Reward0.36 ppm7	A				97.750000
Aquastrike5.5 qts/ A-ft1	A				97.500000
Reward0.25 ppm5	A				97.500000
Aquastrike 4.5 qts / A-Ft7	A				97.250000
Aquathol K and Reward1.8 ppm and 0.36 ppm7	A				97.250000
Aquathol K and Reward1.8 ppm and 0.36 ppm3	A				97.000000
Aquathol K and Reward1.2 ppm and 0.25 ppm1	A				97.000000
Reward0.25 ppm1	A				97.000000
Reward0.25 ppm3	A				97.000000
Reward0.25 ppm7	A				97.000000
Reward0.36 ppm1	A				97.000000
Aquastrike5.5 qts/ A-ft5	A				96.750000
Aquastrike6.5 qts / A-ft1	A				96.750000
Aquathol K and Reward1.2 ppm and 0.25 ppm3	A				96.750000
Aquastrike6.5 qts / A-ft5	A				96.500000
Aquastrike6.5 qts / A-ft7	A				96.250000
Aquathol K and Reward1.2 ppm and 0.25 ppm7	A				96.000000
Aquathol K1.8 ppm5		B			15.000000
Aquathol K1.2 ppm5		B	C		12.500000
Aquathol K1.2 ppm7		B	C		11.250000
Aquathol K1.2 ppm3		B	C	D	8.750000
Aquathol K1.8 ppm1		B	C	D	6.250000
Aquathol K1.8 ppm7		B	C	D	6.250000
Aquathol K1.2 ppm1			C	D	5.000000
Aquathol K1.8 ppm3			C	D	3.750000
Untreated Control00				D	0.000000

Levels not connected by same letter are significantly different
Tukey's HSD (honestly significant difference), is a single-step multiple comparison statistical test to find means that are significantly different from each other.

Figure 3.3. Connecting letters report after running oneway anova and all pairs Tukey-Kramer HSD from trial one 4 WAT evaluation from visual observers.

Ordered Differences Report

Level	- Level	Difference	Std Err Dif	Lower CL	Upper CL	p-Value
Fluridone 10 ppb	Glyphosate 96 LBAE/GAL 1% v/v	236.1360	43.60709	93.429	378.8426	<.0001*
Fluridone 10 ppb	Glyphosate 48 LBAE/GAL 1% v/v	225.9319	43.60709	83.225	368.6385	<.0001*
Fluridone 10 ppb	Reward 0.25 ppm	217.0084	43.60709	74.302	359.7150	0.0002*
Control 00	Glyphosate 96 LBAE/GAL 1% v/v	191.1527	43.60709	48.446	333.8593	0.0016*
Control 00	Glyphosate 48 LBAE/GAL 1% v/v	180.9486	43.60709	38.242	323.6552	0.0036*
Control 00	Reward 0.25 ppm	172.0251	43.60709	29.319	314.7317	0.0070*
Fluridone 5 ppb	Glyphosate 96 LBAE/GAL 1% v/v	171.3370	43.60709	28.630	314.0436	0.0073*
Fluridone 10 ppb	Reward 0.125 ppm	166.2189	43.60709	23.512	308.9255	0.0106*
Control 01	Glyphosate 96 LBAE/GAL 1% v/v	162.2414	43.60709	19.535	304.9481	0.0140*
Fluridone 5 ppb	Glyphosate 48 LBAE/GAL 1% v/v	161.1328	43.60709	18.426	303.8394	0.0151*
Penoxsulam 5 ppb	Glyphosate 96 LBAE/GAL 1% v/v	157.9977	43.60709	15.291	300.7043	0.0187*
Fluridone 5 ppb	Reward 0.25 ppm	152.2094	43.60709	9.503	294.9160	0.0274*
Control 01	Glyphosate 48 LBAE/GAL 1% v/v	152.0373	43.60709	9.331	294.7439	0.0277*
Penoxsulam 5 ppb	Glyphosate 48 LBAE/GAL 1% v/v	147.7936	43.60709	5.087	290.5002	0.0364*
Control 01	Reward 0.25 ppm	143.1139	43.60709	0.407	285.8205	0.0488*
Penoxsulam 5 ppb	Reward 0.25 ppm	138.8702	43.60709	-3.836	281.5768	0.0630
Fluridone 10 ppb	Penoxsulam 10 ppb	138.0477	43.60709	-4.659	280.7543	0.0661
Control 00	Reward 0.125 ppm	121.2356	43.60709	-21.471	263.9422	0.1645
Fluridone 5 ppb	Reward 0.125 ppm	101.4198	43.60709	-41.287	244.1265	0.3867
Penoxsulam 10 ppb	Glyphosate 96 LBAE/GAL 1% v/v	98.0883	43.60709	-44.618	240.7949	0.4348
Control 00	Penoxsulam 10 ppb	93.0644	43.60709	-49.642	235.7710	0.5109
Control 01	Reward 0.125 ppm	92.3243	43.60709	-50.382	235.0309	0.5224
Penoxsulam 5 ppb	Reward 0.125 ppm	88.0806	43.60709	-54.626	230.7872	0.5885
Penoxsulam 10 ppb	Glyphosate 48 LBAE/GAL 1% v/v	87.8842	43.60709	-54.822	230.5908	0.5916
Penoxsulam 10 ppb	Reward 0.25 ppm	78.9607	43.60709	-63.746	221.6674	0.7262
Fluridone 10 ppb	Penoxsulam 5 ppb	78.1383	43.60709	-64.568	220.8449	0.7378
Fluridone 10 ppb	Control 01	73.8946	43.60709	-68.812	216.6012	0.7945
Fluridone 5 ppb	Penoxsulam 10 ppb	73.2487	43.60709	-69.458	215.9553	0.8026
Reward 0.125 ppm	Glyphosate 96 LBAE/GAL 1% v/v	69.9171	43.60709	-72.789	212.6237	0.8418
Fluridone 10 ppb	Fluridone 5 ppb	64.7990	43.60709	-77.908	207.5056	0.8930
Control 01	Penoxsulam 10 ppb	64.1531	43.60709	-78.553	206.8597	0.8986
Penoxsulam 5 ppb	Penoxsulam 10 ppb	59.9094	43.60709	-82.797	202.6160	0.9309
Reward 0.125 ppm	Glyphosate 48 LBAE/GAL 1% v/v	59.7130	43.60709	-82.994	202.4196	0.9322
Reward 0.125 ppm	Reward 0.25 ppm	50.7895	43.60709	-91.917	193.4962	0.9752
Fluridone 10 ppb	Control 00	44.9833	43.60709	-97.723	187.6899	0.9892
Control 00	Penoxsulam 5 ppb	33.1550	43.60709	-109.552	175.8616	0.9989
Control 00	Control 01	28.9113	43.60709	-113.795	171.6179	0.9996
Penoxsulam 10 ppb	Reward 0.125 ppm	28.1712	43.60709	-114.535	170.8778	0.9997
Control 00	Fluridone 5 ppb	19.8157	43.60709	-122.891	162.5223	1.0000
Reward 0.25 ppm	Glyphosate 96 LBAE/GAL 1% v/v	19.1276	43.60709	-123.579	161.8342	1.0000
Fluridone 5 ppb	Penoxsulam 5 ppb	13.3392	43.60709	-129.367	156.0459	1.0000
Glyphosate 48 LBAE/GAL 1% v/v	Glyphosate 96 LBAE/GAL 1% v/v	10.2041	43.60709	-132.502	152.9108	1.0000
Fluridone 5 ppb	Control 01	9.0955	43.60709	-133.611	151.8021	1.0000
Reward 0.25 ppm	Glyphosate 48 LBAE/GAL 1% v/v	8.9234	43.60709	-133.783	151.6300	1.0000
Control 01	Penoxsulam 5 ppb	4.2437	43.60709	-138.463	146.9503	1.0000

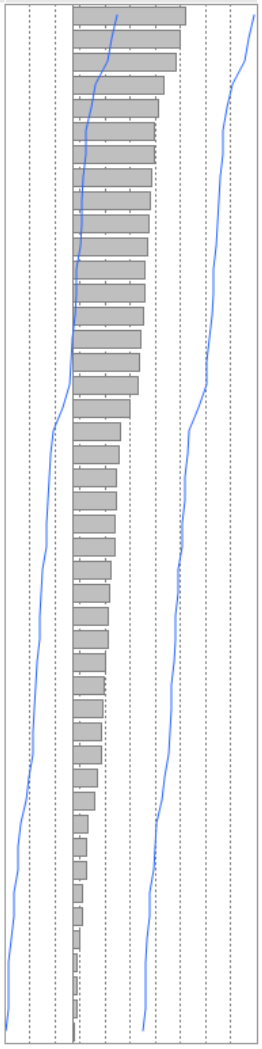

Figure 3.4. Trial 2 oneway analysis of percent change 2 weeks after treatment ordered difference report.

Ordered Differences Report

Level	- Level	Difference	Std Err Dif	Lower CL	Upper CL	p-Value
Fluridone 10 ppb	Glyphosate 96 LBAE/GAL 1% v/v	293.9255	47.95120	137.003	450.8485	<.0001*
Fluridone 10 ppb	Glyphosate 48 LBAE/GAL 1% v/v	289.1046	47.95120	132.182	446.0276	<.0001*
Fluridone 10 ppb	Reward 0.25 ppm	265.6894	47.95120	108.766	422.6123	<.0001*
Control 00	Glyphosate 96 LBAE/GAL 1% v/v	221.2351	47.95120	64.312	378.1581	0.0007*
Control 00	Glyphosate 48 LBAE/GAL 1% v/v	216.4142	47.95120	59.491	373.3372	0.0010*
Fluridone 10 ppb	Reward 0.125 ppm	202.0965	47.95120	45.174	359.0194	0.0029*
Control 01	Glyphosate 96 LBAE/GAL 1% v/v	196.5174	47.95120	39.594	353.4403	0.0042*
Control 00	Reward 0.25 ppm	192.9990	47.95120	36.076	349.9219	0.0054*
Fluridone 5 ppb	Glyphosate 96 LBAE/GAL 1% v/v	192.1926	47.95120	35.270	349.1156	0.0057*
Control 01	Glyphosate 48 LBAE/GAL 1% v/v	191.6965	47.95120	34.774	348.6194	0.0059*
Fluridone 5 ppb	Glyphosate 48 LBAE/GAL 1% v/v	187.3717	47.95120	30.449	344.2947	0.0078*
Fluridone 10 ppb	Penoxsulam 10 ppb	182.9555	47.95120	26.032	339.8784	0.0104*
Penoxsulam 5 ppb	Glyphosate 96 LBAE/GAL 1% v/v	177.8651	47.95120	20.942	334.7881	0.0144*
Penoxsulam 5 ppb	Glyphosate 48 LBAE/GAL 1% v/v	173.0442	47.95120	16.121	329.9672	0.0195*
Control 01	Reward 0.25 ppm	168.2812	47.95120	11.358	325.2042	0.0260*
Fluridone 5 ppb	Reward 0.25 ppm	163.9564	47.95120	7.033	320.8794	0.0335*
Penoxsulam 5 ppb	Reward 0.25 ppm	149.6290	47.95120	-7.294	306.5519	0.0741
Control 00	Reward 0.125 ppm	129.4061	47.95120	-27.517	286.3290	0.1954
Fluridone 10 ppb	Penoxsulam 5 ppb	116.0604	47.95120	-40.863	272.9834	0.3308
Penoxsulam 10 ppb	Glyphosate 96 LBAE/GAL 1% v/v	110.9701	47.95120	-45.953	267.8930	0.3938
Control 00	Penoxsulam 10 ppb	110.2650	47.95120	-46.658	267.1880	0.4030
Penoxsulam 10 ppb	Glyphosate 48 LBAE/GAL 1% v/v	106.1492	47.95120	-50.774	263.0721	0.4580
Control 01	Reward 0.125 ppm	104.6883	47.95120	-52.235	261.6113	0.4781
Fluridone 10 ppb	Fluridone 5 ppb	101.7329	47.95120	-55.190	258.6559	0.5194
Fluridone 5 ppb	Reward 0.125 ppm	100.3636	47.95120	-56.559	257.2865	0.5388
Fluridone 10 ppb	Control 01	97.4082	47.95120	-59.515	254.3311	0.5807
Reward 0.125 ppm	Glyphosate 96 LBAE/GAL 1% v/v	91.8291	47.95120	-65.094	248.7520	0.6591
Reward 0.125 ppm	Glyphosate 48 LBAE/GAL 1% v/v	87.0082	47.95120	-69.915	243.9311	0.7238
Penoxsulam 5 ppb	Reward 0.125 ppm	86.0361	47.95120	-70.887	242.9590	0.7363
Control 01	Penoxsulam 10 ppb	85.5473	47.95120	-71.376	242.4702	0.7426
Penoxsulam 10 ppb	Reward 0.25 ppm	82.7339	47.95120	-74.189	239.6569	0.7772
Fluridone 5 ppb	Penoxsulam 10 ppb	81.2225	47.95120	-75.700	238.1455	0.7949
Fluridone 10 ppb	Control 00	72.6904	47.95120	-84.233	229.6134	0.8810
Penoxsulam 5 ppb	Penoxsulam 10 ppb	66.8950	47.95120	-90.028	223.8180	0.9246
Reward 0.125 ppm	Reward 0.25 ppm	63.5929	47.95120	-93.330	220.5158	0.9439
Control 00	Penoxsulam 5 ppb	43.3700	47.95120	-113.553	200.2930	0.9958
Control 00	Fluridone 5 ppb	29.0425	47.95120	-127.880	185.9655	0.9998
Reward 0.25 ppm	Glyphosate 96 LBAE/GAL 1% v/v	28.2362	47.95120	-128.687	185.1591	0.9999
Control 00	Control 01	24.7178	47.95120	-132.205	181.6407	1.0000
Reward 0.25 ppm	Glyphosate 48 LBAE/GAL 1% v/v	23.4153	47.95120	-133.508	180.3382	1.0000
Penoxsulam 10 ppb	Reward 0.125 ppm	19.1410	47.95120	-137.782	176.0640	1.0000
Control 01	Penoxsulam 5 ppb	18.6522	47.95120	-138.271	175.5752	1.0000
Fluridone 5 ppb	Penoxsulam 5 ppb	14.3275	47.95120	-142.595	171.2504	1.0000
Glyphosate 48 LBAE/GAL 1% v/v	Glyphosate 96 LBAE/GAL 1% v/v	4.8209	47.95120	-152.102	161.7439	1.0000
Control 01	Fluridone 5 ppb	4.3248	47.95120	-152.598	161.2477	1.0000

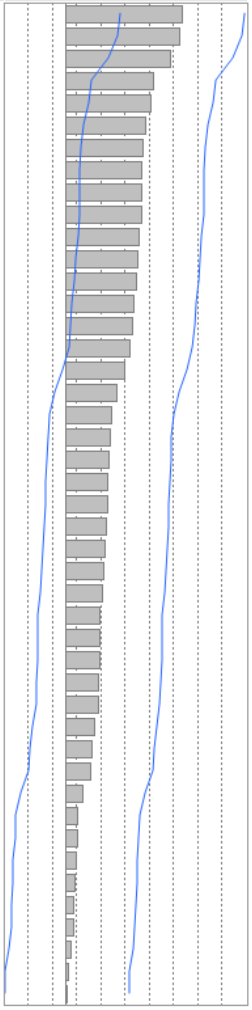

Figure 3.5. Trial 2 oneway analysis of percent change 3 weeks after treatment ordered difference report.

Ordered Differences Report

Level	- Level	Difference	Std Err Dif	Lower CL	Upper CL	p-Value
Fluridone 10 ppb	Glyphosate 48 LBAE/GAL 1% v/v	329.1236	45.75401	179.391	478.8561	<.0001*
Fluridone 10 ppb	Glyphosate 96 LBAE/GAL 1% v/v	326.2999	45.75401	176.567	476.0324	<.0001*
Fluridone 10 ppb	Reward 0.25 ppm	294.5965	45.75401	144.864	444.3291	<.0001*
Control 00	Glyphosate 48 LBAE/GAL 1% v/v	244.5933	45.75401	94.861	394.3259	<.0001*
Control 00	Glyphosate 96 LBAE/GAL 1% v/v	241.7697	45.75401	92.037	391.5022	<.0001*
Control 01	Glyphosate 48 LBAE/GAL 1% v/v	231.6749	45.75401	81.942	381.4074	0.0001*
Control 01	Glyphosate 96 LBAE/GAL 1% v/v	228.8512	45.75401	79.119	378.5837	0.0002*
Fluridone 10 ppb	Reward 0.125 ppm	226.8256	45.75401	77.093	376.5581	0.0002*
Fluridone 10 ppb	Penoxsulam 10 ppb	218.6231	45.75401	68.891	368.3556	0.0004*
Fluridone 5 ppb	Glyphosate 48 LBAE/GAL 1% v/v	218.0370	45.75401	68.304	367.7695	0.0004*
Fluridone 5 ppb	Glyphosate 96 LBAE/GAL 1% v/v	215.2133	45.75401	65.481	364.9459	0.0005*
Control 00	Reward 0.25 ppm	210.0663	45.75401	60.334	359.7989	0.0008*
Control 01	Reward 0.25 ppm	197.1478	45.75401	47.415	346.8804	0.0021*
Fluridone 5 ppb	Reward 0.25 ppm	183.5100	45.75401	33.777	333.2425	0.0056*
Penoxsulam 5 ppb	Glyphosate 48 LBAE/GAL 1% v/v	177.1321	45.75401	27.400	326.8646	0.0088*
Penoxsulam 5 ppb	Glyphosate 96 LBAE/GAL 1% v/v	174.3085	45.75401	24.576	324.0410	0.0106*
Fluridone 10 ppb	Penoxsulam 5 ppb	151.9915	45.75401	2.259	301.7240	0.0438*
Penoxsulam 5 ppb	Reward 0.25 ppm	142.6051	45.75401	-7.127	292.3376	0.0748
Control 00	Reward 0.125 ppm	142.2954	45.75401	-7.437	292.0279	0.0761
Control 00	Penoxsulam 10 ppb	134.0929	45.75401	-15.640	283.8254	0.1174
Control 01	Reward 0.125 ppm	129.3769	45.75401	-20.356	279.1094	0.1483
Control 01	Penoxsulam 10 ppb	121.1744	45.75401	-28.558	270.9069	0.2165
Fluridone 5 ppb	Reward 0.125 ppm	115.7390	45.75401	-33.993	265.4715	0.2722
Fluridone 10 ppb	Fluridone 5 ppb	111.0866	45.75401	-38.646	260.8191	0.3266
Penoxsulam 10 ppb	Glyphosate 48 LBAE/GAL 1% v/v	110.5005	45.75401	-39.232	260.2330	0.3338
Penoxsulam 10 ppb	Glyphosate 96 LBAE/GAL 1% v/v	107.6768	45.75401	-42.056	257.4093	0.3700
Fluridone 5 ppb	Penoxsulam 10 ppb	107.5365	45.75401	-42.196	257.2690	0.3718
Reward 0.125 ppm	Glyphosate 48 LBAE/GAL 1% v/v	102.2979	45.75401	-47.435	252.0305	0.4436
Reward 0.125 ppm	Glyphosate 96 LBAE/GAL 1% v/v	99.4743	45.75401	-50.258	249.2068	0.4842
Fluridone 10 ppb	Control 01	97.4487	45.75401	-52.284	247.1812	0.5139
Fluridone 10 ppb	Control 00	84.5302	45.75401	-65.202	234.2627	0.7030
Penoxsulam 10 ppb	Reward 0.25 ppm	75.9734	45.75401	-73.759	225.7060	0.8129
Penoxsulam 5 ppb	Reward 0.125 ppm	74.8342	45.75401	-74.898	224.5667	0.8258
Reward 0.125 ppm	Reward 0.25 ppm	67.7709	45.75401	-81.962	217.5034	0.8948
Control 00	Penoxsulam 5 ppb	67.4613	45.75401	-82.271	217.1938	0.8974
Penoxsulam 5 ppb	Penoxsulam 10 ppb	66.6316	45.75401	-83.101	216.3642	0.9041
Control 01	Penoxsulam 5 ppb	54.5428	45.75401	-95.190	204.2753	0.9711
Fluridone 5 ppb	Penoxsulam 5 ppb	40.9049	45.75401	-108.828	190.6374	0.9962
Reward 0.25 ppm	Glyphosate 48 LBAE/GAL 1% v/v	34.5270	45.75401	-115.206	184.2595	0.9990
Reward 0.25 ppm	Glyphosate 96 LBAE/GAL 1% v/v	31.7034	45.75401	-118.029	181.4359	0.9995
Control 00	Fluridone 5 ppb	26.5564	45.75401	-123.176	176.2889	0.9999
Control 01	Fluridone 5 ppb	13.6379	45.75401	-136.095	163.3704	1.0000
Control 00	Control 01	12.9185	45.75401	-136.814	162.6510	1.0000
Penoxsulam 10 ppb	Reward 0.125 ppm	8.2025	45.75401	-141.530	157.9350	1.0000
Glyphosate 96 LBAE/GAL 1% v/v	Glyphosate 48 LBAE/GAL 1% v/v	2.8236	45.75401	-146.909	152.5561	1.0000

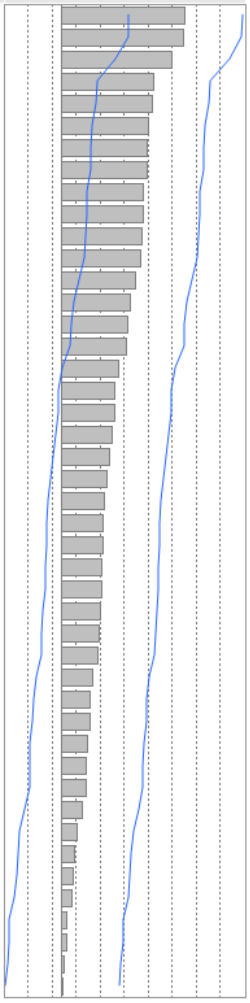

Figure 3.6. Trial 2 oneway analysis of percent change 4 weeks after treatment ordered difference report.

Ordered Differences Report

Level	- Level	Difference	Std Err Dif	Lower CL	Upper CL	p-Value
Control 00	Reward 0.25 ppm	0.1402500	0.0243069	0.060704	0.2197958	<.0001*
Control 00	Glyphosate 48 LBAE/GAL 1% v/v	0.1368750	0.0243069	0.057329	0.2164208	<.0001*
Fluridone 5 ppb	Reward 0.25 ppm	0.1367500	0.0243069	0.057204	0.2162958	<.0001*
Fluridone 5 ppb	Glyphosate 48 LBAE/GAL 1% v/v	0.1333750	0.0243069	0.053829	0.2129208	<.0001*
Control 01	Reward 0.25 ppm	0.1305000	0.0243069	0.050954	0.2100458	<.0001*
Control 00	Glyphosate 96 LBAE/GAL 1% v/v	0.1297500	0.0243069	0.050204	0.2092958	<.0001*
Control 01	Glyphosate 48 LBAE/GAL 1% v/v	0.1271250	0.0243069	0.047579	0.2066708	<.0001*
Fluridone 5 ppb	Glyphosate 96 LBAE/GAL 1% v/v	0.1262500	0.0243069	0.046704	0.2057958	<.0001*
Control 01	Glyphosate 96 LBAE/GAL 1% v/v	0.1200000	0.0243069	0.040454	0.1995458	0.0002*
Control 00	Reward 0.125 ppm	0.1023750	0.0243069	0.022829	0.1819208	0.0029*
Penoxsulam 5 ppb	Reward 0.25 ppm	0.0992500	0.0243069	0.019704	0.1787958	0.0045*
Fluridone 5 ppb	Reward 0.125 ppm	0.0988750	0.0243069	0.019329	0.1784208	0.0047*
Penoxsulam 10 ppb	Reward 0.25 ppm	0.0973750	0.0243069	0.017829	0.1769208	0.0057*
Penoxsulam 5 ppb	Glyphosate 48 LBAE/GAL 1% v/v	0.0958750	0.0243069	0.016329	0.1754208	0.0070*
Penoxsulam 10 ppb	Glyphosate 48 LBAE/GAL 1% v/v	0.0940000	0.0243069	0.014454	0.1735458	0.0089*
Control 01	Reward 0.125 ppm	0.0926250	0.0243069	0.013079	0.1721708	0.0106*
Penoxsulam 5 ppb	Glyphosate 96 LBAE/GAL 1% v/v	0.0887500	0.0243069	0.009204	0.1682958	0.0172*
Penoxsulam 10 ppb	Glyphosate 96 LBAE/GAL 1% v/v	0.0868750	0.0243069	0.007329	0.1664208	0.0216*
Fluridone 10 ppb	Reward 0.25 ppm	0.0821250	0.0243069	0.002579	0.1616708	0.0375*
Fluridone 10 ppb	Glyphosate 48 LBAE/GAL 1% v/v	0.0787500	0.0243069	-0.000796	0.1582958	0.0545
Fluridone 10 ppb	Glyphosate 96 LBAE/GAL 1% v/v	0.0716250	0.0243069	-0.007921	0.1511708	0.1131
Penoxsulam 5 ppb	Reward 0.125 ppm	0.0613750	0.0243069	-0.018171	0.1409208	0.2746
Penoxsulam 10 ppb	Reward 0.125 ppm	0.0595000	0.0243069	-0.020046	0.1390458	0.3155
Control 00	Fluridone 10 ppb	0.0581250	0.0243069	-0.021421	0.1376708	0.3475
Fluridone 5 ppb	Fluridone 10 ppb	0.0546250	0.0243069	-0.024921	0.1341708	0.4361
Control 01	Fluridone 10 ppb	0.0483750	0.0243069	-0.031171	0.1279208	0.6087
Fluridone 10 ppb	Reward 0.125 ppm	0.0442500	0.0243069	-0.035296	0.1237958	0.7201
Control 00	Penoxsulam 10 ppb	0.0428750	0.0243069	-0.036671	0.1224208	0.7547
Control 00	Penoxsulam 5 ppb	0.0410000	0.0243069	-0.038546	0.1205458	0.7988
Fluridone 5 ppb	Penoxsulam 10 ppb	0.0393750	0.0243069	-0.040171	0.1189208	0.8337
Reward 0.125 ppm	Reward 0.25 ppm	0.0378750	0.0243069	-0.041671	0.1174208	0.8629
Fluridone 5 ppb	Penoxsulam 5 ppb	0.0375000	0.0243069	-0.042046	0.1170458	0.8697
Reward 0.125 ppm	Glyphosate 48 LBAE/GAL 1% v/v	0.0345000	0.0243069	-0.045046	0.1140458	0.9168
Control 01	Penoxsulam 10 ppb	0.0331250	0.0243069	-0.046421	0.1126708	0.9341
Control 01	Penoxsulam 5 ppb	0.0312500	0.0243069	-0.048296	0.1107958	0.9535
Reward 0.125 ppm	Glyphosate 96 LBAE/GAL 1% v/v	0.0273750	0.0243069	-0.052171	0.1069208	0.9802
Penoxsulam 5 ppb	Fluridone 10 ppb	0.0171250	0.0243069	-0.062421	0.0966708	0.9994
Penoxsulam 10 ppb	Fluridone 10 ppb	0.0152500	0.0243069	-0.064296	0.0947958	0.9998
Glyphosate 96 LBAE/GAL 1% v/v	Reward 0.25 ppm	0.0105000	0.0243069	-0.069046	0.0900458	1.0000
Control 00	Control 01	0.0097500	0.0243069	-0.069796	0.0892958	1.0000
Glyphosate 96 LBAE/GAL 1% v/v	Glyphosate 48 LBAE/GAL 1% v/v	0.0071250	0.0243069	-0.072421	0.0866708	1.0000
Fluridone 5 ppb	Control 01	0.0062500	0.0243069	-0.073296	0.0857958	1.0000
Control 00	Fluridone 5 ppb	0.0035000	0.0243069	-0.076046	0.0830458	1.0000
Glyphosate 48 LBAE/GAL 1% v/v	Reward 0.25 ppm	0.0033750	0.0243069	-0.076171	0.0829208	1.0000
Penoxsulam 5 ppb	Penoxsulam 10 ppb	0.0018750	0.0243069	-0.077671	0.0814208	1.0000

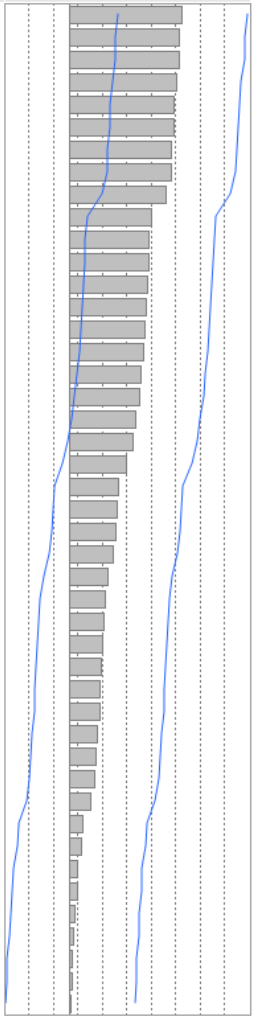

Figure 3.7. Trial 2 oneway analysis of dry biomass in grams by herbicide ordered difference report.

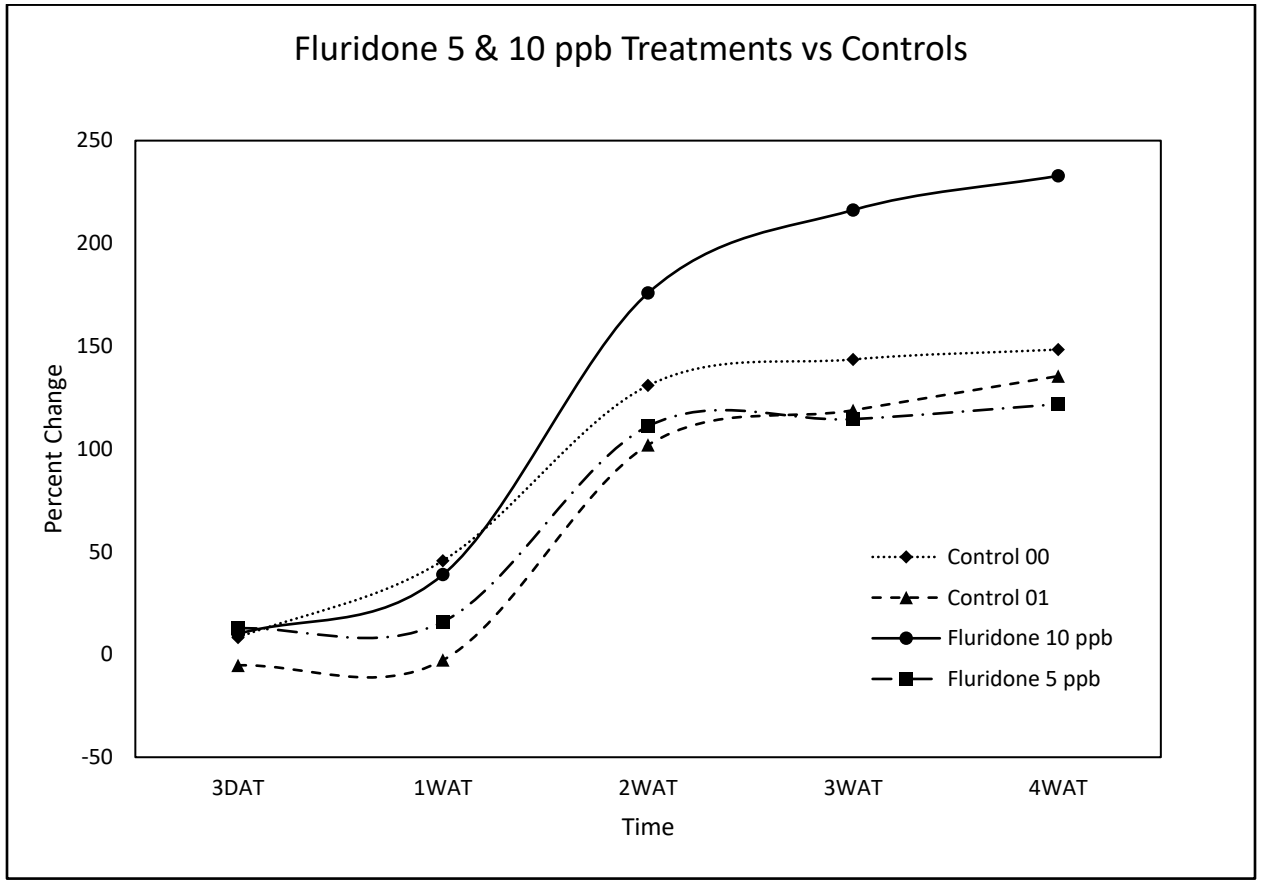

Figure 3.8. Trial 2 percent change ratings fluridone treatments vs controls

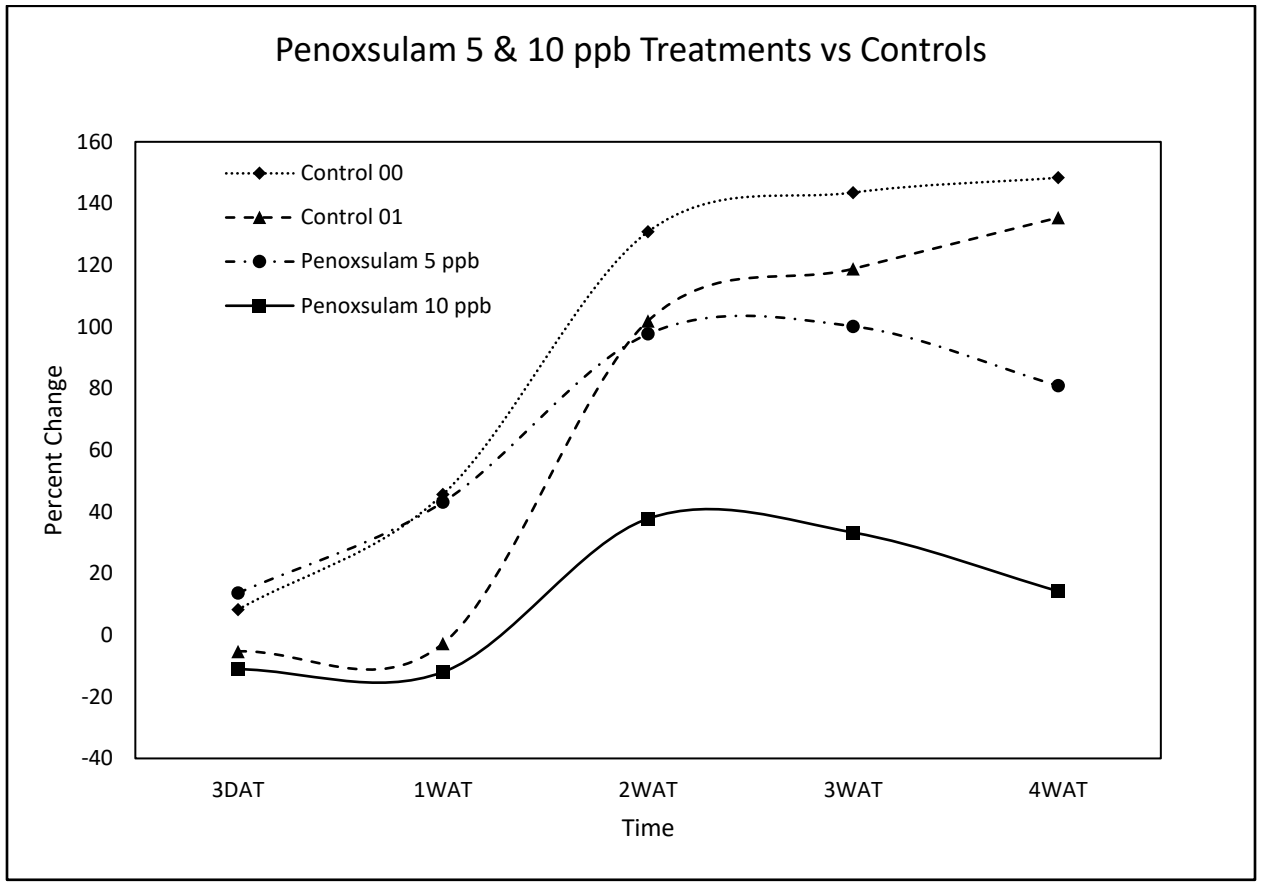

Figure 3.9. Trial 2 percent change ratings penoxsulam treatments vs controls

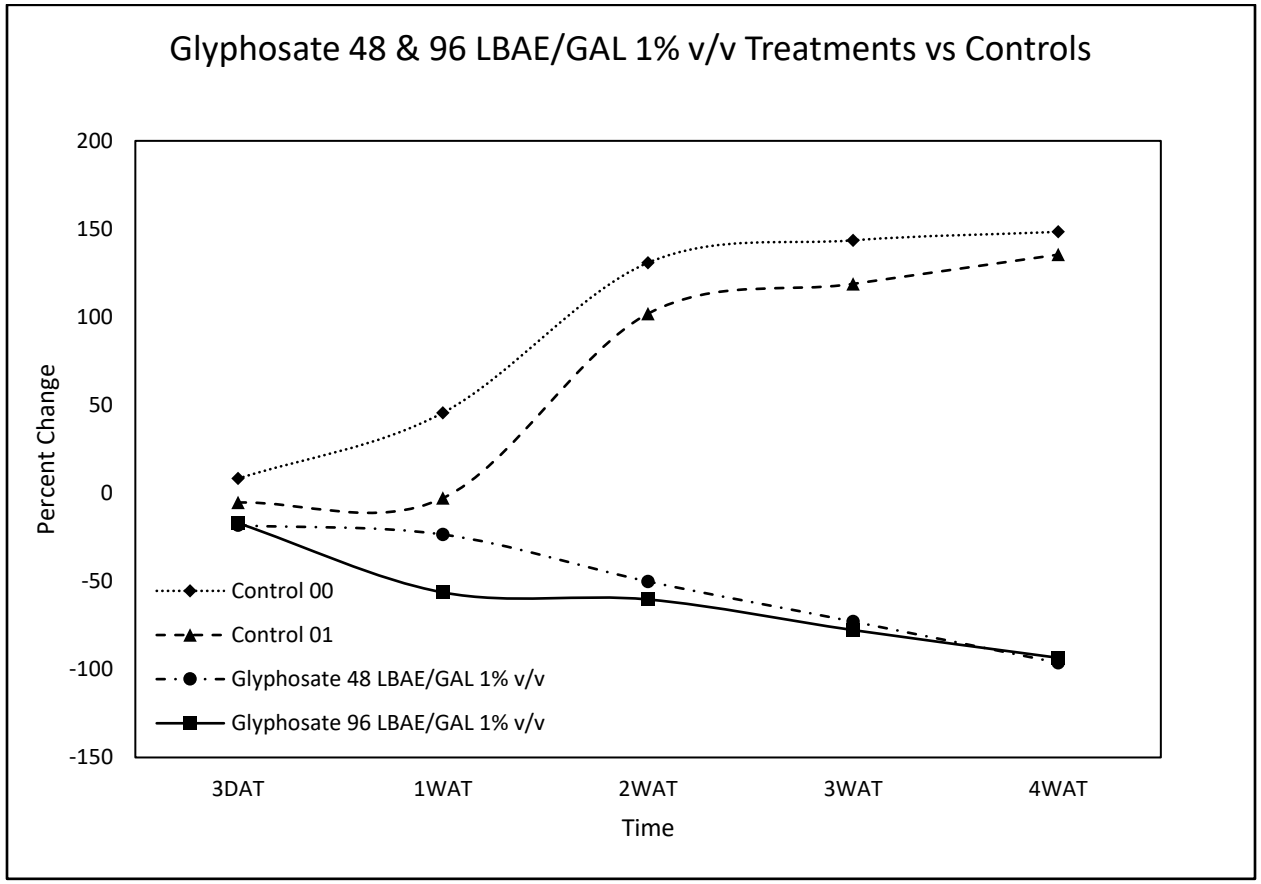

Figure 3.10. Trial 2 percent change ratings glyphosate treatments vs controls

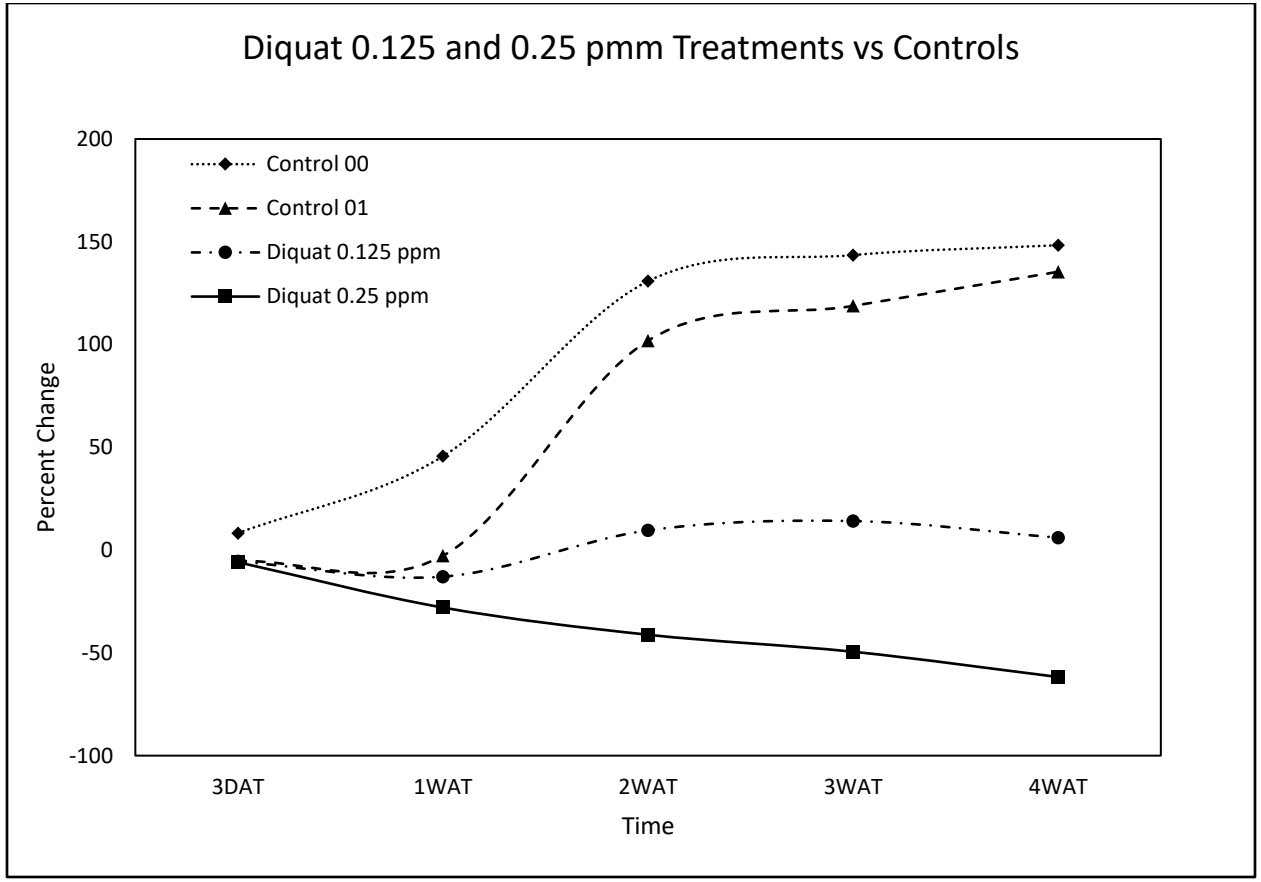

Figure 3.11. Trial 2 percent change ratings diquat treatments vs controls

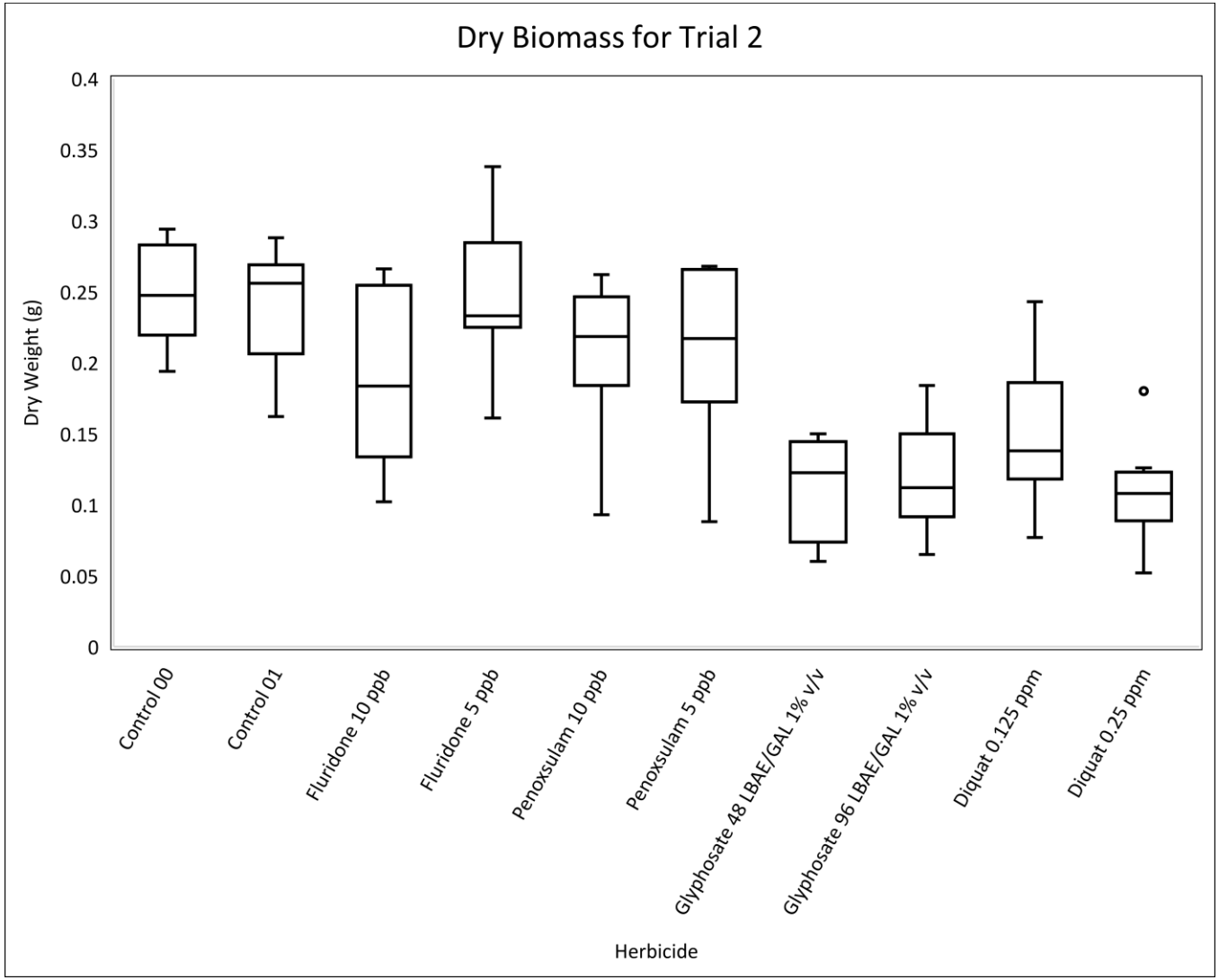

Figure 3.12. Dry biomass in grams Trial 2

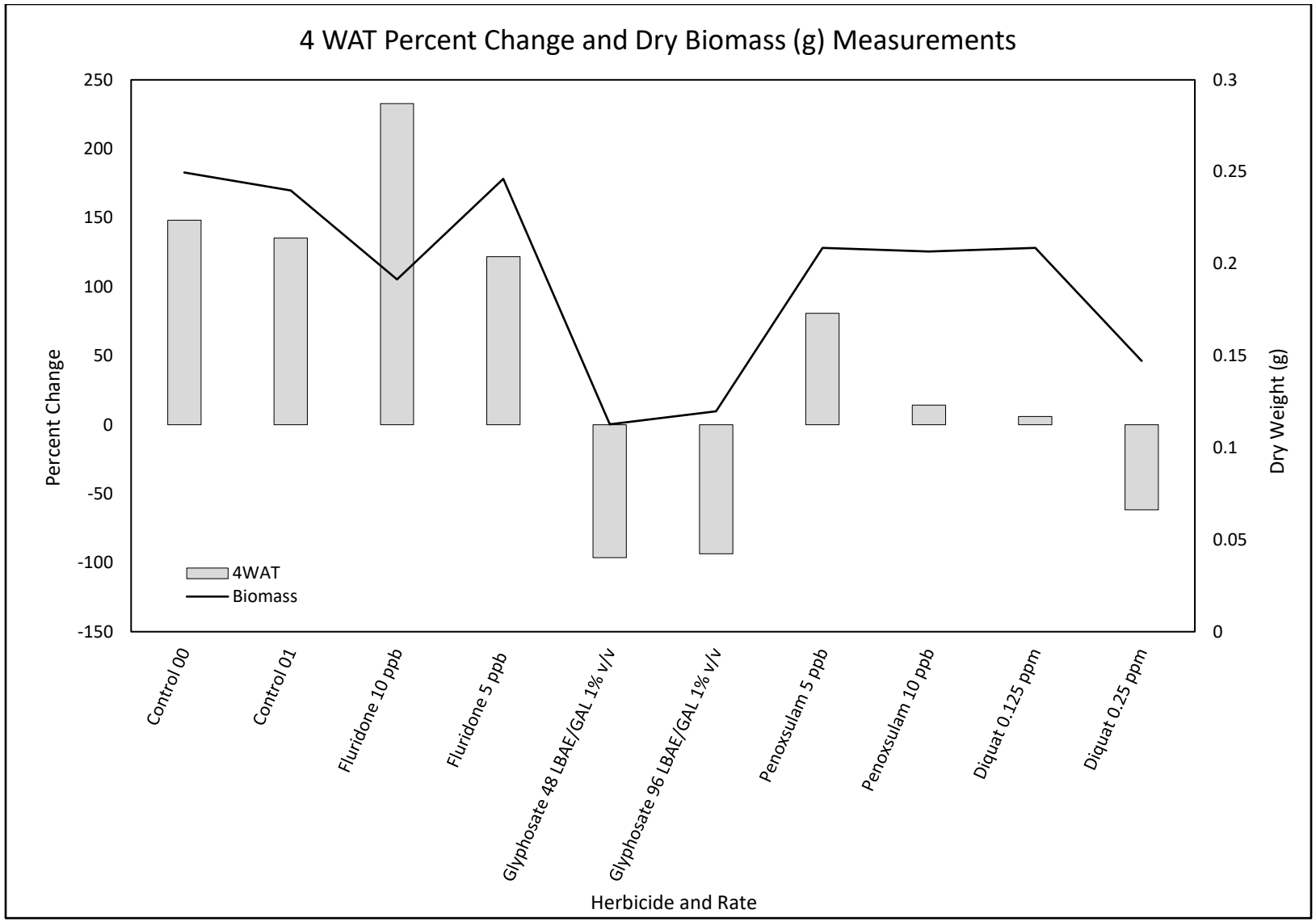

Figure 3.13. Combination graph of dry biomass and 4 WAT evaluations

CHAPTER 4

Utilization of cloud computing to create a convolutional neural network to detect *Pontederia crassipes* (Mart.) Solms, previously known as *Eichhornia crassipes,* and *Salvinia molesta* D.S. Mitchell.

Abstract

Since 2005, computers have undergone continuous improvements in graphics card processing ability providing opportunity for enhanced computer-generated models. Advanced computers and open-sourced technology provide the ability for rapid development of new technologies. Object detection is one such technology. This study used convolutional neural networks and imagery obtained with a Go Pro Hero 5 and Go Pro Hero 6 to detect two invasive aquatic macrophytes. The convolutional neural network was designed to focus on using image classification with the Keras API to identify *Salvinia molesta* D.S. Mitchell and *Pontederia crassipes* (Mart.) Solms. These models were custom built and run using Google Colaboratory. The model yielded results with a validation loss of 0.093 and accuracy of 1.00. The training loss was 0.1312 and maintained an accuracy of 0.98. These models were successful in correctly identifying these two target species in an aquatic environment using open-sourced technology. The ability of producing a usable and functional CNN with open-sourced technology provides researchers the ability to reduce the cost of building a local machine capable of machine learning. The offset of cost does have a reduction of functionality, with Google Collaboratory limiting their server's resources to assure other customers availability of resources. The model's results revealed a *Salvinia molesta* D.S. Mitchell's precision as 0.6470. The recall was 0.9167 for *Salvinia molesta* D.S. Mitchell. The model achieved a precision score of 0.8000 and recall of

0.3333 for *Pontederia crassipes* (Mart.) Solms. The *m*AP obtained for both *Pontederia* crassipes (Mart.) Solms and *Salvinia molesta* D.S. Mitchell was 0.7994. This model was successful in classifications of *Salvinia molesta* D.S. Mitchell, however while *Pontederia crassipes* (Mart.) Solms did have success, it is still in need of improvement to increase the precision and recall. The model's precision and recall for both classifications should be around 0.8500 for both classifications of *Salvinia molesta* D.S. Mitchell and *Pontederia crassipes* (Mart.) Solms.

Introduction

Artificial intelligence research gained popularity in the early 1990's, and implementation has been increasing since Modified National Institute of Standards and Technology (MNIST) databases of handwritten digits comprised of 60,000 training and 10,000 test examples were released (Simard et al., 2003). In 2003, the inclusion of elastic distortions and increased training set size allowed for the highest performance of an error rate of 0.4% was achieved at that time (Simard et al., 2003). Since then, more complex models and upscaled computational resources allowed larger datasets in quantity and file size to be processed (Abadi et al., 2016). Larger datasets may now be processed within TensorFlow with larger clusters registering step times in as little as two seconds (Abadi et al., 2016). TensorFlow is an opensource software obtaining its name from tensors, which are arrays of arbitrary dimensions. TensorFlow is flexible and capable of learning the data randomly selected for the computer to learn from, known as training data. This training over the data can occur over several hours or days depending on dataset and model size (Abadi et al., 2016). Graphical processing units can handle these data but are limited by available memory on the graphical processing unit (Meng et al., 2017). Limitations of local computers graphical processing units are overcome by cloud computing. Google Colaboratory,

hereafter known as Colab, is based upon Jupyter Notebooks (Bisong, 2019). Colab is a runtime fully configured for deep learning with almost 360 GB of GPUs (Meng et al., 2017). This platform provides access to a machine capable of large dataset processing at no cost. Colab notebooks are already preinstalled with the TensorFlow framework for prototyping machine learning models (Bisong, 2019). Results from Carneiro et al. (2018) did test servers against Google Colab and found Colab hardware resources can reach similar performance to dedicated hardware. This platform provides a free powerful hardware options such as GPU and TPUs for free (Bisong, 2019).

Artificial intelligence is rapidly evolving and embedding itself within several industries. The integration of artificial intelligence can be incredibly beneficial, particularly for industries such as the aquatic plant management industries. Implementation of artificial intelligence, specifically machine learning, may increase the efficiency of early detection and rapid response programs for the control of invasive species. Traditionally, the problem of scouting, surveying, and remote sensing, which are components of early detection for invasive species, is how time consuming they can be not only during data collection but also during data processing. The integration of machine-learning technology was hypothesized to be able to adequately detect possible aquatic nuisance species, and this research was designed to investigate this potential use.

Salvinia molesta D.S. Mitchell (giant salvinia) is one of the world's worst aquatic weeds (Holm et al., 1977). Giant salvinia is native to Brazil, South America. Because the rapid growth rate, this floating aquatic fern poses serious threats once introduced to a waterbody. The first case of giant salvinia was documented in 1995 in South Carolina, USA (Johnson, 1995) and since has spread throughout most of the southeastern United States. Slowing the growth of giant

salvinia is daunting especially with giant salvinia buds surviving under the water surface. However, giant salvinia cannot tolerate temperatures less than 3 degrees Celsius (Whiteman & Room, 1991). Giant salvinia's fast growth rate and ability to double size in as little as 6 days (Gaudet 1973; Mitchell & Tur, 1975) and preference for slow moving water bodies such as lakes are currently altering management plans in the upper Lake Marion in South Carolina, USA and recommendations have been made with treatments with endothall (Mudge & Netherland, 2020). Early detection and adequate timing of treatments is advantageous as demonstrated in Mudge et al. (2016).

Pontederia crassipes (Mart.) Solms previously known as *Eichhornia crassipes* (water hyacinth) is another free-floating aquatic macrophyte that has invaded over fifty countries and has the potential to expand its infestation as climate continually changes (Hellmann et al., 2008; Rahel & Olden, 2008; Rodriguez-Gallego, 2004). Water hyacinth's invasion is not bound by areas with already established aquatic vegetative ecosystems or areas lacking aquatic vegetative growth (Mitchell, 1985). This weed is difficult to control because it rapidly reproduces and forms dense interwoven roots and thick mats (Mitchell, 1985). The rapid expansion and growth may be controlled with biological agents in specific locations (Jayanth, 1988), however biological control is not always successful and other techniques are often necessary.

The optimum control method is dependent on site-specific conditions, and no singular method is suitable for each situation (Seagrave, 1988). Due to the rapid growth and spread of water hyacinth, effective management is difficult once populations are established. Biomass studies in nutrient enriched waters in central Florida, USA revealed water hyacinth growing in ten out of twelve months of the year, and during the months of August and September, water hyacinths growth rate's doubling time was around 11.6 days (Reddy & DeBusk, 1984). Rapid

growth and dense mat production with water hyacinth require early detection and rapid response (EDRR) for proper management. If not properly managed, water hyacinth has shown to cause significant impacts on ecosystems including loss of water through evapotranspiration, increased viable habitat for mosquito populations, and decreasing phytoplankton production and dissolved oxygen concentrations (Hunt & Christiansen, 2000; Mangas-Ramirez & Elias Gutierrez, 2004; Meerhoff et al., 2003; Perna & Burrows, 2005; Rommens et al., 2003; Troutman et al., 2007). Controlling water hyacinth is done by several methods, some more cost effective than others. The cost varies based upon infestation, frequency of treatment, and labor costs. Mechanical control of water hyacinth can include both harvesting and shredding with shredding water hyacinth to be the cheaper method (Greenfield, Blankinship & McNabb, 2006). With shredding, these plants decompose within the waterbody negatively altering the nutrient contents of dissolved oxygen (Greenfield et al., 2007).

Chemical control of water hyacinth is one of the most common methods of control in the United States. This type of control includes using submerged or foliar applications, and foliar applications tend to be the more favorable approach. The applications for control of water hyacinth include: glyphosate, 2,4-D amine, diquat, imazamox, imazapyr, imazapic, metsulfuron-methyl, sulfate, and sulfentrazone (Emerine et al., 2010; Gettys et al., 2014; Garlich et al., 2019; Gutierrez et al., 1994; Lopez, 1993; Lugo et al., 1998; Neves et al., 2002; Seagrave, 1988). Higher plant densities of water hyacinth did alter plant response in glyphosate (Lopez, 1993), thus required an additional treatment to achieve plant control. As plant densities increase, chemical control methods may not be the most cost effective method of control.

The use of biological control is a secondary treatment following mechanical or chemical treatments. This provides a conducive environment for weevil populations by providing enough

habitat for the weevils to target the hyacinth but maintain stable populations of weevils when water hyacinth is in low densities. Biological control does require more time for control to increase the population of the biological agent to present significant effects (Center, 1994; Center et al., 1999). The two common weevils for water hyacinth control are *Neochetina eichhorniae* and *N. bruchi*. Although these weevils are native to water hyacinth's range, the control effectiveness is not significant for several years after the first inoculation period (Coetzee, Byrne & Hill, 2007a; Coetzee et al., 2007b; Harley, 1990; Hill & Olckers, 2001; Wilson et al., 2007). Water hyacinth's control can be significant with weevils after several year, thus early detection and rapid response for control is crucial for adequate and effective control.

Using convolutional neural networks for image classification to automate species detection of these two species might simplify and expedite monitoring efforts to detect potential infestations. Multispectral data processing of Worldview-3 satellite data possessing a 1.24 m multispectral resolution, 7.5 m short-wave infrared channel, and a 31 cm panchromatic resolution for a Kaggle competition using an adaptive fully convolutional neural network classified 10 classifications with water and vegetation classes being the highest detected objects (Iglovikov et al., 2017). Deep neural network, Alexnet, was proven to detect and accurately classify underwater vegetation using hydroacoustic data (Patel, 2019). Convolutional neural networks have proven to detect aquatic vegetation, however currently no tools are available to classify floating aquatic macrophytes using convolutional neural networks.

Generation of a model capable of detecting floating macrophytes using a convolutional neural network could provide managers a new tool to rapidly scan publicly available images and extract geolocations to determine if any of these two invasive species are present. Giant salvinia and water hyacinth's rapid growth rate require adequate timing to control these species before

populations become established to limit control measurements. With EDRR monitoring efforts coupled with convolutional neural networks to autonomously detect giant salvinia and water hyacinth, these aquatic nuisances could be controlled before becoming a daunting task. This research aimed to generate a model capable of automatically detecting these two aquatic nuisances using Google Colab, TensorFlow, and Keras API to quickly classify these species using RGB imagery.

Methodology

Giant salvinia and water hyacinth were selected as model species in this initial study on machine learning applications in aquatic plant management. Images were taken with multiple cameras including a GoPro Hero 5, a GoPro Hero 6, and a Panasonic Lumix. These images were collected following standards previously outlined by Mueller et al. (2003). Images were captured in field, laboratory, and mesocosm settings to ensure a broad range of scenarios were encompassed for analysis. Image collection occurred from 10:00-14:00 EST for all imagery collected during all growing months of the year. Each image captured represented unique heights and angles to help strengthen the versatility of the training and testing dataset.

After data collection, each species was separated into their respective directories for classification. Each class was then uploaded to cloud storage on Google Drive to allow access for training through the Google Colab notebook. A total of 1,200 images were utilized to train giant salvinia and 600 images were used to train the water hyacinth. The Keras application program interface, known hereafter as API, was selected for its easy coding and quick experimentation with several optimzers such as Stocastic Gradient Descent (SGD), Adam, Adamax, Nadam, AdaGrad, RMSProp, and AdataDelta to provide little to no changes when moving between

optimizers reducing coding efforts (Ketkar, 2017c). The high-level neural network's API is written in Python and can run on top of TensorFlow. TensorFlow 2.0, and Keras 2.2.5 were the program versions used in this study. Keras allows for easy extensibility, thus new classes and functions are easily added within the algorithm.

Prior to training the model, data were randomly separated into different directories allowing to eliminate data bias. These directories were generated to randomly select images and corresponding files for testing and training. Seventy percent of the data were allotted to the training and 30% were randomly assigned to the testing directory. This process was repeated for each species within the entire data set. However, these parameters are adjustable, and can be easily changed to reflect different values if needed. The model utilized was tf.keras.models.Sequential with an input shape of 600x600 array from three bands. There were 6 separate convolutions, and three dropouts. These dropouts remove neurons and alter the learning of the model to avoid overfitting and allow for the machine to not memorize the dataset. The model selected the RMSprop optimizer with the combination of the loss function as categorical crossentropy, and the activation function as rectified linear activation function (ReLu). RMSprop was selected to for its ability to automatically tune the learning rate from previous stochastic gradients, categorical cross-entropy was selected for the CNN to output the probability over the classes for each image and its outcome to be nonbinary, and ReLu for its output to be positive or otherwise zero (Hinton et al., 2012; Ketkar, 2017a; Ketkar, 2017b) The model summary can be seen in **Table 4.1**. Upon completion of the model, randomly selected images from open sourced platforms with no creative common restrictions were utilized to validate the model. External testing data were comprised of 22 total images:10 containing *Salvinia molesta* D.S. Mitchell, 10 containing *Pontederia crassipes* (Mart.) Solms, and 2 images containing both species.

The precision and recall were determined with true positives (TP), false positives (FP), and false negatives (FN) of the model's classification of either water hyacinth or giant salvinia. The Precision-Recall Curve and average Precision (AP) have been standardized for several object detection studies (Franklin, 2018; Han et al., 2014; Ketkar, 2017d; Zhang et al., 2014), and because of this, the precision, recall, and average precision were calculated based on 22 total images. 10 containing giant salvinia, 10 containing water hyacinth, and 2 that contained both species in the images. To determine the accuracy, Precision-Recall Curve (PRC) was used to determine the proportions of the TP. The formula used to obtain the Precision and recall are as follows:

$$Precision = \frac{TP}{(TP + FP)}$$

$$Recall = \frac{TP}{(TP + FN)}$$

$$mAP = \frac{1}{N}\sum_{i=1}^{N} AP_i$$

Results

The model produced a 98.0% training accuracy with a loss of 0.1312 and a validation accuracy of 100% with a loss of 0.0930. Results were both extremely accurate and precise in identification of the target species with little overfitting of the model. The model's dropouts are

visualized in the graph on the accuracy results validation results can be visualized in **Figure 4.1** and **Figure 4.2**. The training accuracy increases, and the dropout layers can be seen within the model's graph. The dense number of trainable parameters, 63,743,810, provided ample learning points as seen in **Table 4.1**. Training was selected to end upon a callback function allowing the training to commence upon reaching a desired training accuracy of 98 percent accuracy. These model results were then tested against an external dataset for further testing. The testing data returned a 90% accuracy rating for the *Salvinia molesta* and a 40% accuracy in *Pontederia crassipes* (Mart.) Solms during inference **Table 4.2**.

From the PRC, our results obtained from our model revealed a precision score of 0.6470 with giant salvinia. The recall score for giant salvinia was 0.9167. The precision of water hyacinth was 0.8000. The recall for water hyacinth was 0.3333. The *m*AP for water hyacinth and giant salvinia was 0.7994. The *m*AP for the entire model was acceptable, however, the recall of water hyacinth is lower than that of giant salvinia.

Discussion

This application of image classification with a convolutional neural network is especially important in advancing the technology sector within the aquatic plant management industry. These two species selected are two world renowned aquatic invasive weeds. These aquatic nuisance species are likely to continue to spread to new areas as climates continuing to change. With proper implementation of this technology, new populations of these weeds will be autonomously detectable, saving valuable time between detection and control implementation. The development of this system will also benefit the early detection rapid response protocol for new populations within a waterbody. By automizing and training this tool with data mining

open-sourced imagery, vegetation managers can implement this model to increase the likelihood of rapidly identifying invasive species over large quantities images. This tool is capable of processing copious amounts of imagery in minutes. Although this tool does not provide the image classification and location within the image itself like object detection or semantic segmentation, it provides a new approach for rapid detection of species.

This tool is adaptable and allows for new species to be added as more data are collected to address additional species of concern. Adding more diverse imagery from varying environmental ecosystems plagued with water hyacinth and giant salvinia will increase the model's success and rigor in field protocols. Inclusion of new data are needed to provide an alternative response for the model outside of water hyacinth or giant salvinia. This model should further include more imagery of each species, additional species of concern, and also species which are desired. The addition of data will increase training accuracy, precision, recall, and *m*AP. This will provide the model with sufficient data to avoid overfitting to reduce false positives and false negative classifications. The incorporation of more data is needed and total number of images for each species should be in similar quantities per class. The increased amount of imagery will increase the training time of the model. This model was successful in classifying giant salvinia with high recall and precision, however water hyacinth did have a high precision and low recall.

Inclusion of additional imagery will increase the accuracy and precision of this model with classification of these species. The adaptability of this model and easy user interface allows for easy expansion of this classification model. The expansion of this model in classes should be highly considered, and adaptation across multiple classification frameworks and networks should be considered as well. The computing capacity of Google Colab provided enough resources to

train these data, however inclusion of more data may prove to be too much for the free resources causing limitations and timeouts when processing larger data, thus upgrading to Google Colab Pro might be necessary. The model's implementation on a local system should be performed and tested directly against Google Colab to test if there are any differences in precision, recall, accuracy, and training time. Directly testing these results could potentially allow researchers and managers to avoid the cost of building a machine capable of processing these data.

This model could be integrated into a mobile application could provide managers and users an easy way to implement this technology into daily routines with little effort. Extraction of geographical positioning satellite data from the exchangeable image file (EXIF) data would provide information for production of a species habitat range map. This data and use of the model could be integrated to produce species density maps to better understand the species invasion to be included in an integrated vegetation management (IVM) plan. Inclusion of these models in an IVM plan would provide managers a new tool for site evaluation, monitoring treatments, and quality assurance. Prior to using this model at a large scale, it will need a diversified dataset and include species outside of water hyacinth and giant salvinia. Inclusion of new species to the dataset will provide the model the ability to reduce false positives from misclassifications.

Conclusions

Successful identification of the studied species in testing and validation datasets was achieved. These data are easily adaptable and will allow for further adaptation of this model in subsequent years as new invasive species begin to appear in water bodies. Additional data is needed to obtain a more wholistic approach to each species and should be performed prior to

implementation of this model in the field to reduce false positives and false negatives classifications of these species. The amount of imagery for each class in this model from training would need in excess of 1000 images per species for adequate detection.

Google Colab is an excellent resource and should be considered with machine learning projects, however there is a threshold in the amount of data the system will process. Google Colab was able to process the total amount of imagery in this study and provide adequate results. Future models generated could be built upon this one with addition of new data for training and testing by using this framework and model for transfer learning. Generation of new models with new species should consider using Keras because of its easy implementation, however other platforms and frameworks are available and should be tested in classification of these species. Further testing with more optimizers, loss functions, and activation functions will yield different results. Different frameworks outside of keras could provide better results than seen in this study, however, those could provide other challenges including increased cost by having to build a local machine. The model framework should be further evaluated with new classes by selecting different combination of optimizers, activation functions, and loss functions to ultimately increase the model's overall results. This research utilized cloud computing resources and performed successful image classifications on two world renowned invasive aquatic species.

REFERENCES

Abadi, M., Barham, P., Chen, J., Chen, Z., Davis, A., Dean, J., ... & Kudlur, M. (2016). Tensorflow: A system for large-scale machine learning. In *12th {USENIX} Symposium on Operating Systems Design and Implementation ({OSDI} 16)* (pp. 265-283).

Bisong, E. (2019). Google Colaboratory. In *Building Machine Learning and Deep Learning Models on Google Cloud Platform* (pp. 59-64). Apress, Berkeley, CA.

Carneiro, T., Da Nóbrega, R. V. M., Nepomuceno, T., Bian, G. B., De Albuquerque, V. H. C., & Reboucas Filho, P. P. (2018). Performance analysis of Google Colaboratory as a tool for accelerating deep learning applications. *I EEE Access*, *6*, 61677-61685.

Center, T. D. (1994). Biological control of weeds: waterhyacinth and waterlettuce. Pest Management in the Subtropics: Biological Control–A Florida Perspective. *D. Rosen FD Bennett and JL Capinera Intercept Ltd Hampshire UK*, 482-521.

Center, T. D., Dray Jr, F. A., Jubinsky, G. P., & Grodowitz, M. J. (1999). Biological control of water hyacinth under conditions of maintenance management: can herbicides and insects be integrated?. *Environmental Management*, *23*(2), 241-256.

Coetzee, J. A., Byrne, M. J., & Hill, M. P. (2007a). Impact of nutrients and herbivory by *Eccritotarsus catarinensis* on the biological control of water hyacinth, *Eichhornia crassipes*. *Aquatic Botany*, *86*(2), 179-186.

Coetzee, J. A., Byrne, M. J., & Hill, M. P. (2007b). Predicting the distribution of *Eccritotarsus catarinensis*, a natural enemy released on water hyacinth in South Africa. *Entomologia Experimentalis et Applicata*, *125*(3), 237-247.

Emerine, S. E., Richardson, R. J., True, S. L., West, A. M., & Roten, R. L. (2010). Greenhouse response of six aquatic invasive weeds to imazamox. *Journal of Aquatic Plant Management (JAPM)*, *48*, 105.

Franklin, S. E. (2018). Pixel-and object-based multispectral classification of forest tree species from small unmanned aerial vehicles. *Journal of Unmanned Vehicle Systems*, *6*(4), 195-211.

Gaudet, J. J. (1973). Growth of a floating aquatic weed, Salvinia under standard conditions. *Hydrobiologia*, *41*(1), 77-106.

Garlich, N., Guarnieri, C. C. O., Freitas, R. L. G., Cervoni, J. H. C., Cruz, C., & Ferreira, M. C. (2019). Efficacy of imazamox with centrifugal energy spray nozzle on *Eichhornia crassipes* and economic analysis of control viability. *Planta Daninha*, *37*.

Gettys, L. A., Haller, W. T., & Bellaud, M. (2014). Biology and control of aquatic plants. *A Best Management Practices Handbook: Third Edition. Aquatic Ecosystem Restoration Foundation, Marietta, GA*.

Greenfield, B. K., Blankinship, M., & McNabb, T. J. (2006). Control costs, operation, and permitting issues for non-chemical plant control: case studies in the San Francisco Bay-Delta region, California. *Journal of Aquatic Plant Management*, *44*(1), 40-49.

Greenfield, B. K., Siemering, G. S., Andrews, J. C., Rajan, M., Andrews, S. P., & Spencer, D. F. (2007). Mechanical shredding of water hyacinth (*Eichhornia crassipes*): Effects on water quality in the Sacramento-San Joaquin River Delta, California. *Estuaries and Coasts*, *30*(4), 627-640.

Gutierrez E, Arreguin F, Huerto R, Saldana P. (1994). Aquatic weed control. *International Journal of Water Resources Development 10*(3),291-312.

Han, J., Zhang, D., Cheng, G., Guo, L., & Ren, J. (2014). Object detection in optical remote sensing images based on weakly supervised learning and high-level feature learning. *IEEE Transactions on Geoscience and Remote Sensing*, *53*(6), 3325-3337.

Harley, K. L. S. (1990). The role of biological control in the management of water hyacinth, *Eichhornia crassipes*. *Biocontrol News and Information*, *11*(1), 11-22.

Hellmann, J. J., Byers, J. E., Bierwagen, B. G., & Dukes, J. S. (2008). Five potential consequences of climate change for invasive species. *Conservation biology*, *22*(3), 534-543.

Hill, M. P., & Olckers, T. (2000, October). Biological control initiatives against water hyacinth in South Africa: constraining factors, success and new courses of action. In *ACIAR proceedings* (pp. 33-38). ACIAR; 1998.

Hinton, G., Srivastava, N., & Swersky, K. (2012). Neural networks for machine learning lecture 6a overview of mini-batch gradient descent. *Cited on*, *14*(8).

Holm, L. G., Plucknett, D. L., Pancho, J. V., & Herberger, J. P. (1977). *The world's worst weeds. Distribution and biology*. University press of Hawaii.

Hunt, R., & Christensen, I. H. (2000). *Understanding dissolved oxygen in streams: Information kit*. CRC Sugar.

Iglovikov, V., Mushinskiy, S., & Osin, V. (2017). Satellite imagery feature detection using deep convolutional neural network: A kaggle competition. *arXiv preprint arXiv:1706.06169*.

Jayanth, K. P. (1988). Successful biological control of water hyacinth (*Eichhornia crassipes*) by *Neochetina eichhorniae* (Coleoptera: Curculionidae) in Bangalore, India. *International Journal of Pest Management*, *34*(3), 263-266.

Johnson, D. 1995. Giant salvinia found in South Carolina. Aquatics 17(4):22.

Kay, S. H. and S. T. Hoyle. 2001. Mail order, the internet, and invasive aquatic weeds. J. Aquat. Plant Manage. 39:88-91.

Ketkar, N. (2017a). Introduction to keras. In *Deep learning with Python* (pp. 26-28). Apress, Berkeley, CA.

Ketkar, N. (2017b). Introduction to keras. In *Deep learning with Python* (pp. 34). Apress, Berkeley, CA.

Ketkar, N. (2017c). Introduction to keras. In *Deep learning with Python* (pp. 97-111). Apress, Berkeley, CA.

Ketkar, N. (2017d). Introduction to pytorch. In *Deep learning with python* (pp. 195-208). Apress, Berkeley, CA.

Lopez, E. G. (1993). Effect of glyphosate on different densities of water hyacinth. *Journal of Aquatic Plant Management*, *31*, 255-257.

Lugo, A., Bravo-Inclan, L. A., Alcocer, J., Gaytán, M. L., Oliva, M. G., Sánchez, M. D. R., ... & Vilaclara, G. (1998). Effect on the planktonic community of the chemical program used to control water hyacinth (*Eichhornia crassipes*) in Guadalupe Dam, Mexico. *Aquatic Ecosystem Health & Management*, *1*(3-4), 333-343.

Mangas-Ramírez, E., & Elías-Gutiérrez, M. (2004). Effect of mechanical removal of water hyacinth (*Eichhornia crassipes*) on the water quality and biological communities in a Mexican reservoir. *Aquatic Ecosystem Health & Management*, *7*(1), 161-168.

Meerhoff, M., Mazzeo, N., Moss, B., & Rodríguez-Gallego, L. (2003). The structuring role of free-floating versus submerged plants in a subtropical shallow lake. *Aquatic Ecology*, *37*(4), 377-391.

Meng, C., Sun, M., Yang, J., Qiu, M., & Gu, Y. (2017, December). Training deeper models by GPU memory optimization on TensorFlow. In *Proc. of ML Systems Workshop in NIPS*.

Mitchell, D. S. (1985). Surface-floating aquatic macrophytes. In *The ecology and management of African wetland vegetation* (pp. 109-124). Springer, Dordrecht.

Mitchell, D. S., & Tur, N. M. (1975). The rate of growth of *Salvinia molesta* (*S. auriculata* Auct.) in laboratory and natural conditions. *Journal of Applied Ecology*, 213-225.

Mudge, Christopher R., and Michael D. Netherland. 2020. Evaluation of New Endothall and Florpyrauxifen-benzyl Use Patterns for Controlling Crested Floating Heart. APCRP Technical Notes Collection. ERDC/TN APCRP-CC-22. Vicksburg, MS: US Army Engineer Research and Development Center. https://el.erdc.dren.mil/aqua/aqua.html..

Mudge, C. R., Perret, A. J., & Winslow, J. R. (2016). Evaluation of foliar herbicide and surfactant combinations for control of giant salvinia at three application timings. *J. Aquat. Plant Manag.*, *54*, 32-36.

Mueller, J. L., Morel, A., Frouin, R., et al. 2003. Ocean optics protocols for satellite ocean color sensor validation, Revision 4, Volume III: Radiometric measurements and data analysis protocols. National Aeronautical and Space Administration. 4(3):1-78.

Neves, T., Foloni, L. L., & Pitelli, R. A. (2002). Controle químico do aguapé (*Eichhornia crassipes*). *Planta Daninha*, *20*(SPE), 89-97.

Patel, M., Jernigan, S., Richardson, R., Ferguson, S., & Buckner, G. (2019). Autonomous robotics for identification and management of invasive aquatic plant species. *Applied Sciences*, *9*(12), 2410.

Perna, C., & Burrows, D. (2005). Improved dissolved oxygen status following removal of exotic weed mats in important fish habitat lagoons of the tropical Burdekin River floodplain, Australia. *Marine Pollution Bulletin*, *51*(1-4), 138-148.

Rahel, F. J., & Olden, J. D. (2008). Assessing the effects of climate change on aquatic invasive species. *Conservation Biology*, *22*(3), 521-533.

Reddy, K. R., & DeBusk, W. F. (1984). Growth characteristics of aquatic macrophytes cultured in nutrient-enriched water: I. Water hyacinth, water lettuce, and pennywort. *Economic Botany*, *38*(2), 229-239.

Rodriguez-Gallego, L. R., Mazzeo, N., Gorga, J., Meerhoff, M., Clemente, J., Kruk, C., ... & Quintans, F. (2004). The effects of an artificial wetland dominated by free-floating plants on the restoration of a subtropical, hypertrophic lake. *Lakes & Reservoirs: Research & Management*, *9*(3-4), 203-215.

Rommens, W., Maes, J., Dekeza, N., Inghelbrecht, P., Nhiwatiwa, T., Holsters, E., ... & Brendonck, L. (2003). The impact of water hyacinth (*Eichhornia crassipes*) in a eutrophic subtropical impoundment (Lake Chivero, Zimbabwe). I. Water quality. *Archiv für Hydrobiologie*, *158*(3), 373-388.

Seagrave, C. (1988). Aquatic weed control. Farnham, Surrey, UK, Fishing News Books Ltd.

Simard, P. Y., Steinkraus, D., & Platt, J. C. (2003, August). Best practices for convolutional neural networks applied to visual document analysis. In *Icdar* (Vol. 3, No. 2003).

Troutman, J. P., Rutherford, D. A., & Kelso, W. E. (2007). Patterns of habitat use among vegetation-dwelling littoral fishes in the Atchafalaya River Basin, Louisiana. *Transactions of the American Fisheries Society*, *136*(4), 1063-1075.

Whiteman, J. B., & Room, P. M. (1991). Temperatures lethal to *Salvinia molesta* Mitchell. *Aquatic Botany*, *40*(1), 27-35.

Wilson, J. R., Ajuonu, O., Center, T. D., Hill, M. P., Julien, M. H., Katagira, F. F., ... & Van, T. (2007). The decline of water hyacinth on Lake Victoria was due to biological control by Neochetina spp. *Aquatic Botany*, *87*(1), 90-93.

Zhang, D., Han, J., Cheng, G., Liu, Z., Bu, S., & Guo, L. (2014). Weakly supervised learning for target detection in remote sensing images. *IEEE Geoscience and Remote Sensing Letters*, *12*(4), 701-705.

Table 4.1. Contains the model summary from framework produced with Keras in Google Colab.

Model: "Sequential_1"		
Layer (type)	Output Shape	Param #
conv2d_6 (Conv2D)	(None, 596, 596, 64)	864
max_pooling2d_6 (MaxPooling2	(None, 298, 298, 64)	0
dropout_4 (Dropout)	(None, 298, 298, 64)	0
conv2d_7 (Conv2D)	(None, 294, 294, 64)	102464
max_pooling2d_7 (MaxPooling2	(None, 147, 147, 64)	0
dropout_5 (Dropout)	(None, 147, 147, 64)	0
conv2d_8 (Conv2D)	(None, 145, 145, 128)	73856
max_pooling2d_8 (MaxPooling2	(None, 72, 72, 128)	0
dropout_6 (Dropout)	(None, 72, 72, 128)	0
conv2d_9 (Conv2D)	(None, 70, 70, 128)	147584
max_pooling2d_9 (MaxPooling2	(None, 35, 35, 128)	0
conv2d_10 (Conv2D)	(None, 33, 33, 256)	295168
max_pooling2d_10 (MaxPooling	(None, 16, 16, 256)	0
conv2d_11 (Conv2D)	(None, 14, 14, 256)	590080
max_pooling2d_11 (MaxPooling	(None, 7, 7, 256)	0
flatten_1 (Flatten)	(None, 12544)	0
dropout_7 (Dropout)	(None, 12544)	0
dense_6 (Dense)	(None, 4096)	51384320
dense_7 (Dense)	(None, 2048)	8390656
dense_8 (Dense)	(None, 1024)	2098176
dense_9 (Dense)	(None, 512)	524800
dense_10 (Dense)	(None, 256)	131328
dense_11 (Dense)	(None, 2)	514
==========		
Total params: 63,743,810		
Trainable params: 63,743,810		
Non-trainable params: 0		

Table 4.2. Results from inference classifications performed using TensorFlow backend. These results are used in calculation of recall, precision, and *m*AP for the model.

Image	*Pontederia crassipes* (Mart.) Solms	*Salvinia molesta* D.S. Mitchell
sm1	8.15E-13	1.00E+00
sm2	9.19E-11	1.00E+00
sm3	0.8365022	0.16349782
sm4	0.32641342	0.6735866
sm5	0.3265838	0.6734162
sm6	0.01418789	0.98581207
sm7	4.61E-14	1.00E+00
sm8	3.36E-04	1.00E+00
sm9	2.95E-08	1.00E+00
sm10	5.55E-06	1.00E+00
pc1	2.32E-04	1.00E+00
pc2	0.08032066	0.91967934
pc3	1	0.00E+00
pc4	0.00E+00	1.00E+00
pc5	4.24E-07	1.00E+00
pc6	1.00E+00	9.57E-12
pc7	3.26E-01	0.673589
pc8	3.00E-08	1.00E+00
pc9	1.00E+00	0.00E+00
pc10	1.00E+00	3.56E-10
both	0.32641342	0.6735866
both	0.14971724	0.8502827

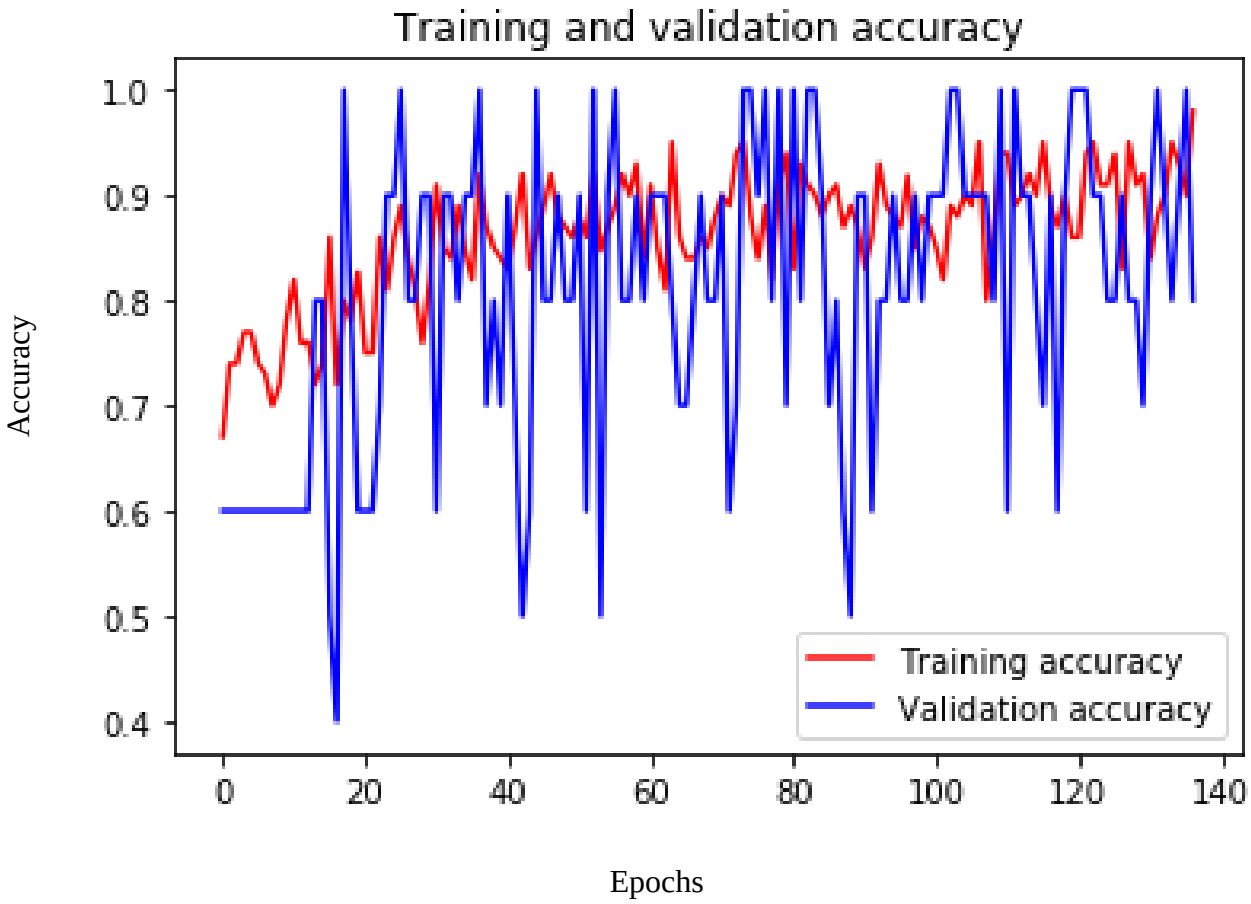

Figure 4.1: Training and validation accuracy generated from the log file using TensorFlow backend.

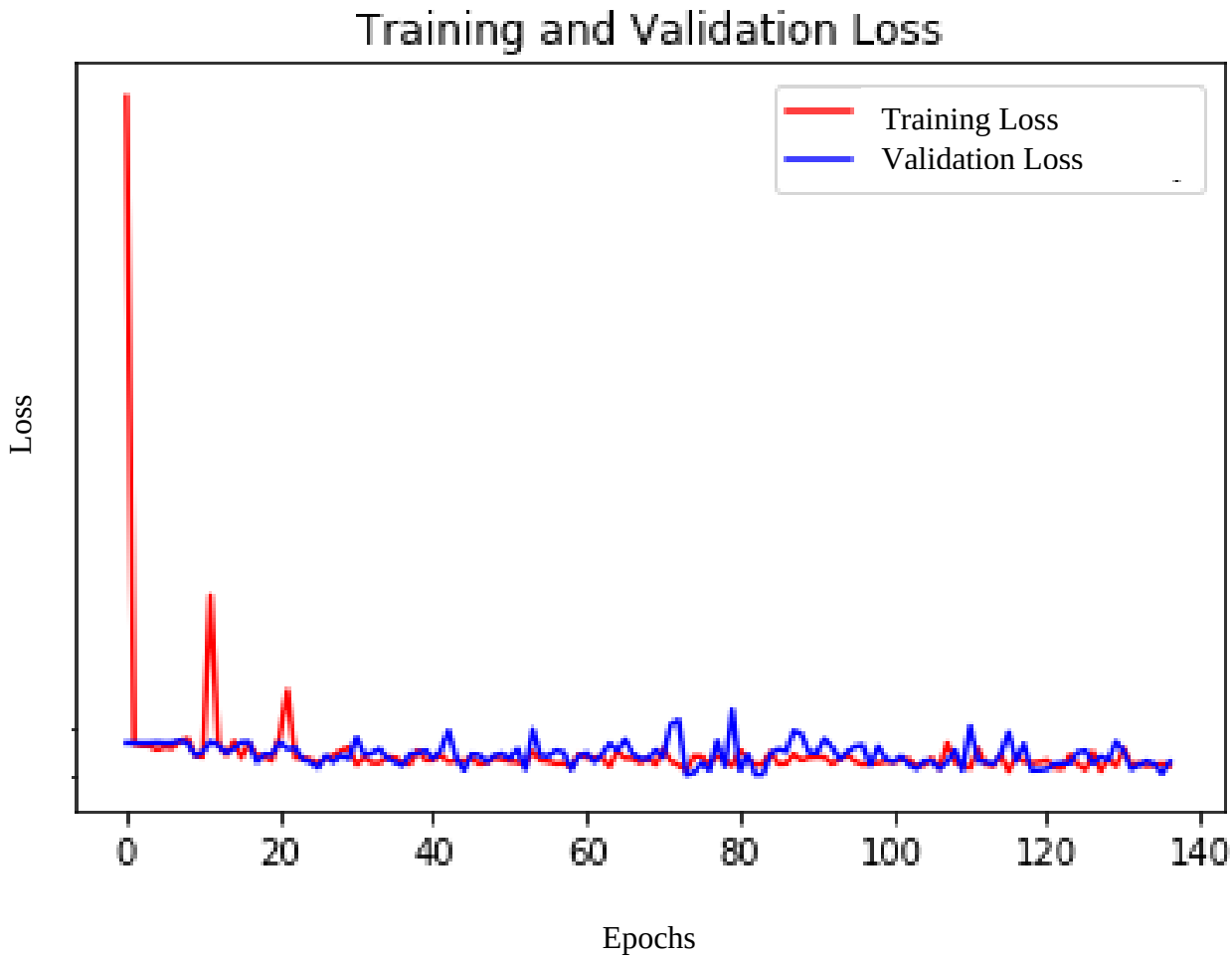

Figure 4.2. Training and Validation Loss generated form the log file using TensorFlow backend.